72-1030

TRANSNUCLEAR

E-21720
November 19, 2004

Ms. Mary Jane Ross-Lee
Spent Fuel Project Office, NMSS
U. S. Nuclear Regulatory Commission
11555 Rockville Pike M/S 0-6-F-18
Rockville, MD 20852

Subject: SAR Rev 1 of the NUHOMS® HD Storage System Docket No. 72-01030.

Dear Ms. Ross-Lee:

In order to accommodate potential customers of the NUHOMS® HD Dry Storage System, Transnuclear, Inc. (TN) has performed evaluations which support the use of Combustion Engineering 14 x 14 fuel assemblies in the 32PTH canister. Accordingly, we have revised the NUHOMS® HD Dry Storage System Safety Analysis Report (SAR) to include information which supports the inclusion of the CE 14x14 as authorized contents for the NUHOMS® HD Dry Storage System. Enclosed are seven (7) copies of Revision 1 pages for the NUHOMS® HD Horizontal Modular Storage System Safety Analysis Report (SAR).

Because the CE 14x14 fuel assembly is smaller in size, weight and contains a lower quantity of fuel than the contents currently described in the SAR, the majority of analyses described in the current SAR are bounding and only a few new analyses were required for the CE fuel. The only structural changes are additional analyses for the cladding stress during the drop accidents and damaged fuel cladding (Appendix 3.9.8). New thermal analyses were performed for the smaller CE fuel assembly and a slightly lower DSC kW rating was selected in order to maintain the current SAR bounding temperatures. The radiological source from the CE assembly is bounded by the current SAR design basis fuel, therefore, additional shielding analyses are not required. As with the current contents, criticality analyses were performed for the CE 14x14 assembly. to define the reactivity parameters, (enrichment, boron water concentration, boron loading in the basket).

Revision bars have been placed in the right hand margin to identify the changes. This revision is being made solely to address the inclusion of the CE 14 x 14 fuel assembly. Therefore, the revisions pertain only to the CE 14 x 14 fuel assembly; however, we have taken this opportunity to make some minor corrections, (typos, etc.). These corrections are identified below.

Page 4-5	Conductivity and Temperature data were reversed for Lead.
Page 4-24	Total Volume value was corrected in the table.
Page 4-25	The $\overline{C}_p$ value was corrected.
Page 4-34	Reference [25] was changed to [31].
Page 4-74	Reference 25 was a duplicate of reference 31.
Table 4-14	Corrected title –Sections 2 to 12

FOUR SKYLINE DRIVE, HAWTHORNE, NEW YORK 10532
Phone: 914-347-2345 • Fax: 914-347-2346 • E-mail: TRANSNCLR@AOL.COM

NMSS01

Table 4-19	Corrected h_c units to BTU/hr-ft^2-^{o}F
Page 5-2	Corrected Advanced NUHOMS... to NUHOMS HD...
Page 6-9	Removed duplicate 1st paragraph under 6.4.1.2.
Table 6-7	Deleted *Core* and corrected value to 0.075"

If you have any questions, please contact me.

Sincerely,

Michael Mason
Chief Engineer

Enclosures: as stated above

Insertion of 32PTH DSC into HSM: After final alignment of the transfer cask, HSM-H, and hydraulic ram, the 32PTH DSC is pushed into the HSM-H by the hydraulic ram.

HSM Closure: Install 32PTH DSC axial retainer and install HSM-H door.

1.2.2.3 Identification of Subjects for Safety and Reliability Analysis

1.2.2.3.1 Criticality Prevention

Criticality is controlled by utilizing the fixed borated neutron absorbing material in the 32PTH DSC basket and the pool water boron loading. During storage, with the cavity dry and sealed from the environment, criticality control measures within the installation are not necessary because water cannot enter the canister during storage.

1.2.2.3.2 Chemical Safety

There are no chemical safety hazards associated with operations of the NUHOMS® HD System. The coating materials used in the design of the 32PTH DSC are chosen to minimize hydrogen generation. Hydrogen monitoring is required during sealing operations to ensure hydrogen concentration levels remain within acceptable limits.

1.2.2.3.3 Operation Shutdown Modes

The NUHOMS® HD System is a totally passive system so that consideration of operation shutdown modes is unnecessary.

1.2.2.3.4 Instrumentation

The NUHOMS® HD System is a totally passive system. No safety-related instrumentation is necessary. The maximum temperatures and pressures are conservatively bounded by analyses. Therefore, there is no need for monitoring the internal cavity of the 32PTH DSC for pressure or temperature during normal operations. The 32PTH DSC is conservatively designed to perform its confinement function during all worst case normal, off-normal, and accident conditions.

1.2.2.3.5 Maintenance and Surveillance

All maintenance and surveillance tasks are described in Chapter 9.

1.2.3 32PTH DSC Contents

The 32PTH DSC is designed to store up to 32 intact PWR Combustion Engineering 14x14 (CE 14x14), Westinghouse 15x15 (WE 15x15), Westinghouse 17x17 (WE 17x17), and/or Framatome ANP Advanced MK BW 17x17 fuel assemblies (Fr 17x17) with or without NFHAs likeVibration Suppressor Inserts (VSI), Burnable Poison Rod Assemblies (BPRAs), or Thimble Plug Assemblies (TPAs). The 32PTH DSC is also designed for storage of up to 16 damaged fuel assemblies, and remaining intact assemblies, utilizing top and bottom end caps. A description of the fuel assemblies including the damaged fuel assemblies is provided in Chapter 2.

The maximum allowable initial enrichment of the fuel to be stored is 5.00 weight % U-235 and the maximum burnup is 60,000 MWd/MTU. The fuel must be cooled at least 5 years prior to storage.

The criticality control features of the NUHOMS® HD System are designed to maintain the neutron multiplication factor k-effective (including uncertainties and calculational bias) at less than 0.95 under normal, off-normal, and accident conditions.

The quantity and type of radionuclides in the SFAs are described and tabulated in Chapter 5. Chapter 6 covers the criticality safety of the NUHOMS® HD System and its parameters. These parameters include rod pitch, rod outside diameter, material densities, moderator ratios, and geometric configurations. The maximum pressure buildup in the 32PTH DSC cavity is addressed in Chapter 4.

2. PRINCIPAL DESIGN CRITERIA

2.1 Spent Fuel to be Stored

The NUHOMS® HD System components have currently been designed for the storage of 32 intact and or up to 16 damaged with remaining intact, Westinghouse 15x15 (WE 15x15), Westinghouse 17x17 (WE 17x17), Framatome ANP Advanced 17x17 MK BW (FR 17x17), and/or Combustion Engineering 14x14 (CE 14x14) PWR fuel assemblies. Additional payloads may be defined in future amendments to this application.

The thermal and radiological characteristics for the PWR spent fuel were generated using the SCALE computer code package [1]. The physical characteristics for the PWR fuel assembly types are shown in Table 2-1. Free volume in the 32PTH DSC cavity is addressed in Chapter 4. Specific gamma and neutron source spectra are given in Chapter 5.

Although analyses in this SAR are performed only for the design basis fuel, any other intact or damaged PWR fuel which falls within the geometric, thermal, and nuclear limits established for the design basis fuel can be stored in the 32PTH DSC.

2.1.1 Detailed Payload Description

This payload consists of 32 PWR UO_2 fuel assemblies with or without Non-Fuel Assembly Hardware (NFAH) which includes Burnable Poison Rod Assemblies, (BPRAs), Vibration Suppression Inserts (VSI) or Thimble Plug Assemblies (TPAs). Each 32PTH DSC can accommodate a maximum of sixteen damaged fuel assemblies, with the remaining assemblies intact. The fuel to be stored in the 32PTH DSC is limited to fuel with a maximum assembly average initial enrichment of 5.00 weight % U-235. The maximum allowable burnup is given as a function of initial fuel enrichment but does not exceed 60,000 MWd/MTU. The minimum cooling time is five years.

The 32PTH DSC may store up to 32 PWR fuel assemblies arranged in accordance with a heat load zoning configuration as shown in Figure 2-1, with a maximum decay heat of 1.5 kW per assembly and a maximum heat load of 34.8 kW per DSC, (33.8 kW per DSC for CE 14x14)

The 32PTH DSC can accommodate up to 16 damaged fuel assemblies which include assemblies with known or suspected cladding defects greater than hairline cracks or pinhole leaks, up to and including broken rods, portions of broken rods and rods with missing sections. Damaged fuel assemblies shall be placed into the sixteen inner most basket fuel compartments, as shown in Figure 2-2, which contain top and bottom end caps that confine any loose material and gross fuel particles to a known, subcritical volume during normal, off-normal and accident conditions and to facilitate handling and retrievability. A visual inspection of assemblies will be performed prior to placement of the fuel in the 32PTH DSC, which may then be placed in storage or transported anytime thereafter without further fuel inspection.

The NUHOMS®-32TH DSC basket is designed with three alternate poison materials: Borated Aluminum alloy, Boron Carbide/Aluminum Metal Matrix Composite (MMC) and Boral®.

For criticality analysis, 90% of B10 content present in the borated aluminum and MMC poison plates is credited, while only 75% is credited for Boral®.

The NUHOMS®-32PTH DSC basket is analyzed for seven alternate basket configurations, depending on the boron loadings and poison materials.

A summary of the alternate poison loadings considered for each poison material as a function of basket types is presented below:

NUHOMS®-32PTH DSC Basket Type	Minimum B10 Aerial Density, gm/cm^2	
	Natural or Enriched Boron Aluminum Alloy / Metal Matric Composite (MMC)	Boral®
IA or IIA	0.007	0.009
IB or IIB	0.015	0.019
IC or IIC	0.020	0.025
ID	0.032	N/A
IE	0.050	N/A

Table 2-2 shows a parametric equation that can be utilized to qualify spent fuel assemblies for the defined decay heat load zones. The decay heat load can be calculated based on a fuel assembly's burnup, cool time, and initial enrichment parameters. This table ensures that the fuel assembly decay heat load is within the appropriate zone. The development of this equation is provided in Appendix 4.16.2.

The maximum fuel cladding temperature limit of 400°C (752°F) is applicable to normal conditions of storage and all short term operations from spent fuel pool to ISFSI pad including vacuum drying and helium backfilling of the NUHOMS®-32PTH DSC per Interim Staff Guidance (ISG) No. 11, Revision 2 [15]. In addition, ISG-11 does not permit thermal cycling of the fuel cladding with temperature differences greater than 65°C (117°F) during DSC drying, backfilling and transfer operations.

The maximum fuel cladding temperature limit of 570°C (1058°F) is applicable to accidents or off-normal thermal transients [15].

Calculations were performed to determine the fuel assembly type which was most limiting for each of the analyses including shielding, criticality, thermal and confinement. These evaluations are performed in Chapters 5 and 6. The fuel assembly classes considered are listed in Table 2-1. It was determined that the Framatome 17x17 is the enveloping fuel design for the shielding, thermal and confinement source term calculation because of its total assembly weight and highest initial heavy metal loading. The bounding source term for shielding analysis is given in Table 2-3. Table 2-4 presents the thermal and radiological source terms for the Non-Fuel Assembly Hardware (NFAH).

Table 2-1
Spent Fuel Assembly Physical Characteristics

Parameter	WE 15x15	WE 17 x 17 Std	FR 17x17 MK BW	WE 17x17 Vantage 5H	WE 17x17 OFA	CE 14x14 Std
Initial Enrichment, wt % U235 (max)	5.00	5.00	5.00	5.00	5.00	5.00
Clad material	Zircaloy, Zirlo	Zircaloy, Zirlo	M5	Zircaloy, Zirlo	Zircaloy, Zirlo	Zircaloy, Zirlo
No of fuel rods	204	264	264	264	264	176
No of guide/instrument tubes	21	25	25	25	25	5
Assembly Length[4]	162.2	162.4	162.4	162.4	162.4	159.5
Max Uranium Loading (MTU)	467	467	476	467	467	385
Assembly Cross Section	8.424 x 8.424	8.426 x 8.426	8.425 x 8.425	8.426 x 8.426	8.426 x 8.426	8.25 x 8.25
Max Assembly Weight with NFAHs[5] (lbs)	1528	1575	1554	1533	1533	1450[6]

(1) Nominal values shown unless stated otherwise
(2) All dimensions in inches
(3) Where there are variations in a reported value for a given design, the values highlighted are chosen for the criticality analysis. Thermal analysis uses the minimum values
(4) Includes irradiation growth
(5) Weights of TPAs and VSIs are enveloped by BPRAs
(6) Without NFAHs

Table 3-12
Maximum axial stresses in the cladding during 75g side drop

Fuel Assembly Type	WE15x15	WE 17x17std	17x17 MkBW	WE 17x17 Vantage5H	WE 17x17OFA	CE 14x14 Std
Fuel Rod OD, D (in) [1][11]	0.4193	0.3713	0.3713	0.3713	0.3573	0.4373
Clad Thickness, t (in) [1][11]	0.0216	0.0198	0.0213	0.0198	0.0198	0.0253
Average Radius, R (in) [2]	0.1989	0.1758	0.1750	0.1758	0.1688	0.2060
Fuel Pallet OD, D_P (in) [1]	0.3659	0.3225	0.3195	0.3225	0.3088	0.3765
Fuel Tube M.I., I_F (in^4) [3]	5.35E-04	3.39E-04	3.60E-04	3.39E-04	3.00E-04	6.97E-04
Fuel Pellet M.I., I_P (in^4) [4]	8.80E-04	5.31E-04	5.12E-04	5.31E-04	4.46E-04	9.86E-04
I_{Total} (in^4) [5]	1.42E-03	8.70E-04	8.71E-04	8.70E-04	7.46E-04	1.68E-03
Span Length, S (in)	27.0	25.0	25.0	25.0	25.0	17.0
Fuel Assbly Weight, W_F (lb) [1]	1,555	1,575	1,575	1,575	1,575	1,450
No.of Rods, N [1]	204	264	264	264	264	176
Active Fuel Length, L (in) [1]	144.0	144.0	144.0	144.0	144.0	137.0
30-Foot Side Drop Equivalent g load	75	75	75	75	75	75
w_s (lb/in) [9]	3.97	3.11	3.11	3.11	3.11	4.51
Moment, M (kip.in) [6]	0.31	0.21	0.21	0.21	0.21	0.14
Bending Stress, S_b (psi) [7]	45,368	43,858	43,771	43,858	49,185	17,908
Internal Pressure, P (psi)	2,235	2,235	2,235	2,235	2,235	2,235
Pressure Axial Stress, $S_{press.}$(psi) [8]	10,289	9,921	9,183	9,921	9,525	9,100
$S=S_b+S_{press.}$ (psi)	55,657	53,778	52,954	53,778	58,710	27,010
Allowable Stress, $S_{all} = S_y$ (psi) [9]	80,500	80,500	80,500	80,500	80,500	80,500

Note:

1. Input data from Chapter 2, Table 2 -1 & Chapter 6, Table 6-4
2. $R = (D-t)/2$
3. $I_F = \pi / 64 \times (D^4 - (D - 2\,t)^4)$
4. $I_P = \pi / 64 \times D_P^4$
5. $I_{Total} = I_F + I_P$
6. $M = 0.1058\, w_s\, S^2$
7. $S_b = M \times (D / 2) / I_{Total}$
8. $S_{Press.} = (P \times R) / (2 \times t)$
9. Yield strength for Zircaloy cladding tube at 750 °F.
10. $w_s = (W_F \times 75g) / N / L$
11. Reduction of wall thickness by 0.0027 inch

APPENDIX 3.9.8
DAMAGED FUEL CLADDING STRUCTURAL EVALUATION

TABLE OF CONTENTS

3.9.8 DAMAGED FUEL CLADDING STRUCTURAL EVALUATION 3.9.8-1

3.9.8.1 Introduction 3.9.8-1

3.9.8.2 Design Input / Data 3.9.8-2

3.9.8.3 Loads 3.9.8-3

3.9.8.4 Evaluation Criteria 3.9.8-5

3.9.8.5 Evaluation Methodology 3.9.8-6

3.9.8.6 Trailer Acceleration from 0 mph to 5 mph during Transfer 3.9.8-8

3.9.8.7 Trailer Deceleration from 5 mph to 0 mph during Transfer 3.9.8-11

3.9.8.8 Normal Loading Condition during Insertion / Retrieval of DSC into / from HSM 3.9.8-13

3.9.8.9 Off-Normal Jammed Canister Loading during Insertion of DSC into HSM 3.9.8-14

3.9.8.10 One Foot End Drop Damaged Fuel Evaluation 3.9.8-15

3.9.8.11 One Foot Side Drop Damaged Fuel Evaluation 3.9.8-16

3.9.8.12 Conclusions 3.9.8-20

3.9.8.13 References 3.9.8-21

LIST OF TABLES

3.9.8-1 Westinghouse 15x15 - K_I Calculation using Fracture Geometry #2

3.9.8-2 Westinghouse 17x17 Std - K_I Calculation using Fracture Geometry #2

3.9.8-3 Framatome 17x17 MKBW - K_I Calculation using Fracture Geometry #2

3.9.8-4 Westinghouse 17x17 Vantage 5H - K_I Calculation using Fracture Geometry #2

3.9.8-5 Westinghouse 17x17 OFA - K_I Calculation using Fracture Geometry #2

3.9.8-6 Combustion Engineering 14x14 - K_I Calculation using Fracture Geometry #2

3.9.8-7 Summary - Maximum Fuel Rod Stresses and Stress Ratios

3.9.8-8 Summary - Computed Fuel Tube Stress Intensity Factors and Ratios

3.9.8-9 Derivation of Tensile Force (T) and Applied Moment (M) Relationship for a Circular Tube

3.9.8-10 Tire Stiffness Calculation

LIST OF FIGURES

3.9.8-1 Fracture Geometry #1: Ruptured Section

3.9.8-2 Fracture Geometry #2: Through-Wall Circumferential Crack in Cylinder Under Bending

3.9.8-3 Stress Intensity Factor Solutions For Several Specimen Configurations

3.9.8 DAMAGED FUEL CLADDING STRUCTURAL EVALUATION

3.9.8.1 Introduction

The purpose of this appendix is to demonstrate structural integrity of the damaged fuel cladding in the NUHOMS® 32PTH DSC following normal and off-normal loading conditions of storage and onsite transfer (required for Part 72 License) and normal condition of offsite transport (required for Part 71 License).

In this appendix, the damaged fuel is defined as: "damaged PWR fuel assemblies are fuel assemblies containing missing or partial fuel rods or fuel rods with known or suspected cladding defects greater than hairline cracks or pinhole leaks. The extent of cladding damage in the fuel rods is to be limited such that a fuel pellet is not able to pass through the damaged cladding during handling and retrievability is assured following Normal/Off-Normal conditions".

This appendix evaluates stresses in the fuel cladding associated with normal and off-normal conditions of on-site transfer/storage and off-site transport. It also presents a fracture mechanics assessment of the cladding using conservative assumptions regarding defect size geometry and amount of oxidation in the cladding material. These evaluations demonstrate the structural integrity of the damaged fuel cladding under normal and off-normal conditions.

The NUHOMS® 32PTH DSC is designed to store 32 intact fuel assemblies, or no more than 16 damaged and the remainder intact, for a total of 32 standard PWR fuel assemblies per canister. All the fuel assemblies, intact or damaged, consist of PWR fuel assemblies with Zircaloy cladding. Damaged fuel assemblies may only be stored in the peripheral compartments of the NUHOMS® 32PTH DSC.

3.9.8.2 Design Input / Data

The design inputs, taken from References [2] and [12], are modified to include the reduction in cladding thickness due to oxidation. They are documented in the following table.

Fuel Assembly Type	WE15x15	WE 17x17std	17x17 MkBW	WE 17x17 Vantage5H	WE 17x17 OFA	CE 14x14 Std	Notes
Fuel Assembly Weight (lb)	1,555	1,575	1,575	1,575	1,575	1,450	(1,2)
No. of Rods	204	264	264	264	264	176	(1)
Active Fuel Length (in)	144.0	144.0	144.0	144.0	144.0	137.0	(1)
No. of Internal Spacers	6	6	6	6	6	7	(3)
Max. Fuel Rod Span (in)	27.0	25.0	25.0	25.0	25.0	17.0	(5)
Fuel Rod OD (in)	0.4193	0.3713	0.3713	0.3713	0.3573	0.4373	(1,4)
Clad Thickness (in)	0.0216	0.0198	0.0213	0.0198	0.0198	0.0253	(1,4)
Fuel Pellet OD (in)	0.3659	0.3225	0.3195	0.3225	0.3088	0.3765	(1)
Fuel Tube Area (in^2)	0.0270	0.0219	0.0234	0.0219	0.0210	0.0327	
Fuel Tube M.I. (in^4)	5.35E-04	3.39E-04	3.60E-04	3.39E-04	3.00E-04	6.97E-04	
Fuel Pellet M.I. (in^4)	8.80E-04	5.31E-04	5.12E-04	5.31E-04	4.46E-04	9.86E-04	
Fuel Tube + Pellet M.I. (in^4)	1.42E-03	8.70E-04	8.71E-04	8.70E-04	7.46E-04	1.68E-03	
Fuel Rod Weight (lb)	7.62	5.97	5.97	5.97	5.97	8.24	(6)
Irradiated Yield Stress (psi)	80,500	80,500	80,500	80,500	80,500	80,500	(7)
Young's Modulus (psi)	10.4E6	10.4E6	10.4E6	10.4E6	10.4E6	10.4E6	(7)

Notes:

1. Data are obtained from Chapter 2, Table 2-1 & Chapter 6, Table 6-4.
2. The fuel assembly weight includes BPRA weight, except CE 14x14
3. The number of internal spacers is obtained from (Ref 12).
4. Include 0.00270 in thickness reduction to account for maximum oxide thickness.
5. Maximum fuel rod span is obtained from (Ref 12) and have been rounded up to whole number.
6. Fuel rod weight = Fuel Assembly Weight / No. of Rods.
7. Data are obtained from Reference 3 at 750°F temperature.

For 235 (tire width mm)/75 (height to width ratio in %) R 17.5 (rim diameter inch) **SLR184** tires:

Tire width = (235 mm)/(25.4mm/in) = 9.25 in

Height of the tire = 75% of 9.25 in = 6.94 in

Diameter of the tire = (17.5 in) + 2*6.94 in = 31.4 in

Total loaded trailer weight = weight of (loaded cask +trailer + skid +ram)

Loaded Cask Weight (with impact limiters) = 250,000 lbs. (conservative, see Chapter 3, Section 3.2.3)

Weight (trailer + skid + ram) = 39,700(trailer)+ 26,500(skid)+ 6,400(ram) [1]
= 72,600 lb

Total Load = 250,000 + 72,600 = 322,600 lb

Load per tire = (322,600 lb)/(32 tires) = 10,081 lb

Area of contact of the tire = (10,081 lbs/135 psi) = 74.7 in^2

Length of compression of the tire = 74.7 in^2 / 9.25 in = 8.08 in

Therefore, deflection of the tire = (31.4/2) - $\{(31.4/2)^2 - (8.08/2)^2\}^{1/2}$ = 0.5287 in

Tire stiffness/tire = (10,081 lb)/(0.5287 in) = 19,068 lb/in

Total tire stiffness for 32 tires = (19,068)(32) = 6.1 x 10^5 lb/in

As per Table 3.9.8-9, the measured tire stiffness = 1500 x 32 = 4.8 x 10^4 lb/in

Conservatively, use tire stiffness of 6.1 x 10^5 lb/in

The force in the fuel assemblies is $F = (K*M)^{1/2} * (v)$

Therefore, load per assembly = F / 32 lb

Equivalent g load in the fuel rods = F / 32 / W

The axial stress in the rod is = F / Fuel Tube Area

Using the methodology described above, the fuel tube axial stresses for the prescribed condition are computed and presented in the following table.

Fuel Assembly Type	WE15x15	WE 17x17 std	17x17 MkBW	WE 17x17 Vantage 5H	WE 17x17 OFA	CE 14x14 Std
Total Fuel Weight (lb)	1,555	1,575	1,575	1,575	1,575	1,450
Fuel Tube Area (in^2)	0.0270	0.0219	0.0234	0.0219	0.0210	0.0327
gap (in) (1)	6.0	6.0	6.0	6.0	6.0	6.0
t (s)	0.211	0.211	0.211	0.211	0.211	0.211
v (in/s)	56.97	56.97	56.97	56.97	56.97	56.97
M ($lb\text{-}s^2/in$)	128.8	130.4	130.4	130.4	130.4	120.1
W (lb)	48.6	49.2	49.2	49.2	49.2	45.3
No. of Fuel Assemblies	32	32	32	32	32	32
K, lb/in	610,000	610,000	610,000	610,000	610,000	610,000
F (lb)	504,946	508,183	508,183	508,183	508,183	487,600
Force / Assembly (lb)	15,780	15,881	15,881	15,881	15,881	15,237
No of Rod / Assembly	204	264	264	264	264	176
Force / Rod (lb)	77.4	60.2	60.2	60.2	60.2	86.6
Equivalent g load	10.1	10.1	10.1	10.1	10.1	10.5
Axial Stress (lb)	2,865	2,747	2,571	2,747	2,864	2,648

Note:

(1) The gap between the fuel assembly and the DSC end component is conservatively assumed to be 6" (the actual length is around 2 in. for the 15x15 and 17x17 assemblies).

The axial stresses in the fuel rods are compressive stresses, and they are significantly less than the irradiated yield stress of the cladding material = 80,500 psi (See table of Section 3.9.8.2). Therefore, the fuel rods will maintain their structural integrity when subjected to the trailer acceleration during transfer.

3.9.8.7 Trailer Deceleration from 5 mph to 0 mph during Transfer

During onsite transfer of the cask from the fuel building to the ISFSI the loaded trailer travels at a maximum constant velocity of 5 mph (88 in/s). Any sudden loads, which may occur during an emergency stop, are transferred from the road bed through the rubber tires, the trailer, the support skid, and the cask to the fuel assemblies. The fuel assemblies inside the canister are subjected to maximum postulated 1g (386.4 in/s ^{2}) equivalent axial transfer load [7]. Therefore, the maximum transfer acceleration is +/- 1g.

The initial velocity is v_i = 88 in/s, the deceleration, g = 386.4 in/s ^{2}

The maximum velocity at impact of the fuel assemblies on the inner bottom cover plate is

v = 88 in/sec - v_f (due to friction) - v_d (due to deceleration)

Where, v_f is a function of work done by the force due to friction (F_f).

Therefore, $(M^* v_f^2)/2 = F_f * d$

Where:

M = mass of the fuel assemblies

F_f = M*g*0.3 (where the coefficient of friction between grid straps and canister is 0.3 [9])

d = gap between fuel assembly and the DSC plug

$v_f = \{(2*F_f*d)/M)\}^{1/2}$

Conservatively assume that cask is tied to the trailer so that it does not move.

v_d is calculated as follows:

Substituting in the kinematics equation $s = s_o + ut + a*t^2/2$ (Section 3.9.8.5)

s_o = 0, u = 88 in/sec, Acceleration, a = 386.4 in/s ^{2} and solving for 't'

$v_d = u + a*t$

Conservatively, ignoring v_d (change in velocity due to deceleration), at contact with the inner bottom cover plate of the DSC the velocity of the fuel assembly is

$v = 88 - v_f$

The contact force on the fuel assembly = $F = (K*M)^{1/2} * (v)$

Where:

M = total mass of the fuel assemblies = (W*n)/g

W = maximum weight of each fuel assembly

n = number of fuel assemblies/canister = 32

K= conservatively use tire stiffness of 6.1 x 10^5 lb/in (Section 3.9.8.6)

$F = (M * K)^{1/2} * v$

Therefore, load per assembly = F / 32

Equivalent g load in the fuel rods = F / 32 / W.

The axial stress in the rod is = F / Fuel Tube Area.

Using the methodology described above, the fuel tube axial stresses for the prescribed condition are computed and presented in the following table.

Fuel Assembly Type	WE15x15	WE 17x17std	17x17 MkBW	WE 17x17 Vantage 5H	WE 17x17 OFA	CE 14x14 Std
Total Fuel Weight (lb)	1,555	1,575	1,575	1,575	1,575	1,450
Fuel Tube Area (in^2)	0.0270	0.0219	0.0234	0.0219	0.0210	0.0327
gap (in) (1)	6.0	6.0	6.0	6.0	6.0	6.0
M ($lb\text{-}s^2/in$)	128.8	130.4	130.4	130.4	130.4	120.1
W (lb)	48.6	49.2	49.2	49.2	49.2	45.3
F_f (lb)	14,928	15,120	15,120	15,120	15,120	13,920
v_f, (in/s)	37.3	37.3	37.3	37.3	37.3	37.3
v, (in/s)	50.7	50.7	50.7	50.7	50.7	50.7
K, lb/in	610,000	610,000	610,000	610,000	610,000	610,000
F (lb)	449,390	452,271	452,271	452,271	452,271	433,952
Force / Assembly (lb)	14,043	14,133	14,133	14,133	14,133	13,561
No of Rod / Assembly	204	264	264	264	264	176
Force / Rod (lb)	68.8	53.5	53.5	53.5	53.5	77.1
Equivalent g load	9.0	9.0	9.0	9.0	9.0	9.4
Axial Stress (lb)	2,550	2,445	2,288	2,445	2,549	2,356

Note:

(1) The gap between the fuel assembly and the DSC end component is conservatively assumed to be 6".

The axial stresses in the fuel rods are compressive stresses, and they are significantly less than the irradiated yield strength of the cladding material = 80,500 psi (See table of Section 3.9.8.2). Therefore, the fuel rods will maintain their structural integrity when subjected to the trailer deceleration during transfer.

3.9.8.10 One Foot End Drop Damaged Fuel Evaluation

During off site transport (Part 71) the damaged fuel assemblies need to be evaluated for 1 foot end drop. The transport operation is carried out using the MP 187H Cask, with the DSC and the impact limiters in the horizontal position.

The maximum g load acting on the damaged fuel rod subjected to 1 foot end drop = 30g

The fuel tube axial stresses for the prescribed condition are computed and presented in the following table.

Fuel Assembly Type	WE15x15	WE 17x17 Std	17x17 MkBW	WE 17x17 Vantage 5H	WE 17x17 OFA	CE 14x14 Std
Total Fuel Weight (lb)	1,555	1,575	1,575	1,575	1,575	1,450
Fuel Tube Area (in^2)	0.0270	0.0219	0.0234	0.0219	0.0210	0.0327
1-Foot End Drop Equivalent g load	30	30	30	30	30	30
Force / Assembly (lb)	46,650	47,250	47,250	47,250	47,250	43,500
No of Rod / Assembly	204	264	264	264	264	176
Force / Rod (lb)	228.7	179.0	179.0	179.0	179.0	247.2
Axial Stress (lb)	8,469	8,172	7,649	8,172	8,523	7,558

The axial stresses in the fuel rods are compressive stresses, and they are significantly less than the irradiated yield stress of the cladding material = 80,500 psi (see table of Section 3.9.8.2). Therefore, the fuel rods will maintain their structural integrity when subjected to the 1 foot end drop load.

3.9.8.11 One Foot Side Drop Damaged Fuel Evaluation

During off site transport (Part 71) the damaged fuel assemblies need to be evaluated for 1 foot side drop. The transport operation is carried out using the MP 187H Cask, with the DSC and the impact limiters in the horizontal position.

The maximum g load acting on the damaged fuel rods under 1 foot side drop load = 30g. The damaged fuel rod structural integrity under 1 foot side drop load is assessed by computing the bending stress in the rod and comparing it with the yield stress of the cladding material. The fracture assessment of the damaged fuel rod structural integrity is made by using two fracture geometries (ruptured sections) as described below.

It is assumed that the damaged fuel tube is burst at the spacers (supports) location, which is the location of maximum bending moment. The loading assumed is on the opposite side of the rod at the burst location. The following two geometries, used for the fracture evaluation of the damaged fuel rods, are based on these assumptions.

Fracture Geometry #1: The first geometry is shown in Figure 3.9.8-1. In this damage mode the fuel tube is assumed to bulge from diameter D to diameter W ($W \geq D$) and rupture to a hole of diameter (2a) at the bulge location. It is assumed that $(2a/w) = 0.5$ for this geometry.

Fracture Geometry #2: The second geometry is shown in Figure 3.9.8-2. The stress intensities factors for this geometry are determined using the solution for a tube with a crack subjected to pure bending moment given in Reference 13. This evaluation is based on a crack length to diameter ratio of 0.5 (or $2a/D_m=0.5$).

The basis for the 0.5 crack length to equivalent plate width/diameter ratio for fracture geometries #1 and #2 is the experimental tests on "as received" Zircalloy fuel tubes with measured burst temperatures of up to 909°C, which showed flaw opening to diameter ratios of 0.4 to 0.5 [16]. The $(2a/W)$ or $(2a/D_m)$ ratios used in this appendix are 0.5.

3.9.8.11.1 Structural Integrity Evaluation with Fracture Geometry #1

The fracture geometry #1 (Ruptured Section) is shown in Figure 3.9.8-1. With reference to Figure 3.9.8-1, the methodology for computing the stress intensity factor K_I is as follows:

Fuel Rod OD = D

Oxidized Clad Thickness = t

Average radius, R = (D-t)/2

I = net tube MI + net fuel MI, where it is conservatively assumed that the net tube MI is equal to one half of the total tube MI, and the net fuel MI is equal to one half of the total fuel MI.

Span Length = S

Assume (2a/W) = 0.5, where 2a = ruptured hole diameter,

W = bulged fuel tube diameter ≥ D.

Stress Intensity Factor, $K_I = (Y)(P*a^{1/2})/(t*W)$, [Reference 14, Fig. 8.7(c)]

Where:

Y = 2.11 {established using (2a/W) = 0.5 (for Forman et al. case) in Figure 3.9.8-3 }

P = average tensile force at the crack which is expressed as a function of moment on the cross section as:

$= (2MR^2t)/I$ (See Table 3.9.8-8)

$W = \pi R$

$M = 0.1058(W_s*S^2)$ (See Appendix 2 of Reference 3)

W_s = 30g Fuel Rod Weight / Length

Bending Stress = MD / 2I

Using the methodology described above, the stress intensity factors, K_I, for the prescribed condition are computed and presented in the following table.

Fuel Assembly Type	WE15x15	WE 17x17Std	17x17 MkBW	WE 17x17 Vantage 5H	WE17x17 OFA	CE 14x14 Std
Fuel Rod OD, D (in)	0.4193	0.3713	0.3713	0.3713	0.3573	0.4373
Clad Thickness, t (in)	0.0216	0.0198	0.0213	0.0198	0.0198	0.0253
Average Radius, R (in)	0.1989	0.1758	0.1750	0.1758	0.1688	0.2060
Fuel Tube M.I. (in^4)	5.35E-04	3.39E-04	3.60E-04	3.39E-04	3.00E-04	6.97E-04
Fuel Pellet M.I. (in^4)	8.80E-04	5.31E-04	5.12E-04	5.31E-04	4.46E-04	9.86E-04
I (in^4)	7.08E-04	4.35E-04	4.36E-04	4.35E-04	3.73E-04	8.42E-04
Span Length, S (in)	27.0	25.0	25.0	25.0	25.0	17.0
(2a/W)	0.5	0.5	0.5	0.5	0.5	0.5
Y	2.11	2.11	2.11	2.11	2.11	2.11
W (in)	0.62	0.55	0.55	0.55	0.53	0.65
Fuel Assembly Weight (lb)	1,555	1,575	1,575	1,575	1,575	1,450
No. of Rods	204	264	264	264	264	176
Active Fuel Length (in)	144.0	144.0	144.0	144.0	144.0	137.0
1-Foot Side Drop Equivalent g load	30	30	30	30	30	30
W_s (lb/in)	1.59	1.24	1.24	1.24	1.24	1.80
Moment, M (kip. in)	0.12	0.08	0.08	0.08	0.08	0.06
Bending Stress (psi)	36,294	35,086	35,017	35,086	39,348	14,326
P (kip)	0.296	0.231	0.246	0.231	0.248	0.141
K_I (ksi $in^{1/2}$)	18.3	16.6	16.4	16.6	18.2	7.3

The computed stress intensity factor is compared with experimentally obtained plane strain fracture toughness, K_{IC} of irradiated Zircaloy cladding material as reported in [15].

Reference15 reports a K_{IC} = 35 ksi $in^{1/2}$ at approximately 300°F which is greater than highest computed stress intensity factor, K_I of 18.3 ksi $in^{1/2}$ presented in the above table.

Therefore, the structural integrity of the damaged fuel rods, which are conservatively assumed to rupture as shown in Figure 3.9.8-1, will be maintained.

3.9.8.11.2 Structural Integrity Evaluation with Fracture Geometry #2

This geometry is shown in Figure 3.9.8-2. Stress intensity factors are computed for a crack in a fuel tube subjected to a uniform bending moment (M) using formulae given in Reference 13. As per Reference 13, page 472:

$$K_I = \sigma (\pi * R_m * \theta)^{1/2} F(\theta)$$

where,

$$F(\theta) = 1 + 6.8*(\theta/\pi)^{3/2} - 13.6*(\theta/\pi)^{5/2} + 20.0*(\theta/\pi)^{7/2}$$

σ = Bending Stress due to Uniform Moment 'M'

R_m = Average radius of the fuel tube

2θ = Angle which the crack makes at the center of the tube

K_I = Stress Intensity Factor at the crack

The K_I is computed for all the different fuel assemblies, and the results for all the fuel assemblies are presented in Table 3.9.8-1, 3.9.8-2, 3.9.8-3, 3.9.8- 4 and 3.9.8-5.

Based on the computed K_I using Fracture Geometries #1 & #2, a summary of the comparisons is presented as follows:

	Fracture Geometry #1 K_I	Fracture Geometry #2 K_I
WE 15x15	18.3	27.8
WE 17x17 Std.	16.6	25.3
17x17 MKBW	16.4	25.1
WE 17x17 Vantage 5H	16.6	25.3
WE 17x17 OFA	18.2	27.8
CE 14x14 Std	7.3	11.2

3.9.8.12 Conclusions

The maximum computed stresses in the fuel rods and their ratios to the irradiated yield stress of the cladding material are summarized in Table 3.9.8-6. From Table 3.9.8-6, it can be concluded that stresses for all load cases considered are significantly less than the yield stress of the Zircaloy cladding material (computed stresses are 4% to 49% of the yield stress).

It is important to note that, the stresses in the fuel rods for all analyzed normal and off normal load cases are compressive stresses (less than the critical buckling stress), except for the 1-foot transport condition side drop load.

For the 1-foot side drop it is demonstrated by using fracture mechanics procedures (by comparing computed stress intensity factors to critical crack initiation fracture toughness in Table 3.9.8-7), that the damaged fuel rods will maintain their structural integrity.

This calculation demonstrates that the damaged fuel assemblies in the NUHOMS® 32PTH DSC will retain their structural integrity when subjected to normal condition of storage and on site transfer loads. The damaged fuel assembly will also maintain their integrity when subjected to one-foot drop and vibration loads during normal condition of offsite transport. Therefore, the retrievability of the damaged fuel assemblies is assured when subjected to any of these normal and off normal loads.

Table 3.9.8-6

Combustion Engineering 14x14 - K_I Calculation using Fracture Geometry #2

OD (in) =	0.4373
t (in) =	0.0253
R / t =	8.64
Rm (in) =	0.2060
M (kip-in) =	0.06
a / Rm =	0.5
Theta (radian) =	0.52
I (in^4) =	8.42E-04
Bending Stress (ksi) =	14.33
E (ksi) =	10,400

Theta (rad)	Theta/pi	Half Length (in)	F(Theta)	K_I (ksi $in^{1/2}$)
0.05	0.0159	0.0103	1.0132	2.6
0.10	0.0318	0.0206	1.0363	3.8
0.15	0.0477	0.0309	1.0646	4.8
0.20	0.0637	0.0412	1.0966	5.7
0.25	0.0796	0.0515	1.1312	6.5
0.30	0.0955	0.0618	1.1677	7.4
0.35	0.1114	0.0721	1.2058	8.2
0.40	0.1273	0.0824	1.2450	9.1
0.45	0.1432	0.0927	1.2853	9.9
0.50	0.1592	0.1030	1.3265	10.8
0.51	0.1623	0.1051	1.3348	11.0
0.52	0.1655	0.1071	1.3432	11.2
0.55	0.1751	0.1133	1.3686	11.7
0.60	0.1910	0.1236	1.4117	12.6
0.65	0.2069	0.1339	1.4557	13.5
0.70	0.2228	0.1442	1.5009	14.5

Table 3.9.8-7

Summary - Maximum Fuel Rod Stresses and Stress Ratios

Normal and Off Normal Load Case	Maximum [1] Stress (psi)	Stress [2] Ratio
On site Transport and Transfer Operations	2,865	0.04
One-foot End Drop (Part 71)	8,523	0.11
One-foot Side Drop (Part 71)	39,348	0.49

Notes:
(1) Maximum stress for all fuel assemblies.
(2) Stress ratio = maximum stress / 80,500 (yield stress for Zircaloy cladding).

Table 3.9.8-8

Summary - Computed Fuel Tube Stress Intensity Factors and Ratios

Fracture Geometry	Max K_I (1) (ksi $in^{1/2}$)	K_{IC} (2) (ksi $in^{1/2}$)	Ratio Max K_I / K_{IC}
Geometry #1	18.3	35.0	0.52
Geometry #2	27.8	35.0	0.79

Notes:

1. Maximum K_I for all fuel assemblies.
2. K_{IC} = Crack initiation fracture toughness (plane strain fracture toughness).

Table 3.9.8-9

Derivation of Tensile Force (T) and Applied Moment (M) Relationship for a Circular Tube

Consider a circular tube of average radius "R", thickness "t" subjected to a bending moment "M".

At angle "θ" from the neutral axis (N/A), for a segment of the tube with angle "dθ"

Area = $A = t*R*d\theta$,

Tensile stress = $\sigma = (M*R*\sin\theta)/I$

Where, I = moment of inertia of the section

Therefore,

Tensile Force = $\Delta P = (M*R*\sin\theta/I) *(t*R*d\theta)$

Total Tensile Force = $P = \int (M*R*\sin\theta/I) *(t*R*d\theta)$

Where, limits of integral are from angle "$\theta = 0$" to angle "$\theta = \pi$"

Therefore, $P = (M*R^2 *t / I) \int \sin\theta \, d\theta$

$= (M*R^2 *t / I) [-\cos\theta]_0^{\pi}$

$= 2*M*R^2 *t / I$

Table 3.9.8-9 (continued)

Derivation of Tensile Force (T) and Applied Moment (M) Relationship for a Circular Tube

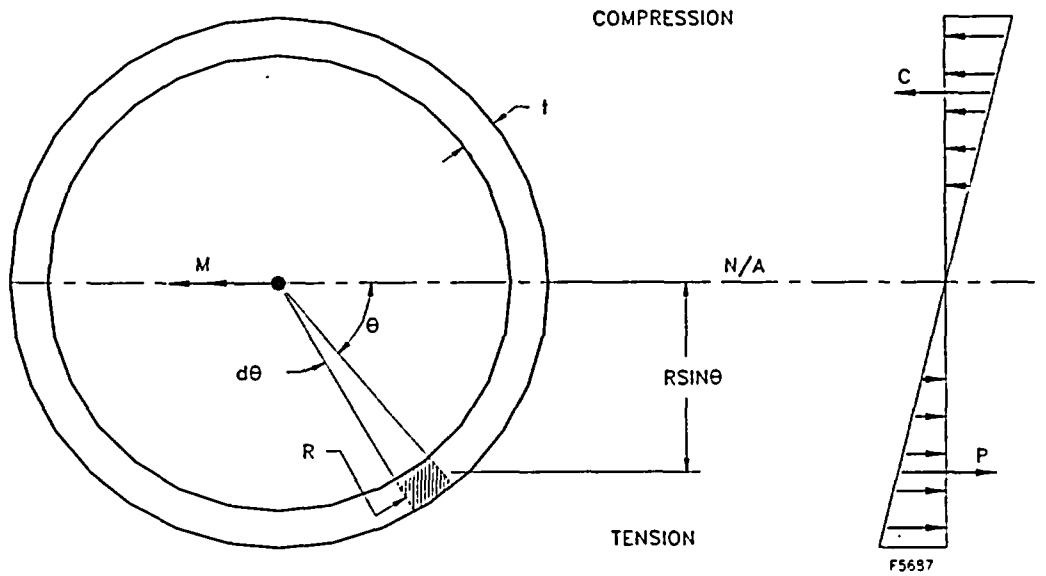

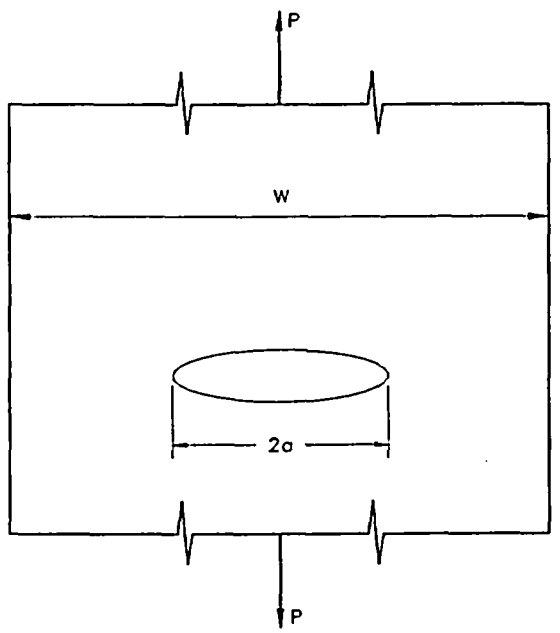

M = Applied moment
P = Resultant tensile force
R = Average radius of fuel tube
t = Thickness of fuel tube
I = Moment of inertia of fuel tube
2a = Crack width

$W = \pi R$

$P = \frac{2MR^2t}{I}$

Table 3.9.8-10

Tire Stiffness Calculation

The on-site transfer trailer has four axles with eight 235/75R 17.5 SLR 184 tires per axle (total of 32 tires). The tire stiffness is estimated based on tire measurements as follows:

For 235 (tire width in mm)/75 (height-to-width ratio in %) R 17.5 (rim diameter in inches) SLR184:
Tire width 235mm/25.4mm/in =9.25 inch

Height of tire = 75% of 9.25= 6.94 inch

Tire diameter = 17.5+2*6.94= 31.4 inch.

From trailer tire measurements:

	a (height) - in	b (width) - in	c (ground top) - in
A (front right tire)	6.5	7.4	30.0
B (front left tire)	7.3	7.4	30.8
C (rear right tire)	4.8	7.3	31.3
D (rear left tire)	4.0	7.2	31.4

Tire pressure: 140-145 psi

Trailer weight: 39,700 lbs.

Skid weight: 26,500 lbs

RAM weight: 6,400 lbs.

Average c dimension at front= (30+30.8)/2=30.4 inches

Average c dimension at rear = (31.3+31.4)/2=31.4 inches

Tire height: 33 inches, at approximately 145 psi pressure

Weight per tire (excluding RAM weight): 66,200/32=2070 lbs/tire

Weight per tire (assuming RAM weight is distributed on 8 tires): 6400/8= 1600 lb/tire

Front 8 tires: 2070+1600=3670 lbs/tire.

Table 3.9.8-10 (continued)

Tire Stiffness Calculation

All other tires: 2070 lbs/tire

Stiffness is determined as:

K_{front} = 3670/(33-30.4)=1411 lbs/in

$K_{all\ others}$ = 2070/(33-31.4)=1294 lbs/in

Use K/tire =1500 lbs/inch.

Total stiffness = 32x 1500= 4.8E 4 lbs/in

CHAPTER 4
THERMAL EVALUATION

Table of Contents

4. **THERMAL EVALUATION** 4-1
- 4.1 **Discussion** 4-1
- 4.2 **Summary of Thermal Properties of Materials** 4-3
- 4.3 **Thermal Evaluation for Normal and Off-Normal Conditions** 4-9
  - 4.3.1 Thermal Models for Normal and Off-Normal Conditions 4-9
  - 4.3.2 Maximum Temperatures for Normal and Off-Normal Conditions 4-20
  - 4.3.3 Minimum Temperatures for Normal and Off-Normal Conditions 4-20
  - 4.3.4 Maximum Internal Pressures for Normal and Off-Normal Conditions 4-20
  - 4.3.5 Maximum Thermal Stresses for Normal and Off-Normal Conditions 4-20
  - 4.3.6 Evaluation of Thermal Performance for Normal and Off-Normal Conditions 4-21
- 4.4 **Thermal Evaluation for Accident Conditions** 4-22
  - 4.4.1 Thermal Models for Accident Conditions 4-22
  - 4.4.2 Maximum Temperatures for Accident Conditions 4-27
  - 4.4.3 Maximum Internal Pressures for Accident Conditions 4-28
  - 4.4.4 Maximum Thermal Stresses for Accident Conditions 4-28
  - 4.4.5 Evaluation of Thermal Performance for Accident Conditions 4-28
- 4.5 **Thermal Evaluation for Loading and Unloading Conditions** 4-29
  - 4.5.1 Vacuum Drying 4-29
  - 4.5.2 Reflooding 4-34
- 4.6 **Maximum Internal Pressure** 4-36
  - 4.6.1 Average Gas Temperature 4-36
  - 4.6.2 Amount of Initial Helium Backfill 4-37
  - 4.6.3 Free Gas within Fuel Assemblies / BPRA 4-38
  - 4.6.4 Total Amount of Gases within DSC 4-38
  - 4.6.5 Maximum DSC Internal Pressures 4-38
  - 4.6.6 Maximum Pressure in Annulus 4-39
- 4.7 **Axial Decay Heat Profile** 4-40
- 4.8 **Effective Fuel Properties** 4-43
  - 4.8.1 Discussion 4-43
  - 4.8.2 Summary of Material Properties 4-43
  - 4.8.3 Effective Fuel Conductivity 4-45
  - 4.8.4 Effective Fuel Density and Specific Heat 4-46
  - 4.8.5 Conclusion 4-47
- 4.9 **Effective Conductivity of Fluids in the Transfer Cask** 4-48
  - 4.9.1 Effective Conductivity in the Shielding Panel 4-48
  - 4.9.2 Effective Water Conductivity in Annulus between TC and DSC 4-50
- 4.10 **Justification of the Assumed Hot Gap Sizes** 4-52
  - 4.10.1 Radial Gap between Basket Rails and DSC shell 4-52
  - 4.10.2 Radial Gap between Lead and the Cask Structural Shell 4-53

4.11 Heat Transfer Coefficients 4-55
4.11.1 Total heat Transfer Coefficient to Ambient 4-55
4.11.2 Free Convection Coefficients 4-55
4.12 Effective Conductivity of Air in Closed Cavity of HSM-H 4-63
4.13 Thermal-Hydraulic Equations for the HSM-H 4-65
4.14 Thermal Evaluation of DSC Containing Damaged Fuel 4-68
4.14.1 Normal / Off-Normal Conditions 4-68
4.14.2 Accident Conditions 4-68
4.14.3 Effective Properties of Damaged Fuel 4-70
4.14.4 Evaluation of DSC Thermal Performance with Damaged Fuel 4-71
4.15 References 4-73
4.16 Appendices 4-75

4-38 Total Free Gas Volume verses Burnup Rate
4-39 Comparison of the Axial Heat Profiles in the FE Model and in Ref. [4]
4-40 Finite Element Model of Fuel Assemblies
4-41 Effective Transverse Fuel Conductivity in Helium
4-42 Effective Transverse Fuel Conductivity for Vacuum Conditions
4-43 Effective Axial Fuel Conductivity
4-44 Schematic Flow Paths through HSM-H
4-45 Temperature Regions around DSC in the HSM-H Cavity
4-46 Location of the Damaged Fuel Assemblies in the Basket
4-47 Typical FE Models of Damaged (Reconfigured) Fuel WE17x17OFA
4-48 Transverse Effective Fuel Conductivity verses Pitch Size
4-49 Effective Transverse Conductivity of Damaged (Reconfigured) Fuel
4-50 Temperature Distributions in the DSC containing 16 Damaged Fuel Assemblies for Normal / Off-Normal Transfer Conditions
4-51 Temperature Distributions in the DSC containing 16 Damaged Fuel Assemblies for Accident Conditions

4. THERMAL EVALUATION

4.1 Discussion

The NUHOMS®-32PTH DSC is designed to passively reject decay heat during storage and transfer for normal, off-normal, and accident conditions while maintaining temperatures and pressures within specified limits. Objectives of the thermal analyses performed for this evaluation include:

- Determination of maximum and minimum temperatures with respect to material limits to ensure components perform their intended safety functions,
- Determination of temperature distributions to support the calculation of thermal stresses,
- Determination of maximum DSC internal pressures for normal, off-normal, and accident conditions, and
- Determination of the maximum fuel cladding temperature, and to confirm that this temperature will remain sufficiently low to prevent unacceptable degradation of the fuel during storage.

To establish the heat removal capability, several thermal design criteria are established for the System. These are:

- Maximum temperatures of the containment structural components must not adversely affect the containment function.
- To maintain the stability of the neutron shield resin in the transfer cask (TC) during normal transfer conditions, a maximum allowable temperature of 320°F is set for the neutron shield material [1].
- A maximum fuel cladding temperature limit of 400°C (752°F) has been established for normal conditions of storage and for short-term storage operations such as transfer and vacuum drying [2]. During off-normal storage and accident conditions, the fuel cladding temperature limit is 570°C (1058°F) [2].
- A maximum temperature limit of 327°C (620°F) is considered for the lead in the transfer cask, corresponding to the melting point [3].

- The ambient temperature range for normal operation is 0 to 100°F (-18 to 38°C). The minimum and maximum off-normal ambient temperatures are -20°F (-29°C) and 115°F (46°C) respectively. In general, all the thermal criteria are associated with maximum temperature limits and not minimum temperatures. All materials can be subjected to a minimum environment temperature of -20°F (-29°C) without adverse effects.

- The maximum DSC internal pressure during normal and off-normal conditions must be below the design pressures of 15 psig and 20 psig respectively. For accident cases, the maximum DSC internal pressure must be lower than 70 psig during storage and lower than 120 psig during transfer operation.

The NUHOMS®-32PTH DSC is analyzed based on a maximum heat load of 34.8 kW from 32 fuel assemblies with a maximum heat load of 1.5 kW per assembly. For CE14x14 fuel assembly the maximum total heat load is limited to 33.8 kW. The loading requirements described in Section 4.3.1.3 are used to develop the bounding load configurations.

A description of the detailed analyses performed for normal/off-normal conditions is provided in Section 4.3, and accident conditions in Section 4.4. The thermal analyses performed for the loading and unloading conditions are described in Section 4.5. DSC internal pressures are discussed in Section 4.6.

The analyses consider the effect of the decay heat flux varying axially along a fuel assembly. The axial decay heat profile for a PWR fuel assembly is based on [4]. Section 4.7 describes the calculated peaking factors and the methodology to apply the axial heat profile in the model.

Fuel assemblies are considered as homogenized materials in the fuel compartments. The effective thermal conductivity of the fuel assemblies used in the thermal analysis is based on the conservative assumption that heat transfer within the fuel region occurs only by conduction and radiation where any convection heat transfer is neglected. The lowest effective properties among the applicable fuel assemblies are selected to perform the thermal analysis. Section 4.8 presents the calculation that determines the bounding effective thermal properties of the applicable fuel assemblies.

The thermal evaluation concludes that with a design basis heat load of 34.8 kW and the loading requirements described in Section 4.3.1.3, all design criteria are satisfied.

9. Poison Plates

Neutron poison plates in the basket type I are borated aluminum alloy or MMC. The minimum conductivity of the borated material must be equal or larger than the 145 W/m-K at 100°C. It is assumed that the conductivity of the borated aluminum alloy/MMC remains unchanged at higher temperatures. The measured conductivities of the available borated aluminum alloys for the entire range of 20°C to 400°C are much higher than the above requirement [7 and 8].

Basket type II is designed to use Boral® absorber as neutron poison plate. The Boral® absorber possesses orthotropic thermal conductivity. To avoid any uncertainty, conductivity values of Boral® are set conservatively to zero. An equivalent conductivity is calculated for a pair of Boral® and aluminum-1100 plates in thermal analyses. For calculation of the equivalent conductivity, the paired plates are considered as parallel thermal resistances. Since the temperature gradients along the plates are much higher than the temperature gradients across the plates, this assumption is reasonable. The following equation is used to calculate the equivalent thermal conductivity of paired plates.

$$k_{eq} = \frac{k_{Al}\, t_{Al} + k_p\, t_p}{t_{total}} = \frac{k_{Al}\, t_{Al}}{t_{total}}$$

t_{total} = Total thickness of the basket plate = 0.5"
k_{Al} = Thermal conductivity of aluminum plate (Al 1100)
t_{Al} = Thickness of the aluminum plate (t_{total} - t_p -tolerance)
t_p = Thickness of the Boarl plate = 0.075"

Temp (°F)	k - Al-1100 [6] (Btu/hr-ft-°F)	k_{eq} for Basket Type II (Btu/hr-in-°F)
70	133.1	9.34
100	131.8	9.25
150	130.0	9.12
200	128.5	9.02
250	127.3	8.93
300	126.2	8.86
350	125.3	8.79
400	124.5	8.74
650	121.3[3]	8.51

Basket type II contains Boral® plates with a nominal core thickness of 0.05 in.

Total Boral® plate thickness is 0.075±0.004 in. from reference [9]

The minimum thickness of the Al-1100 plate (0.421") is considered to calculate the equivalent conductivity.

The minimum required thermal conductivities of the paired aluminum and poison plates will be verified via testing as described in Chapter 9.

To minimize the thermal resistance of the basket during fire period, the conductivity of poison plate is considered to be equal to the aluminum conductivity. Conductivity of the poison plate is set equal to the minimum value of 145 W/m-K (6.98 Btu/hr-in-°F) during the cool down period to maximize the thermal resistance. Specific heat and density of poison plate is set equal to those of aluminum for transient runs.

[3] Extrapolated from the values in [ASME]

6. SA-240, Type 304 Stainless Steel

Temperature (°F)	Conductivity (Btu/hr-ft-°F) [6]	Conductivity (Btu/hr-in-°F)	Diffusivity (ft^2/hr) [6]	Specific Heat (Btu/lbm-°F)[2]	Density (lbm/in^3) [3]
70	8.6	0.717	0.151	0.117	0.29
100	8.7	0.725	0.152	0.117	
150	9.0	0.750	0.154	0.120	
200	9.3	0.775	0.156	0.122	
250	9.6	0.800	0.158	0.125	
300	9.8	0.817	0.160	0.126	
350	10.1	0.842	0.162	0.128	
400	10.4	0.867	0.165	0.129	
450	10.6	0.883	0.167	0.130	
500	10.9	0.908	0.170	0.131	
550	11.1	0.925	0.172	0.132	
600	11.3	0.942	0.174	0.133	
650	11.6	0.967	0.177	0.134	
700	11.8	0.983	0.179	0.135	
750	12.0	1.000	0.181	0.136	
800	12.2	1.017	0.184	0.136	

7. Aluminum Alloy 1100

Temperature (°F)	Conductivity (Btu/hr-ft-°F) [6]	Conductivity (Btu/hr-in-°F)	Diffusivity (ft^2/hr) [6]	Specific Heat (Btu/lbm-°F)[2]	Density (lbm/in^3) [6]
70	133.1	11.092	3.67	0.214	0.098
100	131.8	10.983	3.61	0.216	
150	130.0	10.833	3.50	0.219	
200	128.5	10.708	3.42	0.222	
250	127.3	10.608	3.35	0.224	
300	126.2	10.517	3.28	0.227	
350	125.3	10.442	3.23	0.229	
400	124.5	10.375	3.17	0.232	

8. Lead

Temperature (K)	Conductivity (W/m-K) [5]	Temperature (°F)	Conductivity (Btu/hr-in-°F)	Specific Heat (Btu/lbm-°F) [3]	Density (lbm/in^3) [3]
200	36.7	-100	1.767	0.03	0.393
250	36.0	10	1.733		
300	35.3	80	1.700		
400	34.0	260	1.637		
500	32.8	440	1.579		
600	31.4	620	1.512		

[2] Thermal diffusivity is $\alpha = \frac{k}{\rho c_p}$, this equation is used to calculate the specific heat.

4.3 Thermal Evaluation for Normal and Off-Normal Conditions

4.3.1 Thermal Models for Normal and Off-Normal Conditions

The finite element models are developed using the ANSYS computer code [16]. ANSYS is a comprehensive thermal, structural, and fluid flow analysis package. It is a finite element analysis code capable of solving steady-state and transient thermal analysis problems in one, two, and three dimensions. Heat transfer via a combination of conduction, radiation, and convection can be modeled by ANSYS.

Three finite element models are used for evaluation of the normal and off-normal storage and transfer conditions:

- A transfer cask model (OS-187H) to determine temperature distributions within the cask body and neutron shielding. This model also includes the DSC shell and the helium gap between the DSC and the cask inner surface.
- A DSC model including the basket and the homogenized fuel assemblies to determine temperature distributions within the DSC and its contents.
- A HSM-H model including the DSC shell and shield plugs to determine temperature distribution in the HSM-H concrete structure, the supporting rails, and the DSC shell.

The analysis starts first with evaluating the transfer cask or the HSM-H model. The resultant temperatures of the DSC shell are then applied as boundary conditions to the exterior nodes of the DSC model. This approach allows modeling of sufficient detail within the DSC while keeping the overall size of the individual models reasonable.

Ambient temperatures between 0 and 100°F are considered as normal, long-term transfer and storage conditions. Minimum and maximum off-normal ambient temperatures are -20°F and 115°F. Should these extreme temperatures ever occur, they would be expected to last for a short period of time. Nevertheless, these ambient temperatures are conservatively assumed to occur for a significant duration to result in a steady-state temperature distribution in the NUHOMS®-32PTH system components.

Since the normal conditions are bounded by the off-normal conditions, the finite element models are evaluated only for off-normal conditions. The thermal stresses and the DSC internal pressures for the normal conditions are therefore conservatively calculated based on the resultant temperatures for the off-normal conditions.

4.3.1.1 Steady State Transfer Cask Model (OS187H)

OS187H transfer cask is designed to provide structural and radiological protection for the DSC during transfer operation while providing passive heat removal for the canisterized spent fuel. The three-dimensional finite element model of the OS187H transfer cask represents a 180° symmetric section of the TC and includes the geometry and material properties of the DSC shell and shield plugs, inner shell, gamma shell (lead), and structural shell of the transfer cask, as well as the shielding panel, cask lid, cask bottom plate, and the solid neutron shields. Properties of pure water are assumed for the liquid neutron shield contained in the shielding panel.

The neutron shield panel consists of a cylindrical shell welded to the cask structural shell and supported by 17 rings. Each of the 15 inner supporting rings has four holes to allow filling and draining of water in or out of the panel. The water in the neutron shield panel is modeled as 16 individual, cylindrical segments using SOLID70 elements. Effective conductivities are calculated for individual segments in Section 4.9 to model the combination of the conduction and convection heat transfer through the water contained in the shielding panel.

Radiation between the DSC outer shell and the cask inner shell is modeled using radiation LINK31 elements. The LINK elements connect the outermost nodes of the DSC shell to the inner most nodes of the transfer cask in the radial and axial directions. A macro[4] is written to retrieve the average surface area of the elements attached to each LINK31 element and apply it as a real constant to the corresponding LINK31 element.

Since the outer diameter of DSC is very close to the inner diameter of the cask, the radiating surfaces of the DSC and cask can be considered as parallel planes. The effective emissivity for the radiation exchange between the parallel planes is calculated as follows and applied as real constant to radiation LINK31 elements.

$$\varepsilon_{eff} = \frac{1}{\left(\frac{1}{\varepsilon_1} + \frac{1}{\varepsilon_2} - 1\right)} = 0.2987$$

A surface emissivity of 0.46 for stainless steel (see Section 4.2) is used for ε_1, ε_2 in the above equation to calculate the real constant of ε_{eff}. The value of ε_{eff} remains unchanged for all the radiation LINK elements.

Following assumptions are considered in developing the model:

a) DSC in centered axially in the transfer cask. This assumption reduces the axial heat transfer and hence maximizes the DSC shell temperature, which in turn results in higher fuel cladding temperature in the DSC model.

b) The total decay heat load (34.8 kW) is considered evenly distributed over the radial inner surface of the DSC cavity. The applied heat flux is:

$$\text{Decay heat flux} = \frac{Q}{\pi D_i L} = 3.34 \text{ Btu/hr-in}^2 \quad \text{or} \quad 3.25 \text{ Btu/hr-in}^2 \text{ for CE 14x14 only}$$

where,
Q = total decay heat load = 34.8 kW (118,748 Btu/hr) or 33.8 kW (115,336 Btu/hr) for CE14x14 only

[4] See Appendix 4.16.1 for macros

The circumference of the DSC model is divided into eight regions with linearly progressive bulk temperatures. The first region covers the area between the supporting rails from an angle of -90° to -64.2°. The second region begins from the center line of the supporting beam at -60° to -45°. The surface of the DSC shell from -64.2° to -60° is located above the upper edge of the slots in the slotted plate. The free convection is therefore restricted over this area. For conservatism, this area is considered as a dead zone with no free convection. The other circumferential regions are equal in size and each covers 22.5° of the DSC shell. Figure 4-9 shows the regions of the DSC lower half. Correlation of free convection over horizontal cylinder is considered to calculate the convection coefficients for circumferential DSC regions.

Similar to the DSC circumference, the cross section of the HSM-H cavity is divided into different regions to apply the convection boundary conditions. Energy and hydraulic equations are combined to calculate the bulk air temperatures for various ambient temperatures. Section 4.13 shows the regions and describes briefly the methodology to calculate the bulk air temperatures in the HSM-H cavity.

Convection on HSM-H end walls is calculated using free convection correlations for vertical surfaces at HSM-H average bulk air temperature (T_s). Convection on the lower part of the side wall, below the side heat shield, is determined using free convection correlation for vertical surfaces at cold region temperature (T_0). For the space between the side wall and the side heat shield, free convection correlation for a narrow channel is used to determine the free convection coefficient. For the HSM-H ceiling and the HSM-H basemat, correlations for flat horizontal surfaces are used to determine free convection coefficients. Air temperatures for the convection on the basemat and ceiling are cold region temperature (T_0) and exit air temperature (T_{exit}). respectively. The calculation methods of free convection coefficients are discussed in detail in Section 4.11. Figure 4-10 shows the convection boundary conditions applied in the HSM-H model.

Insolance is applied as a constant heat flux on the roof and front wall of the HSM-H, which are exposed to the ambient. The value of the solar heat flux is taken from [17] averaged over a 24 hour period. The insolance is applied as a constant heat flux over the SURF152 elements superimposed on the SOLID70 elements on the HSM-H roof and front wall. A solar absorptivity of 1.0 is assumed for the concrete surface. The values of the applied heat fluxes are listed below:

Shape	Insolance [17] (gcal/cm^2)	Averaged over 24 hr (Btu/hr-in^2)
HSM roof	800	0.8537
HSM front wall	200	0.2134

Insolance is not considered for the minimum ambient temperature of -20°F.

Convection and radiation from the roof and the front wall are combined together as a total convection coefficient. The calculation of the total convection coefficient is discussed in Section 4.11.

The decay heat load is considered to be distributed evenly on the radial inner surface of the DSC for the steady state runs in this analysis. The applied decay heat flux is:

$$Decay\ heat\ flux = \frac{Q}{\pi D_i L} = 3.34 \quad \text{Btu/hr-in}^2 \text{ or } 3.25 \text{ Btu/hr-in}^2 \text{ for CE 14x14 only}$$

where,

Q = total decay heat load = 34.8 kW (118,748 Btu/hr) or 33.8 kW (115,336 Btu/hr) for CE14x14 only
Di = inner DSC diameter = 68.75"
L = DSC cavity length = 164.5"

In the event that the side heat shields are not equipped with fins, applying the maximum decay heat load of 34.8 kW increases the maximum component temperatures within the HSM-H. In order to limit the maximum concrete temperature below the values considered for the structural analyses in Chapter 3, the maximum decay heat load is decreased for the HSM-H modules without fins on the side heat shields. The maximum decay heat load for the HSM-H modules with un-finned aluminum side heat shields is 32.0 kW, which gives a uniform heat flux of 3.07 Btu/hr-in^2.

$$Decay\ heat\ flux = \frac{Q}{\pi D_i L} = 3.07 \quad \text{Btu/hr-in}^2 \text{ for HSM-H with un-finned aluminum side heat shields}$$

Q_1 = 32.0 kW = 109,194 Btu/hr

For the HSM-H modules with galvanized side heat shields, the maximum decay heat load is limited to 26.1 kW.

$$Decay\ heat\ flux = \frac{Q}{\pi D_i L} = 2.51 \quad \text{Btu/hr-in}^2 \text{ for HSM-H with galvanized steel side heat shields}$$

Q_2 = 26.1 kW = 89,061 Btu/hr

It is assumed that soil has a temperature of 70°F at 10' below the HSM-H basemat for hot conditions. The soil temperature for cold condition (-20°F) is assumed to be 45°F. These assumptions are consistent with the assumptions in the thermal analysis of the standardized HSM design [19]. The HSM-H basemat is considered to be a 4' thick concrete slab. Due to low conductivity of concrete and soil, the model is insensitive to the thickness of the basemat / soil and the soil temperature. The heat flux and fixed temperature boundary conditions applied in the model are shown in Figure 4-11.

4.3.1.3 Steady State 32PTH DSC Model

The 32PTH DSC is a high integrity stainless steel welded pressure vessel that provides confinement of radioactive material, encapsulates the fuel in a helium atmosphere, and when placed in the transfer cask, provides radiological shielding.

A three dimensional finite element model of the 32PTH DSC is developed using ANSYS [16] to determine the maximum fuel cladding temperature. The DSC model includes the DSC shell, shield plugs, basket rails, basket, and fuel assemblies. The fuel assemblies are modeled as homogenized regions within the fuel compartments. The effective thermal properties for the homogenized fuel are calculated in Section 4.8.

The following conservative assumptions are considered in developing the finite element model to maximize the fuel cladding temperature:

- No convection occurs within the DSC cavity,
- The basket containing the fuel assemblies is centered axially in the DSC cavity,
- Heat transfer across the contact gaps within the basket occurs only by gasous conduction.

The following gaps are considered between components in the model at thermal equilibrium:

- 0.010" gap between each two adjacent basket plates except for the following cases:
  - between the aluminum inserts and the stainless steel rails – this gap is considered to be at least 0.020"
  - between the aluminum and the poison plates, when applicable. The aluminum plate and the poison plate are sandwiched between fuel compartments. For ease of modeling the 0.010" gaps are placed on both sides of the paired plates. No gap is considered between the paired aluminum and poison plates.
- 0.010" gap between the basket plates and aluminum rails
- 0.100" radial gap between rails and inner shell (see Section 4.11 for justification)

The axial cold gap of 0.07" between the stainless steel support plates and the aluminum plates is divided into a 0.01" axial gap at the bottom and a 0.060" axial gap at the top of the stainless steel plate. All dimensions of the canister are at nominal values. Details of the finite element model are shown in Figures 4-12 to 4-14.

Five basket types in two categories are designed for NUHOMS-32PTH DSC. Relevant characteristics of these basket types are listed below.

Basket type	I	II
A	Boron Aluminum, or Metal Matrix Composites (MMC) Maximum thickness 0.187"	Boral® Maximum thickness 0.075"
B		
C		
D		Not applicable
E		Not applicable

Aluminum plates are to be paired with the poison plates to make a nominal thickness of 0.5". The conductivity of the borated aluminum/MMC plate depends on the boron content and the fabrication procedure. To bound the maximum component temperature, the maximum thickness of the boron containing plate (0.1875") is considered in the model for basket type I.

Paired Boral®/ aluminum plates are used in basket type II. An effective conductivity is calculated for the paired Boral® / aluminum plates, as discussed in Section 4.2. Other combination of aluminum and poison plates that satisfies the conductivity requirements in Chapter 9 can be used in the basket.

Heat transfer from the fuel regions occurs only by conduction through the basket plates and the rails. Conduction and radiation heat transfer are considered between the rails and the DSC shell. Conduction through components is modeled using SOLID70 elements.

Radiation between the rails and the DSC shell is modeled using radiation LINK31 elements using the same methodology as described in Section 4.3.1.1. Axial radiation is also considered between the top and bottom surfaces of the fuel assemblies to the shield plugs. The emissivity of the heavily oxidized top and bottom surfaces of the fuel assemblies are considered to be 0.9.

Steady State Boundary conditions for the DSC Model

The nodal temperatures of the DSC shell are retrieved from the transfer cask or HSM-H models described in Sections 4.3.1.1 and 4.3.1.2, and applied to the corresponding nodes in the DSC model via a macro described in Appendix 4.16.1.

The SOLID70 elements representing the homogenized fuel are given heat generating boundary conditions in the region of the active fuel length. Active fuel length is considered to be 144" [20] beginning at approximately 4.0" above the bottom of the fuel assembly [20]. Fuel assembly has a total length of 162" in the model. Peaking factors to apply the axial decay heat profile for the homogenized fuel region are calculated in Section 4.7.

The maximum heat load per canister is 33.8 kW for CE14x14 fuel assemblies and 34.8 kW for other fuel assemblies. Since CE14x14 fuel assembly has a shorter active fuel length than the other assemblies, a lower total heat load is considered for CE14x14 assembly to avoid a high heat generating rate. The maximum decay heat per assembly is 1.5 kW. Heat load zoning, as illustrated below, is used to maximize the number of higher heat load assemblies per DSC. The loading requirements are as follows.

For CE14x14 Assemblies

- Q_{zi} is the maximum decay heat per assembly in zone i
- Total Decay Heat ≤ 33.8 kW
- 4 fuel assemblies in zone 1 with $Q_{z1} \leq 0.775$ kW
- 20 fuel assemblies in zone 2 with $Q_{z2} \leq 1.068$ kW
- 8 fuel assemblies in zone 3 with $Q_{z3} \leq 1.5$ kW

$Q_{z1} \leq Q_{z2} \leq Q_{z3}$

For other fuel Assemblies

- Q_{zi} is the maximum decay heat per assembly in zone i
- Total Decay Heat ≤ 34.8 kW
- 4 fuel assemblies in zone 1 with
  - total decay heat ≤ 3.2 kW
  - $Q_{z1a} \leq 1.05$ kW in the lower compartments
  - $Q_{z1b} \leq 0.8$ kW in the upper compartments
- 20 fuel assemblies in zone 2 with $Q_{z2} \leq 1.1$ kW
- 8 fuel assemblies in zone 3 with $Q_{z3} \leq 1.5$ kW
- $Q_{z1} \leq Q_{z2} \leq Q_{z3}$

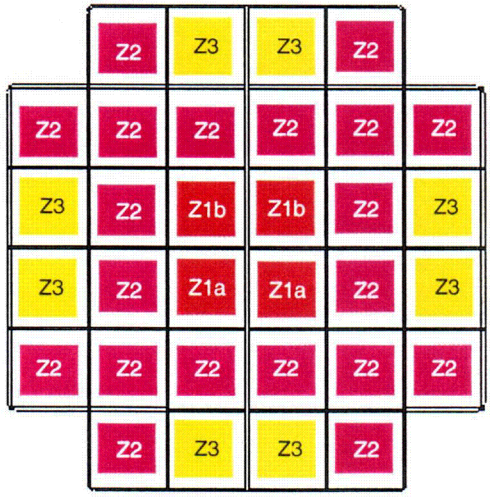

Heat generation rates as a function of spent fuel parameters are calculated in Appendix 4.16.2. Five extreme loading configurations are considered to bound the maximum component temperatures. The loading configurations are shown in Figure 4-15. In the first configuration, the heat load in the core compartments is maximized, so that zone 1 has a uniform heat load of 0.8

C01

kW per assembly and zone 2 has a heat load of 1.1 kW per assembly. Since the total heat load is limited to 34.8 kW, the heat load of zone 3 is 1.2 kW per assembly.

The heat load in the peripheral compartments is maximized in loading configuration 2, so that zone 3 has a heat load of 1.5 kW per assembly and zone 2 has a heat load of 1.1 kW per assembly. Since the total heat load is limited to 34.8 kW, the heat load of zone 1 is 0.2 kW per assembly. A heat load of 0.2 kW per assembly for a fuel assembly in zone 1 is rather unrealistic. To have a more realistic estimation of maximum component temperatures loading configuration 3 is considered, in which zone 1 has a heat load of 0.55 kW per assembly and zone 3 has a heat load of 1.5 kW per assembly. Zone 2 is divided into two subdivisions. The first subdivision includes the fuel assemblies around the central assemblies with a heat load of 0.925 kW per assembly and the second subdivision located at the periphery has a heat load of 1.1 kW per assembly.

In loading configuration 4, the heal load in zone 1 and zone 3 are maximized, so that the central and peripheral compartments have maximum heat load. The heat load is 1.5 kW per assembly in zone 3 and 0.8 kW per assembly in zone 1. The remaining heat load is divided uniformly over assemblies in zone 2, which gives a heat load of 0.98 kW per assembly.

To investigate the effect of non-uniform loading in zone 1, loading configuration 5 is considered, in which the two lower compartments in zone 1 have a heat load of 1.05 kW per assembly. It gives a heat load of 0.55 kW per assembly for the two upper compartments in zone 1 based on the loading restrictions.

Similar to load configuration 1, the heat load in the core compartments is maximized for CE14x14 assemblies in load configuration 6. The heat load of zone 3 is 1.17 kW per assembly.

Load configuration 7 is similar to configuration 4, the heat load in zones 1 and 3 are maximized to investigate the effect of the maximum heat load in zone 3 on the cladding temperature.

The seven loading configurations discussed above are considered only for the maximum ambient temperature of 115°F during transfer operation. For the other conditions loading configuration 1 is evaluated, which gives the maximum DSC component temperatures for high enriched fuel assemblies in basket type I.

Heat generating rate for each segment of the active fuel region is calculated as follows:

$$\dot{q}''' = \frac{\left(\frac{Q}{4a^2 L_a}\right)}{0.984}$$

where

Q = Heat load per assembly defined for each loading zone
a = half width of fuel compartment = 8.7"/2 = 4.35"
L_a =Active fuel length = 137 for CE14x14 / 144" for other assemblies
PF = Peaking Factor from Section 4.7

The area beneath the peaking factor curve shown in Section 4.7 is 0.984. The heat generating value is divided by this factor to avoid any reduction of the total heat load in the model. The total

heat load applied in the model is verified by retrieving the reaction solution from the solved model and comparing it to the maximum heat load value. Typical applied boundary conditions are shown in Figure 4-16.

4.3.2 Maximum Temperatures for Normal and Off-Normal Conditions

Steady state thermal analyses are performed using the maximum decay heat load of 34.8 kW (33.8 kW for CE14x14) per canister, 115°F ambient temperature, and the maximum insolation per reference [17]. Insolation is averaged over a 12 hour period for transfer conditions and over a 24 hour period for storage conditions.

The temperature distributions within the TC, the HSM-H, and the DSC models are shown in Figures 4-17 to 4-23. Summaries of the maximum component temperatures are listed in Tables 4-1 and 4-2. The maximum component temperatures for 34.8 kW heat load bounds the temperatures calculated for 33.8 kW heat load as shown in Table 4-1.

The maximum temperatures calculated for off-normal conditions bound the values for the normal conditions. Therefore, thermal stress and DSC internal pressures for both normal and off-normal conditions are calculated based on the temperatures resulted from the maximum off-normal conditions (115°F ambient) for conservatism.

4.3.3 Minimum Temperatures for Normal and Off-Normal Conditions

Temperature distributions under the minimum ambient temperatures of –20°F with no insolation and the maximum design heat load are determined under steady state conditions to maximize the temperature gradients in the TC, the HSM-H and the DSC. Figures 4-24 and 4-25 show the temperature distributions for transfer operations and storage conditions at -20°F respectively. Tables 4-3 and 4-4 summarize the results of these analyses.

The resultant DSC and transfer cask temperatures for the -20°F ambient during transfer and storage are used to calculate the thermal stresses for the normal conditions at 0°F ambient.

4.3.4 Maximum Internal Pressures for Normal and Off-Normal Conditions

Maximum internal pressure within the NUHOMS®-32PTH DSC is calculated in section 4.6.

4.3.5 Maximum Thermal Stresses for Normal and Off-Normal Conditions

Maximum thermal stresses during normal and off-normal conditions of storage and transfer are calculated in Chapter 3.

4.3.6 Evaluation of Thermal Performance for Normal and Off-Normal Conditions

The thermal analysis for normal and off-normal conditions of transfer and storage concludes that the NUHOMS®-32PTH System design meets all applicable requirements.

The maximum component temperatures calculated using conservative assumptions are lower than the allowable limits. The maximum TC seal temperature (255°F / 124°C) during off-normal transfer conditions is well below the 400°F long-term limit specified for continued seal function. The maximum solid neutron shield temperature (265°F / 129°C) is below allowable limit of 320°F (160°C) and no degradation of the solid neutron shielding material is expected. The maximum pressure within the neutron shielding panel (38.5 psia / 23.8 psig) corresponding to the average temperature of the liquid neutron shield (265°F / 129°C) is below the set point of the pressure relief valve (54.7 psia / 40 psig).

If the side heat shield is equipped with fins, the maximum local temperature of the HSM-H concrete structure is lower than 200°F as required in [21]. If the side heat shields are not equipped with fins, the maximum local temperature of concrete is slightly above 200°F but does not exceed 225°F. The concrete structure of the HSM-H is made using Type II cement with fine aggregates satisfying ASTM C33 or equivalents as defined in NUREG-1536 [22], when the side heat shields are not equipped with the fins.

The calculated maximum fuel cladding temperature is lower than the temperature limit of 752°F (400°C) considered for normal conditions of storage and short-term operations in [2]. The comparison of the resultant maximum temperatures with the allowable limits is listed below:

Component	Transfer Conditions [6]	Allowable / Design Limit
Cask Lid Seal	205°F	400°F
Cask Bottom Plate Seal	190°F	400°F
Lead	337°F	621°F
Liquid Neutron Shield (Temp / Press)	265°F / 23.8 psig	45 psig
Solid Neutron Shield	213°F	320°F
Fuel Cladding	723°F	752°F

Component	Storage Conditions [6]	Allowable / Design Limit
Concrete in module with finned aluminum side heat shields @ 34.8 kW	190°F	200°F
Concrete in module with un-finned aluminum side heat shields @ 32.0 kW	202°F	225°F
Concrete in module with un-finned galvanized steel side heat shields @ 26.1 kW	201°F	225°F
Fuel Cladding @ 34.8 kW	684°F	752°F for normal conditions / 1058°F for off-normal conditions

The maximum DSC internal pressures for normal and off-normal storage conditions are 5.9 and 10.7 psig respectively. The maximum DSC internal pressure for normal transfer conditions is 6.4 psig and for off-normal transfer conditions is 11.2 psig. The DSC internal pressures are lower than the design pressure limits of 15 psig for normal and 20 psig for off-normal storage and transfer conditions.

[6] The TC and HSM-H models are run only with off-normal conditions at 115°F ambient. The resultant temperatures are used to evaluate the thermal performance for both normal and off-normal conditions. The fuel cladding temperature remains in all cases below the normal allowable limit of 752°F.

4.4 Thermal Evaluation for Accident Conditions

Three hypothetical accident cases during transfer operation are relevant for thermal evaluation:

- Loss of the TC liquid neutron shield due to damages on the shielding panel
- Loss of helium gas in annulus between the DSC and the TC
- Postulated fire engulfing the TC

It is considered in all the above cases that the transfer cask contains a fully loaded DSC. The fire accident is postulated in which maximum amount of 300 gallons of diesel fuel is spilled onto the ground in such a way as to completely engulf the transfer cask. Subsequent to the fire accident, it is assumed that the seals for the TC lid and the bottom cover plate will burn, and the liquid neutron shield will be released and evaporates completely. Therefore, the fire accident scenario bounds the loss of liquid neutron shield and the loss of helium gas in the accident cases. The fire accident case is analyzed to give the bounding fuel cladding temperature for the transfer accident cases.

Since the HSM-H is located outdoors, there is a remote probability that the air inlet and outlet openings will become blocked by snow or by debris from events such as flooding, high wind, and tornados. The perimeter security fence around ISFSI and the location of the air inlet and outlet openings reduces the probability of such an event. Nevertheless, it is conservatively considered in this analysis that all the inlet and outlet openings become blocked.

The thermal mass of the HSM-H, the construction of the vent openings, and the location of the fuel on the transfer vehicle limit the effect of a fire accident for the HSM-H. Therefore, the worst case fire accident is bounded by the fire accident case during transfer operation.

A new model is developed to evaluate the fire accident case during transfer operation. The HSM-H model described in Section 4.3 is slightly modified to evaluate the blocked vent accident case during storage. The DSC model is unchanged for this evaluation. Details of the models are discussed in section 4.4.1.

4.4.1 Thermal Models for Accident Conditions

4.4.1.1 Transient Transfer Cask Model

To determine the temperature distribution in the transfer cask and the DSC for fire accident case, a three dimensional model is developed using ANSYS [16]. This model is created by selecting the nodes and elements of the DSC model described in Section 4.3 at z-axis from 56.06" to 86.07". The shells of TC including the annulus are then modeled around the DSC using SOLID70 elements. LINK31 elements are created using the same methodology as described in Section 4.3.1.1 to simulate the radiation between the DSC shell and the TC inner shell. The three dimensional model represents a slice of the DSC within the transfer cask. The TC slice model is shown in Figure 4-26. Axial length of the slice model is 30".

It is assumed that the helium gas in the annulus will remain in place during the burning period to maximize the heat input from fire into the transfer cask. For the same reason, all the air gaps in the transfer cask were removed during the burning period. To eliminate the uncertainties about the maximum poison plate conductivity, the conductivity of poison plate is set equal to that of aluminum 1100 during the fire.

The effective conductivity of liquid neutron shield (water) is calculated using the methodology discussed in Section 4.9. The liquid neutron shield (water) will be released at high temperatures (~417°F) when its saturation pressure exceeds the set point of the pressure relief value (40 psig). The average temperature of liquid neutron shield drops to 212°F (boiling point of water) when the pressure relief valve opens. After this point, the energy of fire will be consumed to evaporate the liquid neutron shield and the temperatures remain constant until the liquid shield is evaporated completely. Nevertheless, an effective conductivity of 2.25 Btu/hr-in-°F is considered for the liquid neutron shield to bound the problem and to maximize the heat input from the fire into the transfer cask. The selected value (2.25 Btu/hr-in-°F) is higher than the effective conductivity values calculated for the liquid neutron shield during fire in Section 4.9.

During the cool down period all the air gaps are replaced. Subsequent to the fire, it is assumed that the TC seals are burned and air has replaced water in the shielding panel. The properties of air are therefore given to the elements in the shielding panel and to the elements in the annulus between the DSC and the transfer cask during the cool down period. Convection and radiation through the air in the shielding panel are combined together in form of an effective conductivity. Section 4.9 describes the calculation of the effective conductivity for the air within the shielding panel. Convection is not considered for the air in the annulus. As mentioned in Section 4.3.1.1, radiation in annulus is modeled using LINK31 elements.

Boundary Conditions for the Fire Accident Case

Initial temperatures for the transfer cask slice model are transferred from the steady-state models at 115°F ambient conditions.

Fire is assumed to have an average flame temperature of 1475°F and an emissivity of 0.9. The cask surface emissivity is set to 0.8 during the fire. These assumptions are in compliance with 10CFR71.73 [17].

It is assumed that the diesel fuel creates a pool diameter of about 200 inches, which is the approximate length of the transfer cask. Considering a volume of 300 gallons and a minimum burning rate of 0.15 in/min [23] give a burning time of 14.5 minutes for diesel fuel. A burning time of 15 minutes is considered conservatively for analytical purposes.

A forced convection value of 4.5 Btu/hr-ft^2-F is considered during the burning time as concluded in [23]. The calculation of the heat transfer coefficients on the transfer cask during fire accident are described in Section 4.11.1.

Heat generation corresponding to loading configuration 1 is considered for the solid elements representing the homogenized fuel during the burning time and the cool down period.

A peaking factor of 1.1 is considered for this evaluation. Adiabatic boundary conditions are applied over the vertical end surfaces of the slice model. This model is conservative regarding the fuel cladding temperature since the axial heat transfer is restricted and the maximum peaking factor is applied to the heat generating rate.

4.4.1.2 Transient HSM-H Model

A slightly modified HSM-H model discussed in Section 4.3.1 is used to determine the temperature distribution in the HSM-H and the 32PTH DSC shell for the blocked vent accident case. The basket and its content including the fuel assemblies are homogenized for the transient run required for the blocked vent analysis. The effective thermal properties of the homogenized DSC content are calculated as follows.

Effective Properties of the Homogenized Basket

Volume and weight of the basket components are calculated in chapter 3. The relevant values are listed below for calculation of the effective basket properties.

	Volume	Weight	C_p	C_p x M
Component	in^3	lbm	Btu/lbm-°F	Btu/°F
Fuel Assemblies	148488	50720	0.068	3449
Basket, Stainless Steel	75928	22019	0.116	2554
Basket, Aluminum	79952	7835	0.218	1708
Total	610662	80574	---	7711

The equations for calculating the average basket density and heat capacity are:

$$\overline{\rho} = \frac{basket\ weight + fuel\ assemblies\ weight}{total\ cavity\ volume}$$

$$\overline{C}_p = \frac{weight\ of\ SS \times C_{p,ss} + weight\ of\ Al \times C_{p,ss} + weight\ of\ fuel \times C_{p,fuel}}{basket\ weight + fuel\ assemblies\ weight}$$

total cavity volume = $\pi/4 \times D_i^2 \times L$
D_i = DSC inner diameter = 68.75"
L = cavity length = 164.5"
$C_{p,ss}$ = 0.116 Btu/lbm-°F @ 100°F [6]
$C_{p,Al}$ = 0.218 Btu/lbm-°F @ 100°F [6]
$C_{p,fuel}$ = 0.068 Btu/lbm-°F @ 400°F [Section 4.8]

Specific heat capacities of stainless steel and aluminum increase at higher temperatures as shown in Section 4.2. Initial basket temperature for blocked vent case is higher than 100°F. Selecting lower heat capacity values for stainless steel and aluminum at 100°F is conservative since it reduces the amount of stored heat in the basket and results in a higher fuel cladding temperature.

The heat capacity of the fuel assembly is selected at 400°F, which is lower than the average off-normal temperature of the fuel assemblies in the 32PTH DSC model. Similar to stainless steel and aluminum, selecting lower heat capacity values for fuel assemblies is conservative.

The resultant effective density and specific heat capacity of the basket are:

$\overline{\rho} = 0.132$ lbm/in^3

$\overline{C}_p = 0.096$ Btu/lbm-°F

To calculate the axial and the transverse effective conductivities of the basket a 15" long slice of the basket is created by selecting the nodes and elements of the 32PTH DSC shell and basket from the finite element model described in section 4.3.1.3. DSC shell elements are unselected prior to run the slice model. The basket slice model is shown in Figure 4-27.

To calculate the axial effective conductivity of the basket, constant temperature boundary conditions are applied at the top and bottom of the slice model. No heat generation is considered for the fuel elements in this case. The axial effective conductivity is calculated using the following equation:

$$k_{eff,axl} = \frac{Q \times L}{A \times \Delta T}$$

where,

Q = Amount of heat leaving the upper face of the slice model – reaction solution of the uppermost nodes (Btu/hr)

L = Length of the model = 15"

A = Surface area of the upper (or bottom) face of the model = $\pi/2 \times r_i^2 = 1856$ in^2

r_i = Inner radius of the DSC shell = 34.375"

$\Delta T = (T_1 - T_2)$ =Temperature difference between upper and lower faces of the model (°F)

T_1 = Constant temperature applied on the lower face of the model (°F)

T_2 = Constant temperature applied on the upper face of the model (°F)

In determining the temperature dependent axial effective conductivities an average temperature, equal to $(T_1 + T_2)/2$, is used for the basket temperature. The resulting axial effective conductivities of the basket are listed below.

T_1 (°F)	T_2 (°F)	T_{avg} (°F)	$Q_{reaction}$ (Btu/hr)	$k_{eff,axl}$ (Btu/hr-in-°F)
300	400	350	12380	1.0005
400	500	450	12533	1.0128
500	600	550	12734	1.0291
600	700	650	12928	1.0448
700	800	750	13096	1.0583
800	900	850	13280	1.0732
900	1000	950	13449	1.0869
1000	1100	1050	13627	1.1013
1100	1200	1150	13762	1.1122

To calculate the transverse effective conductivity of the basket, constant temperature boundary conditions are applied on the outermost nodes of the slice model and heat generating conditions

are applied on the fuel elements. The heat generation rates are calculated based on the loading configuration 1 shown in Figure 4-15 with a peaking factor of 1.1.

The following equation from [15] determines the maximum temperature for long solid cylinders with uniformly distributed heat sources.

$$T = T_o + \frac{\dot{q}\, r_o^2}{4k}\left[1-\left(\frac{r}{r_o}\right)^2\right]$$

with T_o = Temperature at the outer surface of the cylinder (°F)
T = Maximum temperature of cylinder (°F)
$\dot{q}$ = Heat generation rate (Btu/hr-in^3)
r_o = Outer radius =34.375"
r = Inner radius = 0 for slice model
k = Conductivity (Btu/hr-in-°F)

The above equation is rearranged to calculate the transverse effective conductivity of the basket.

$$\dot{q} = \frac{Q}{V} = \frac{Q}{\frac{\pi r_o^2}{2} L} \quad \rightarrow \quad k_{eff,rad} = \frac{2Q}{4\pi L \Delta T}$$

with Q = Amount of heat leaving the periphery of the slice model – reaction solution of the outermost nodes (Btu/hr)
L = length of the model = 15"
$\Delta T = (T - T_o)$ = Difference between maximum and the outer surface temperatures in (°F)

Since the surface area of the fuel assemblies at the basket cross section is much larger than the other components, assuming a uniform heat generation is a reasonable approximation to calculate the radial, effective conductivity. In determining the temperature dependent transverse effective conductivities an average temperature, equal to $(T_{max} + T_o)/2$, is used for the basket temperature. The resulting transverse effective conductivities of the basket are listed below.

T_o (°F)	T_{max} (°F)	T_{avg} (°F)	$Q_{reaction}$ (Btu/hr)	$k_{eff,rad}$ (Btu/hr-in-°F)
100	491	296	6914	0.1876
200	568	384	6914	0.1993
300	647	474	6914	0.2114
400	728	564	6914	0.2237
500	810	655	6914	0.2366
600	894	747	6914	0.2495
700	980	840	6914	0.2620
800	1068	934	6914	0.2737
900	1160	1030	6914	0.2821
1000	1254	1127	6914	0.2888

Boundary Conditions for the Blocked Vent Case

The initial temperatures for the HSM-H model are calculated using the same convection and radiation boundary conditions as described in Section 4.3.1.2 for the maximum ambient temperature of 115°F (105°F daily average temperature).

4.5.1.3 Boundary Conditions for Procedure C

The same boundary conditions as those described for procedure B are considered for Procedure C except that the 32PTH DSC is backfilled with helium after drainage of the annulus water. It is considered that it takes three hours until the helium replaces the air and water vapor within the DSC cavity completely. Before helium backfill, the model considers air conductivity for the DSC back fill gas. After the three hour period, the conductivity of back fill gas is changed to that of helium, and the fuel effective conductivities are changed to those calculated for helium atmosphere.

4.5.1.4 Evaluation of Vacuum Drying Procedure

Transient simulation of vacuum drying procedures gives the time-temperature history of the fuel assemblies with the maximum decay heat load of 34.8 kW. Duration of the vacuum process is limited to the time at which the maximum temperature of the fuel assemblies is close to the allowable limit of 752°F (400°C) [2]. A margin of about 20°F is considered for conservatism in determining the time limit. The maximum fuel cladding temperatures are summarized in Table 4-8. Typical temperature distributions at the end of vacuum drying process are shown in Figure 4-34. Histories of the maximum component temperatures are shown in Figures 4-35 to 4-37.

As Table 4-8 shows, the vacuum drying can proceed up to 36 hours, if procedure A is followed. For procedure B, the time limit to complete the vacuum drying is 14 hours after drainage of the annulus water or 28 hours after complete drainage of DSC water, whichever is the limiting time.

Backfilling the transfer cask must start within12 hours after completion of the vacuum drying, if one chooses to follow procedure B. The time limit to start backfilling the transfer cask with helium is significantly longer, if procedure A is followed. For procedure C, backfilling of the transfer cask with helium must start within 42 hours after complete DSC drainage or 28 hours after drainage of the annulus water based on the time-temperature history curve shown in Figure 4-37.

Should the decay heat load be lower than 34.8 kW, the time frame will increase for completion of the vacuum drying process. At some decay heat load, the maximum fuel cladding temperature remains always below the allowable limit regardless of the vacuum drying duration. To determine the decay heat load at which the time limitation is not required, models of procedure A to C are investigated separately assuming steady state conditions. Uniform heat generating boundary conditions are applied on the fuel assemblies in the steady state analysis. The results summarized in Table 4-9 show that the fuel cladding temperature remains always below the allowable limit for 23.2 kW decay heat load using procedure A. Similarly, there is no time limit for vacuum drying with 16.0 kW and 22.4 kW using procedures B and C respectively.

Vacuum drying procedures A to C preclude any thermal cycling of fuel cladding. Backfilling the DSC with helium gas causes a one time temperature drop, which is not considered as a repeated thermal cycling. Re-evacuation of the DSC under helium atmosphere does not reduce the pressure sufficiently to decrease the thermal conductivity of helium. Therefore, evacuation and re-pressurizing the DSC under helium atmosphere proceed on a descending curve to the minimum steady state temperatures, and does not include any thermal cycling. It concludes that the limit of 65°C (118°F) considered for thermal cycling is not applicable for NUHOMS®-32PTH system.

4.5.2 Reflooding

For unloading operations, the DSC will be filled with the spend fuel pool water through the siphon port. During this filling, the DSC vent port is maintained open with effluents routed to the plant's off-gas monitoring system.

When the pool water is added to a DSC cavity containing hot fuel and basket components, some of the water will flash to steam causing internal cavity pressure to rise. The steam pressure is released through the vent port. The initial flow rate of the reflood water must be controlled such that the internal pressure in the DSC cavity does not exceed 20 psig. This is assured by monitoring the maximum internal pressure in the DSC cavity during reflood event. The reflood of the DSC is considered as a "Service Level D" event and the design pressure of the DSC is 120 psig. Therefore, there is sufficient margin in the DSC internal pressure during the reflooding event to ensure that the DSC will not be over pressurized.

The maximum fuel cladding temperature during reflooding process is significantly less than the vacuum drying condition owing to the presence of water/steam in the DSC cavity. Hence, the peak cladding temperature during the reflooding operation will be less than 734°F calculated for procedure A in Section 4.5.1 when water circulates in the annulus between the DSC and transfer cask.

To evaluate the effects of the thermal loads on the fuel cladding during reflooding operations, a conservative high fuel rod temperature of 750°F and a conservative low quench water temperature of 50°F are used.

The following material properties, corresponding to 750°F, are used in the evaluation.

Modulus of elasticity, $E = 10.4 \times 10^6$ psi $= 7.17 \times 10^{10}$	(Pa)	[26]
Modulus of rigidity, $G = 2.47 \times 10^{10}$	(Pa)	[31]
Thermal expansion coefficient, $\alpha = 6.72 \times 10^{-6}$	(1/K)	[31]
Yield stress, Sy = 80,500 psi $= 5.55 \times 10^8$	(Pa)	[26]
Poisson's ratio, $\upsilon = \frac{E}{2G} - 1$		[27]

The fuel cladding stress is evaluated as a hollow cylinder with an outer surface temperature of T (50°F), and the inner surface temperature of T+ΔT (750°F) using the following equations from [27].

Maximum circumferential stresses are:

(outer surface) $\sigma_{to} = \frac{\Delta T \cdot \alpha \cdot E}{2(1-\upsilon)\ln(r_o / r_i)}\left(1 - \frac{2 r_i^2}{(r_o^2 - r_i^2)}\ln(\frac{r_o}{r_i})\right)$ tension

(inner surface) $\sigma_{ti} = \frac{\Delta T \cdot \alpha \cdot E}{2(1-\upsilon)\ln(r_o / r_i)}\left(1 - \frac{2 r_o^2}{(r_o^2 - r_i^2)}\ln(\frac{r_o}{r_i})\right)$ compression

The longitudinal stresses are equal to the tangential stresses [27]. The maximum stresses calculated for the fuel assembly types to be stored in the NUHOMS-32PTH are summarized in the following table.

	WE15x15	WE17x17Std	17x17MkBW	WE17x17OFA	CE14x14
OD fuel rod (in)	0.422	0.374	0.374	0.360	0.440
Clad thickness (in)	0.0243	0.0225	0.0240	0.0225	0.028
ID Clad (in)	0.3734	0.3290	0.3260	0.3150	0.3840
σ_{to} max (Pa)	1.64E+08	1.64E+08	1.63E+08	1.63E+08	1.63E+08
σ_{to} max (psi)	23,768	23,719	23,644	23,676	23,654
σ_{ti} max (Pa)	1.78E+08	1.78E+08	1.79E+08	1.78E+08	1.79E+08
σ_{ti} max (psi)	25,787	25,835	25,910	25,879	25,900

σ_max (psi) = 25,910

The maximum stress is 25,910 psi. The calculated maximum stress is much less than the yield stress of 80,500 psi. Therefore, cladding integrity is maintained during reflooding operation.

4.6 Maximum Internal Pressure

The following methodology is used to determine the maximum pressures within the 32PTH DSC during storage and transfer conditions:

- Average cavity gas temperatures are derived from component temperatures.
- The amount of helium present within the canister after the initial backfilling is determined via the ideal gas law.
- The total amount of free gas within the fuel assemblies, including both fill and fission gases, is calculated based on data reported in [28].
- The amount of released gas from the fuel rods into the DSC cavity is determined based on the maximum fraction of the ruptured fuel rods considered in NUREG 1536 [22].
- The amount of helium gas is added to the amount of released gases to make the total amount of gases in the 32PTH DSC cavity.
- Finally, the maximum cavity pressures are determined via the ideal gas law.

The design pressures for the NUHOMS®-32PTH DSC are summarized in the following table.

Condition	Maximum Allowable Pressure For Storage (psig)	Maximum Allowable Pressure for Transfer (psig)
Normal	15	15
Off-Normal	20	20
Accident	70	120

Based on the ideal gas law, the internal pressure of the DSC increases as the average gas temperature increases. Since the DSC normal operating temperatures are bounded by the off-normal temperatures, the maximum internal pressure of the DSC is conservatively calculated based on the off-normal temperatures for both the normal and the off-normal conditions. The average cavity gas temperatures are calculated for loading configuration 1 and HSM-H with unfinned side heat shields at 34.8 kW, which give the maximum component temperatures.

The maximum fractions of the fuel rods that can rupture and release their free gases to DSC cavity for normal, off-normal, and accident cases are 1, 10, and 100% respectively as considered in NUREG 1536 [22].

4.6.1 Average Gas Temperature

To determine the average gas temperature, volume average temperatures of the elements representing the helium gaps (T_{void}) and the homogenized fuel assemblies (T_{fuel}) are calculated discretely from the thermal models. Although the average temperature of the homogenized fuel elements includes the fuel rods and the helium gas between them, this average temperature is considered as the average gas temperature within fuel compartments. The following volumes are considered to calculate the gas average temperature:

Gas volume in the fuel compartments = Volume of the fuel compartments – Volume of the fuel rods
Volume of the fuel compartment = 8.7 x 8.7 x 162 x 32 = 392,377 in^3
Volume of the fuel rods = 148,488 in^3 [Chapter 3]
Gas volume in the fuel compartments ($V_{He,comp}$) = 243,889 in^3

Average peaking factor is:

$$P_j = \frac{A_j}{H_j}$$

P_j = Average peaking factors of fuel region j
H_j= Height of fuel region i

The following Figure depicts this methodology. The resultant average peaking factors for active fuel length of 144" are listed in Table 4-11.

Calculation of the Average Peaking Factor

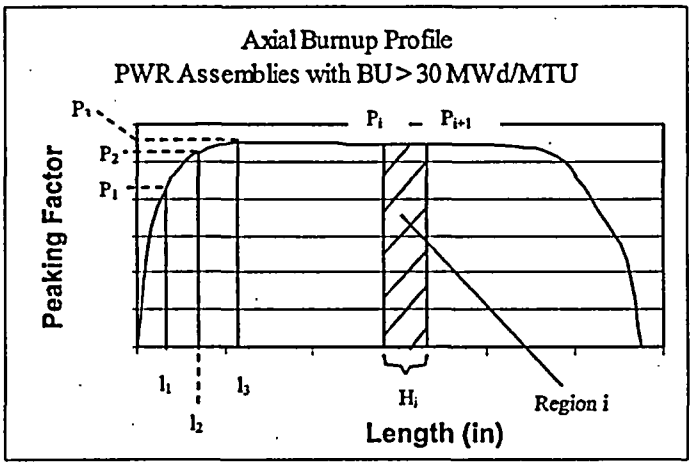

The height of each region is converted to the corresponding local coordination in the finite element model to apply the peaking factors in the model. The peaking factors applied in the model are listed below.

For WE and MkBW Fuel Assemblies (Active Fuel Length =144")

Region No.	Height from bottom of active fuel		Z-axis in FEM		Peaking Factor
	from	To	from	to	
1	0	1.32	4	5.32	0.107
2	1.32	7.0675	5.32	11.0675	0.582
3	7.0675	14.5	11.0675	18.5	0.908
4	14.5	22.0675	18.5	26.0675	1.048
5	22.0675	37.0675	26.0675	41.0675	1.100
6	37.0675	57.69	41.0675	61.69	1.104
7	57.69	66.9425	61.69	70.9425	1.096
8	66.9425	82.0675	70.9425	86.0675	1.094
9	82.0675	97.0675	86.0675	101.0675	1.095
10	97.0675	111.9425	101.0675	115.9425	1.088
11	111.9425	121.26	115.9425	125.26	1.046
12	121.26	127.0675	125.26	131.0675	0.955
13	127.0675	136.26	131.0675	140.26	0.743
14	136.26	144	140.26	148	0.374

For CE14x14 Fuel Assembly (Active Fuel Length =137")

Region No.	Height from bottom of active fuel		Z-axis in FEM		Peaking Factor
	from	To	from	to	
1	0	5.5	5.5	11.0675	0.441
2	5.5	11.0675	11.0675	18.5	0.874
3	11.0675	18.5	18.5	26.0675	1.041
4	18.5	26.0675	26.0675	41.0675	1.100
5	26.0675	41.0675	41.0675	61.69	1.103
6	41.0675	61.69	61.69	65.32	1.097
7	61.69	65.32	65.32	78.51	1.094
8	65.32	78.51	78.51	95.32	1.095
9	78.51	95.32	95.32	110.32	1.091
10	95.32	110.32	110.32	120	1.054
11	110.32	120	120	125.32	0.974
12	120	125.32	125.32	136.75	0.732
13	125.32	137	136.75	142.5	0.321

A comparison between the axial burnup profile from Reference [4] and the axial burnup profile used in the finite element model is shown in the Figure 4-39.
Figure 4-39 shows that the calculated axial profile perfectly matches the data from reference [4] except for the very ends of the active fuel. The small discrepancy at the very ends is due to the size of the regions and has a minimum effect on the thermal evaluation.

4.8 Effective Fuel Properties

4.8.1 Discussion

The NUHOMS®-32PTH DSC finite element models simulate the effective thermal properties of the fuel with a homogenized material occupying the volume within the basket where the fuel assemblies are stored. Effective values for density, specific heat, and conductivity are determined for this homogenized material for use in the finite element models.

The 32PTH DSC is capable of handling a variety of spent PWR fuel assemblies. In order to determine conservative thermal properties of the homogenized fuel assembly, all of the PWR fuel assembly types to be stored in the 32PTH DSC are studied. WE and MkBW fuel assemblies are considered in one category with active fuel length of 144". The lowest effective thermal conductivity, density, and specific heat of this fuel assembly group are selected to apply in the finite element model. Use of these properties would conservatively predict bounding maximum temperatures for the components of the NUHOMS®-32PTH DSC. The effective fuel properties for CE14x14 assembly are considered separately since CE14x14 assembly has a shorter active fuel length.

The characteristics of the fuel assemblies to be stored in the 32PTH DSC are listed in Table 4-12.

4.8.2 Summary of Material Properties

1. UO_2, Fuel Pellets

Conductivity and specific heat for fuel pellets are taken from [30] and listed below.

Temperature (°C)	k (cal/s-cm-°C) [30]	Temperature (°F)	k (Btu/hr-in-°F)
25	0.025	77	0.503
100	0.021	212	0.423
200	0.018	392	0.362
300	0.015	572	0.302
500	0.0132	932	0.266
700	0.0123	1292	0.248
800	0.0124	1472	0.250

Temperature (°C)	C_p (cal/g-°C) [30]	Temperature (°F)	C_p (Btu/lbm-°F)
0	0.056	32	0.056
100	0.063	212	0.063
200	0.0675	392	0.068
400	0.0722	752	0.072
1200	0.079	2192	0.079

The density of fuel pellets (UO_2) is 10.96 g/cc = 0.396 lbm/in^3 [30].

2. Zircaloy-4, Cladding

Table B-2.I of Reference [31] lists measured and calculated values of thermal conductivity for zircaloy-4 at various temperatures. The measured values used in this calculation are listed below.

Temperature (K)	k (W/m-K) [31]	Temperature (°F)	k (Btu/hr-in-°F)
373.2	13.6	212	0.655
473.2	14.3	392	0.689
573.2	15.2	572	0.732
673.2	16.4	752	0.790
773.2	18.0	932	0.867
873.2	20.1	1112	0.968

Table B-1.1 of [31] lists specific heat values for Zircaloy as a function of temperature.

Temperature (K)	C_p (J/kg-K) [31]	Temperature (°F)	C_p (Btu/lbm-°F)
300	281	80	0.067
400	302	260	0.072
640	331	692	0.079
1090	375	1502	0.090

The density of Zircaloy is 6.56 g/cm3 = 0.237 lbm/in3, as defined in [30].

Table B-3.11 of [31] lists the measured emissivity values for fuel cladding. For ease of calculation a temperature independent emissivity of 0.8 is set for zircaloy4 in this calculation.

$\varepsilon zirc = 0.80$

3. Helium

Temperature (K)	Conductivity [5] (W/m-k)	Temperature (°F)	Conductivity (Btu/hr-in-°F)
200	0.1151	-100	0.0055
250	0.1338	-10	0.0064
300	0.150	80	0.0072
400	0.180	260	0.0087
500	0.211	440	0.0102
600	0.247	620	0.0119
800	0.307	980	0.0148
1000	0.363	1340	0.0175

4. Air at low pressure (0.1 bar)

Temperature (K)	Conductivity [5] (W/m-k)	Temperature (°F)	Conductivity (Btu/hr-in-°F)
200	0.0180	-100	0.0009
300	0.0263	80	0.0013
400	0.0336	260	0.0016
500	0.0403	440	0.0019
600	0.0466	620	0.0022
800	0.0577	980	0.0028
1000	0.0681	1340	0.0033

The air conductivity at low pressure is used to calculate the effective transverse conductivity for vacuum drying conditions.

5. Stainless Steel SA-240, Type 304

A stainless steel emissivity of 0.3, a value lower than the measured values from Reference [14], is used in the analysis for conservatism.

4.8.3 Effective Fuel Conductivity

4.8.3.1 Transverse Effective Conductivity

The purpose of the effective conductivity in the transverse direction of a fuel assembly is to relate the temperature drop of a homogeneous heat generating square to the temperature drop across an actual assembly cross section for a given heat load. This relationship is established by the following equation obtained from Reference [32]:

$$k_{eff} = \frac{Q}{4L_a(T_c - T_o)}(0.29468)$$

where:

k_{eff} = Effective thermal conductivity (Btu/hr-in.-°F)
Q = Assembly head generation (Btu/hr)

$Q = 4 \times Q_{react} \times L_a$ for WE and MkBW assemblies with quarter symmetric models

$Q = Q_{react} \times L_a$ for CE14x14 assembly with full-scale model

Q_{react} = Reaction solution retrieved from the ANSYS model (Btu/hr-in)
L_a = Assembly active length (in.)
T_o = Maximum temperature (°F)
T_s = Surface temperature (°F)

Discrete finite element models of the fuel assemblies to be stored in the NUHOMS®-32PTH DSC are developed using the ANSYS computer code [16]. These two-dimensional models simulate heat transfer by radiation and convection and include the geometry of the fuel rods and fuel pellets. Helium or air properties are used as the fill gas in the fuel assembly. A fuel assembly decay heat load of 0.8 kW [9] is used for heat generation. An active length of 144" is

[9] 0.8 kW is the maximum decay heat load for the fuel assemblies in the center of the basket.

assumed for WE and MkBW assemblies. The active fuel length of CE14x14 assembly is considered to be 137".

The finite element models are used to calculate the maximum radial temperature difference with isothermal boundary conditions. All components are modeled using 2-D PLANE55 thermal solid elements. LINK32 elements are placed on the exteriors of the fuel assembly components to set up the creation of the radiation super-element. The compartment wall is modeled using LINK32 elements and used only to set up the surrounding surface for the creation of the radiation matrix super-element using the /AUX12 processor in ANSYS. All LINK32 elements are unselected prior to solution of the thermal problem. The thermal properties used in the model are described in Section 4.8.2, and the fuel assembly geometries are shown in Table 4-12. A typical ANSYS finite element model of fuel assemblies is shown in Figures 4-40 for fuel assemblies WE 17x17 and CE14x14.

Several computational runs were made for each model using isothermal boundary temperatures ranging from 100 to 1000°F. In determining the temperature dependent effective conductivities of the fuel assemblies an average temperature, equal to $(T_o + T_s)/2$, is used for the fuel temperature. The transverse effective conductivity is calculated in helium for storage and transfer conditions. For vacuum drying conditions, the conductivity of helium is replaced by air conductivity at low pressure. The vacuum drying of the DSC generally does not reduce the pressure sufficiently to reduce the thermal conductivity of the water vapor and air in the DSC cavity [33]. Therefore, air conductivity at low pressures is assumed for the backfill gas for vacuum drying conditions and the effect of water vapor conductivity is neglected.

4.8.3.2 Axial Effective Conductivity

The backfill gas, fuel pellets, and zircaloy behave like resistors in parallel. However, due to the small conductivity of the fill gas and the axial gaps between fuel pellets, credit is only taken for the zircaloy in the determination of the axial effective conductivities.

$$kaxial = \frac{cladding\ area}{4a^2} \times cladding\ conductivity$$

with a = half of compartment width = 8.7"/2 = 4.35"

4.8.4 Effective Fuel Density and Specific Heat

Volume average density and weight average specific heat are calculated to determine the effective density and specific heat for each fuel assembly type separately. The equations to determine the effective density and specific heat are shown below.

$$\rho_{eff} = \frac{\sum \rho_i V_i}{V_{assembly}} = \frac{\rho_{UO2}\ V_{UO2} + \rho_{Zr4}\ V_{Zr4}}{4a^2 L_a}$$

$$C_{P,eff} = \frac{\sum \rho_i V_i C_{Pi}}{\sum \rho_i V_i} = \frac{\rho_{UO2}\ V_{UO2}\ C_{P,UO2} + \rho_{Zr4}\ V_{Zr4}\ C_{P,Zr4}}{\rho_{UO2}\ V_{UO2} + \rho_{Zr4}\ V_{Zr4}}$$

4.8.5 Conclusion

The effective transverse conductivity values are plotted in Figure 4-41. Among WE and MkBW assemblies, fuel type WE17x17 OFA has the lowest conductivity for the range of 100 to 700°F under helium atmosphere. For temperatures higher than 700°F, fuel assembly 17x17 MK BW has the lowest transverse conductivity. To bound the transverse effective conductivity, the lowest effective conductivity value in each temperature range is selected to apply in the thermal analysis. The effective transverse conductivity of CE14x14 is used separately in a DSC model with 137" active fuel length.

The calculated transverse effective conductivties for vacuum drying conditions are plotted in Figure 4-42. As Figure 4-42 shows, fuel assembly 17x17MK BW has the lowest conductivity for vacuum drying conditions, which are used in thermal analysis for vacuum conditions.

The axial effective conductivity for each fuel type is calculated using the equation from Section 4.8.3.2. The resultant values are listed in Table 4-13 and plotted in Figure 4-43. The lowest axial effective conductivity belongs to fuel type WE 15x15 among WE and MkBW assemblies. This value is used in all DSC models except for the DSC model containing CE14x14 fuel assemblies. The latest model uses the CE14x14 axial conductivity shown separately in Figure 4-43.

Effective density of each fuel type is calculated using the corresponding equation from Section 4.8.4. Since using the lowest density results in the highest cladding temperature for accident conditions, the density of fuel assembly WE 17x17 OFA is the bounding density. The calculated effective density values are listed in Table 4-13.

Effective specific heat values are calculated as a function of temperature using the corresponding equation from Section 4.8.4. Properties of fuel pellets and fuel cladding from Section 4.8.2 are linearly interpolated for this purpose. The lowest specific heat belongs to the fuel type WE15x15. Since the lowest specific heat results in the highest cladding temperature for transient calculations, specific heat of fuel type WE 15x15 is selected for thermal analysis as the bounding property. The calculated effective specific heat values are listed in Table 4-13.

Since CE14x14 fuel assembly is analyzed only for steady state transfer conditions, the effective density and the effective specific heat are not calculated for this fuel type.

The bounding effective fuel properties used in the finite element models for WE and MkBW assemblies are listed in Section 4.2.

4.9 Effective Conductivity of Fluids in the Transfer Cask

4.9.1 Effective Conductivity in the Shielding Panel

Heat transfer in the shielding panel occurs by conduction and convection through the fluid (water) contained in the shielding. The shielding panel consists of 16 cylindrical segments. Each segment can be considered as two concentric, horizontal cylinders. The following correlation from [5] is used to calculate the free convection coefficient for water within each of the panel segments.

$$k_{con} = Nu\ k_w$$

k_{con} = effective conductivity for conduction and convection from inner to outer cylinder
k_w = conductivity of water

$$Nu = [Nu_{COND}, Nu_l]_{\max}$$

$$N_{COND} = \frac{\ln(D_o / D_i)}{\cosh^{-1}\left[\left(D_o^2 + D_i^2 - 4E^2\right)/2D_oD_i\right]} \qquad \text{conduction}$$

$$Nu_l = 0.603\,\overline{C}_l \frac{(\ln D_o / D_i)\,Ra^{1/4}}{\left[(L/D_i)^{3/5} + (L/D_o)^{3/5}\right]^{5/4}} \qquad \text{laminar flow}$$

where,

$$Ra = \frac{g\beta(T_i - T_o)L^3}{\nu^2} \times \Pr \qquad \text{with} \qquad L = (D_o - D_i)/2 \qquad \text{and}$$

$$\overline{C}_l = \tfrac{4}{3}\frac{0.503}{[1 + (0.492/\Pr)^{9/16}]^{4/9}}$$

All water properties are evaluated at average temperature:

$$T_{avg} = (T_o + T_i)/2$$

T_o = average temperature of the outer cylinder
T_i = average temperature of the inner cylinder

Diameter of the inner cylinder is 81.7", and diameter of outer cylinder is 91.825". The average inner and outer temperatures are initially unknown. Iterative solution of the ANSYS [16] model combined with the above correlations determines the inner and outer temperatures, and the effective conductivity. The iteration continues until the difference between the applied coefficient in the ANSYS model and the calculated coefficient is less than 5% for the off-normal conditions at 115°F ambient. To ease the analysis, this criterion is increased to 10% for the off-normal conditions at -20°F ambient, which is less sensitive for thermal evaluations.

Water properties are reported in Section 4.2. The calculated effective conductivity values and their verifications are shown in the Table 4-14 and 4-15 for normal and off-normal transfer conditions.

The same methodology as described above is used to calculate the effective conductivity of liquid neutron shield during the burning period of fire accident case.

4.15 References

1. Cogema Logistics, "Qualification du Materiau Vyal B", Rapport d'essaias n° 99 023-1
2. USNRC, SFPO, Interim Staff Guidance – 11, Rev. 3, "Cladding Considerations for the Transportation and Storage of Spend Fuel"
3. Perry, R. H., Chilton, C. H., "Chemical Engineers' Handbook", 5th Edition, 1973
4. USDOE, "Topical Report on Actinide-Only Burnup Credit for PWR Spent Nuclear Fuel Packages", Department of Energy, Report No. DOE / RW0472, Rev. 2, 1998
5. Rohsenow, W. M., Hartnett, J. P., Ganic, E. N. , "Handbook of Heat Transfer Fundamentals", 2nd Edition, 1985
6. ASME Boiler and Pressure Vessel Code, Section II, Part D, "Material Properties", 1998 and 2000 addenda
7. Issard, Herve, "ACL Progress on Boralyn Development", Cogema Logistics presented in "Transnuclear Group Technical Exchange Meeting", October 11, 2002
8. Final Documentation Package TN-68, P.O. # EP-2001-022, Section G, "Thermal Conductivity Measurements of Borated Aluminum Specimens", Rev. 0
9. AAR Brooks & Perkins Advanced Structures Division, "Boral® The Neutron Absorber – Product Performance", Report 624
10. Zoldners, N. G., "Thermal Properties of Concrete under Sustained Elevated Temperatures", ACI Publications, Paper SP 25-1, American Concrete Institute, Detroit, MI, 1970
11. Cavanaugh, Kevin, "Guide to Thermal Properties of Concrete and Masonary Systems", Reported by ACI Committee 122, Report # ACI 122R-02, American Concrete Institute, Detroit, MI, 2002
12. Bentz, D. P., "A Computer Model to Predict the Surface Temperature and Time-of-wetness of Concrete Pavements and Bridge Decks", Report # NISTIR 6551, National Institute of Standards and Technology, 2000
13. Siegel, Robert, Howell, R. H., "Thermal Radiation Heat Transfer", 4th Edition, 2002
14. Azzazy Technology Inc., "Emissivity Measurements of 304 Stainless Steel", Report Number ATI-2000-09-601, 2000
15. Kreith, Frank, "Principles of Heat Transfer", 3rd Edition, 1973
16. ANSYS Computer Code and User's Manuals, Rev. 6.0
17. USNRC, Code of Federal Regulations, Part 71, "Packaging and Transportation of Radioactive Material", 2003
18. "ASHRAE Handbook Fundamentals", 4th Edition, 1983
19. Transnuclear, Inc., "Standardized NUHOMS® Horizontal Modular Storage System for Irradiated Nuclear Fuel", Final Safety Analysis Report, Rev. 7
20. Viebrock, J. M., Douglas, H. M., "Domestic Light Water Reactor Fuel Design Evolution", Vol. III, Nuclear Assurance Corporation, 1981
21. American Concrete Institute, "Code Requirements for Nuclear Safety Related Concrete Structures (ACI-349-01) and Commentary (ACI 349R-01)", 2001
22. USNRC, SFPO, NUREG-1536, "Standard Review Plan for Dry Cask Storage Systems - Final Report", 1997.
23. Gregory, J. J., Mata, R., Keltner, N. R., "Thermal Measurements in a Series of Long Pool Fires", SANDIA Report, SAND 85-0196, TTC-0659,1987
24. Parker O-Ring Handbook, 5700, Y2000 Edition, 1999

25. Not used
26. Chun, R., Witte, M., Schwartz, M., "Dynamic Impact Effects on Spent Fuel Assemblies", Lawrence Livermore National Laboratory, Report UCID-21246, 1987
27. Young, W. C., "Roark's Formulas for Stress and Strain", 6th Edition, 1989
28. Plannel, et. al., "Extended Fuel Burnup Demonstration Program – Topical Report – Transport Considerations for Transnuclear Casks", DOE/ET 34014-11, TN-E4226, Transnuclear, Inc. 1983
29. Brookmire, et. al., "Storage of Burnable Poison Rod Assemblies and Thimble Plug Devices in Dry Storage Casks Surry ISFSI", NE-1162, Rev. 0, 1998
30. Oak Ridge National Laboratory, RSIC Computer Code Collection, "SCALE, A Modular Code System for Performing Standardized Computer Analysis for Licensing Evaluation for Workstations and Personal Computers", NUREG/CR-0200, Rev. 6, ORNL/NUREG/CSD-2/V3/R6
31. USNRC, SFPO, NUREG/CR-0497, "A Handbook of Materials Properties for Use in the Analysis of Light Water Reactor Fuel Rod Behavior", MATPRO - Version II, EG&G Idaho, Inc., TREE-1280, 1979
32. SANDIA Report, SAND90-2406, "A Method for Determining the Spent Fuel Contribution to Transport Cask Containment Requirements", 1992.
33. Diament, R.M.E., "Thermal and Acoustic Insulation", 1986
34. Kreith, Frank, "The CRC Handbook of Thermal Engineering", 2000
35. "ASHRAE Handbook, Fundamentals" – SI Edition, 1997
36. I.E. Idelchik, "Handbook of Hydraulic Resistance", 3rd Edition, 1994

Table 4-1
Maximum Component Temperatures during Transfer Operations at 115°F ambient

Component	Maximum Temperature 34.8 kW (°F)	Allowable Maximum Temperature (°F)
DSC shell	475	
Cask inner shell	340	
Lead gamma shielding	337	621 [3]
Cask structural shell	280	
Neutron shield panel	263	
Cask lid inner plate *	275	
Cask lid outer plate	217	
Solid neutron shield	265	320 [1]
Cask lid seal †	240	400 [24]
Bottom plate seal ‡	255	400 [24]
Liquid neutron shield (Bulk temperature) §	265	
Liquid neutron shield (Maximum temperature)	275	

	Maximum Temperature (°F) 34.8 kW					Allowable Max. Temp. (°F)
Basket Type	Type I				Type II	
Component	Conf. # 1	Conf. # 2	Conf. # 3	Conf. # 4	Conf. # 1	
Fuel cladding	719	705	700	715	723	752 [2]
Fuel compartment	693	667	673	689	697	
Basket Al plates	692	666	672	688	696	
Basket rails	561	559	559	558	561	

	Maximum Temperature (°F) 33.8 kW for CE14x14 Fuel Assembly		Allowable Max. Temp. (°F)
Basket Type	Type I		
Component	Configuration # 6	Configuration # 7	
Fuel cladding	717	712	752 [2]
Fuel compartment	689	685	
Basket Al plates	689	684	
Basket rails	555	552	
DSC Shell	467	467	

* Temperatures of cask lid, solid neutron absorber, and seals are from the transfer cask sub-models.
† Maximum temperature of cask body at seal location
‡ Maximum temperature of ram access ring at seal location
§ Bulk temperature is the volumetric average temperature of the elements in shielding segments 8 and 9, see Figure 4-2.

Table 4-11
Average Peaking Factors for Active Fuel Length of 144"

	Height from Bottom of Active Fuel (in)	P_i [4]	P_i (interpolated)	A_i	$P_{avg,i}$
1	0	0.000			
	1.32		0.215	0.142	0.107
2	4.00	0.652			
	7.0675		0.773	3.346	0.582
3	12.00	0.967			
	14.5		1.000	6.751	0.908
4	20.00	1.074			
	22.0675		1.081	7.933	1.048
5	27.99	1.103			
6	36.00	1.108			
	37.0675		1.108	16.506	1.100
7	44.01	1.106			
8	52.00	1.102			
	57.69		1.098	22.766	1.104
9	60.00	1.097			
	66.9425		1.094	10.143	1.096
10	68.00	1.094			
11	76.00	1.094			
	82.0675		1.095	16.549	1.094
12	84.00	1.095			
13	92.00	1.096			
	97.0675		1.095	16.432	1.095
14	99.99	1.095			
15	108.00	1.086			
	111.943		1.073	16.191	1.088
16	116.01	1.059			
	121.26		1.001	9.743	1.046
17	124.00	0.971			
	127.068		0.882	5.543	0.955
18	132.00	0.738			
	136.26		0.591	6.826	0.743
19	140.00	0.462			
	144		0.000	2.892	0.374
20	144.00	0.000			

Table 4-11 – Continued
Average Peaking Factors for Active Fuel Length of 137"

	Height from Bottom of Active Fuel (in)	P_i [4]	P_i (interpolated)	A_i	$P_{avg,i}$
1	0	0.000			
	5.5675		0.725	2.452	0.441
2	11.41	0.967			
	13		0.989	6.497	0.874
3	19.03	1.074			
	20.5675		1.080	7.877	1.041
4	26.63	1.103			
	34.25	1.108			
5	35.5675		1.108	16.500	1.100
6	41.87	1.106			
	49.47	1.102			
7	56.19		1.098	22.757	1.103
8	57.09	1.097			
	59.82		1.096	3.981	1.097
9	64.69	1.094			
	72.31	1.094			
10	73.01		1.094	14.435	1.094
11	79.91	1.095			
	87.53	1.096			
12	89.82		1.096	18.410	1.095
13	95.13	1.095			
	102.75	1.086			
14	104.82		1.079	16.366	1.091
15	110.37	1.059			
	114.5		1.011	10.207	1.054
16	117.97	0.971			
	119.82		0.914	5.183	0.974
17	125.59	0.738			
	131.25		0.532	8.362	0.732
18	133.19	0.462			
	137		0.000	1.845	0.321
19	137	0.000			

Table 4-12
Characteristics of Fuel Assemblies

Fuel Type	WE 15x15	WE 17x17 Standard/ Vantage 5H	Framatome 17x17 MK BW	WE 17x17 OFA	CE14x14
Active fuel length	142-144	144	144	144	137
Pellet OD	0.3649-0.3669	0.3225	0.3195	0.3088	0.3765
Rod OD	0.422	0.374	0.374	0.360	0.440
Clad wall thickness	0.0243	0.0225	0.0240	0.0225	0.028
Rod pitch	0.563	0.496	0.496	0.496	0.580
No. of fuel rods	204	264	264	264	176
No. of Guide/Instrument tubes	21	25	25	25	5
Guide tube OD	0.484-0.545	0.429-0.482	0.482	0.429-0.482	1.115
Guide tube wall thickness	0.015	0.016	0.016	0.016	0.04
Instrument tube OD	0.545	0.474-0.545	0.482	0.474-0.545	---
Instrument tube wall thickness	0.015	0.015-.016	0.016	0.015-.016	---

All Dimensions are in inches

Table 4-13 – Continued
Effective Fuel Properties for CE14x14

Transverse Effective Fuel Conductivity in Helium

Fuel Type			CE 14x14	
T_o (°F)	T_c (°F)	T_{avg} (°F)	Q_{react} (Btu/hr-in)	k (Btu/hr-in-°F)
100	181	140	19.968	0.0182
225	291	258	19.969	0.0222
350	404	377	19.969	0.0271
475	519	497	19.970	0.0331
600	637	618	19.970	0.0402
725	755	740	19.970	0.0483
850	875	863	19.970	0.0577

Axial Effective Conductivity

Fuel type	CE 14x14
No of fuel rods	176
OD fuel rod (in)	0.440
Clad thickness (in)	0.028
No of guides tubes	5
OD guide tubes (in)	1.115
Wall thickness (in)	0.04
No of Instrument tubes	---
OD Instrument tube (in)	---
Wall thickness (in)	---
Fuel type	**CE 14x14**
Cladding area (in^2)	7.05
Compartment area (in^2)	75.69
Temperature	k-axial
(°F)	(Btu/hr-in-°F)
212	0.0610
392	0.0642
572	0.0682
752	0.0736
932	0.0808

Table 4-14 – Continued
Effective Conductivity of Liquid Neutron Shielding – Sections 2 to 12

Ti	To	Tavg	Tavg	k	β	ν	Pr	C_l	Ra	Nu_COND	Nu_l	Nu	k_eff
(°F)	(°F)	(°F)	(K)	(W/m-K)	(1/K)	(m^2/s)	(---)	(---)	(---)	(---)	(---)	(---)	(Btu/hr-in-°F)
156.5	143.5	150	339	0.658	4.844E-04	4.460E-07	2.79	0.5819	1.024E+09	1.00	25.92	25.92	0.821
166.5	153.5	160	344	0.663	5.186E-04	4.104E-07	2.54	0.5780	1.179E+09	1.00	26.67	26.67	0.851
176.5	163.5	170	350	0.668	5.528E-04	3.749E-07	2.29	0.5737	1.357E+09	1.00	27.42	27.42	0.882
186.5	173.5	180	356	0.671	5.858E-04	3.552E-07	2.16	0.5712	1.510E+09	1.00	28.03	28.03	0.906
196.5	183.5	190	361	0.674	6.187E-04	3.355E-07	2.03	0.5684	1.679E+09	1.00	28.65	28.65	0.929
206.5	193.5	200	367	0.677	6.517E-04	3.158E-07	1.90	0.5654	1.866E+09	1.00	29.26	29.26	0.953
216.5	203.5	210	372	0.680	6.846E-04	2.962E-07	1.77	0.5622	2.076E+09	1.00	29.88	29.88	0.978
226.5	213.5	220	378	0.682	7.167E-04	2.802E-07	1.66	0.5593	2.282E+09	1.00	30.44	30.44	0.999
236.5	223.5	230	383	0.683	7.481E-04	2.681E-07	1.58	0.5570	2.478E+09	1.00	30.94	30.94	1.018
246.5	233.5	240	389	0.685	7.794E-04	2.559E-07	1.50	0.5545	2.690E+09	1.00	31.44	31.44	1.037
256.5	243.5	250	394	0.686	8.108E-04	2.437E-07	1.42	0.5518	2.920E+09	1.00	31.94	31.94	1.056
266.5	253.5	260	400	0.688	8.421E-04	2.315E-07	1.34	0.5490	3.171E+09	1.00	32.43	32.43	1.074
276.5	263.5	270	406	0.688	8.815E-04	2.231E-07	1.29	0.5471	3.441E+09	1.00	32.99	32.99	1.093
286.5	273.5	280	411	0.688	9.210E-04	2.147E-07	1.24	0.5451	3.731E+09	1.00	33.54	33.54	1.111
296.5	283.5	290	417	0.688	9.604E-04	2.063E-07	1.19	0.5430	4.044E+09	1.00	34.09	34.09	1.129
306.5	293.5	300	422	0.687	9.906E-04	1.990E-07	1.15	0.5411	4.323E+09	1.00	34.54	34.54	1.143
316.5	303.5	310	428	0.685	1.007E-03	1.934E-07	1.12	0.5396	4.528E+09	1.00	34.85	34.85	1.150
326.5	313.5	320	433	0.684	1.023E-03	1.877E-07	1.08	0.5381	4.745E+09	1.00	35.17	35.17	1.157

Table 4-19
Total Heat Transfer Coefficient during Fire

T_{amb} = 1475 °F
L = 92.2 in
F_{12} = 1.0
ε = 0.9

T_s (°F)	T_f (°F)	h_c (Btu/hr-ft^2-°F)	h_r (Btu/hr-in^2-°F)	H_t (Btu/hr-in^2-°F)
226	1475	4.5	0.095	0.126
251	1475	4.5	0.096	0.127
276	1475	4.5	0.098	0.129
301	1475	4.5	0.100	0.131
326	1475	4.5	0.101	0.133
351	1475	4.5	0.103	0.134
376	1475	4.5	0.105	0.136
401	1475	4.5	0.107	0.138
426	1475	4.5	0.109	0.140
451	1475	4.5	0.111	0.142
476	1475	4.5	0.113	0.144
501	1475	4.5	0.115	0.146
526	1475	4.5	0.117	0.148
551	1475	4.5	0.119	0.151
576	1475	4.5	0.121	0.153
601	1475	4.5	0.124	0.155
626	1475	4.5	0.126	0.157
651	1475	4.5	0.128	0.159
676	1475	4.5	0.131	0.162
701	1475	4.5	0.133	0.164
726	1475	4.5	0.135	0.167
751	1475	4.5	0.138	0.169
776	1475	4.5	0.140	0.171
801	1475	4.5	0.143	0.174
826	1475	4.5	0.145	0.176
851	1475	4.5	0.147	0.179
876	1475	4.5	0.150	0.181
901	1475	4.5	0.152	0.184
926	1475	4.5	0.155	0.186
951	1475	4.5	0.155	0.186

Configuration 1

	1.1	1.2	1.2	1.1	
1.1	1.1	1.1	1.1	1.1	1.1
1.2	1.1	0.8	0.8	1.1	1.2
1.2	1.1	0.8	0.8	1.1	1.2
1.1	1.1	1.1	1.1	1.1	1.1
	1.1	1.2	1.2	1.1	

Configuration 2

	1.1	1.5	1.5	1.1	
1.1	1.1	1.1	1.1	1.1	1.1
1.5	1.1	0.2	0.2	1.1	1.5
1.5	1.1	0.2	0.2	1.1	1.5
1.1	1.1	1.1	1.1	1.1	1.1
	1.1	1.5	1.5	1.1	

Configuration 3

	1.1	1.5	1.5	1.1	
1.1	1.1	0.925	0.925	1.1	1.1
1.5	0.925	0.55	0.55	0.925	1.5
1.5	0.925	0.55	0.55	0.925	1.5
1.1	1.1	0.925	0.925	1.1	1.1
	1.1	1.5	1.5	1.1	

Configuration 4

	0.98	1.5	1.5	0.98	
0.98	0.98	0.98	0.98	0.98	0.98
1.5	0.98	0.80	0.80	0.98	1.5
1.5	0.98	0.80	0.80	0.98	1.5
0.98	0.98	0.98	0.98	0.98	0.98
	0.98	1.5	1.5	0.98	

Configuration 5

	1.1	1.2	1.2	1.1	
1.1	1.1	1.1	1.1	1.1	1.1
1.2	1.1	0.55	0.55	1.1	1.2
1.2	1.1	1.05	1.05	1.1	1.2
1.1	1.1	1.1	1.1	1.1	1.1
	1.1	1.2	1.2	1.1	

Figure 4-15
Thermally Bounding Loading Configurations Considered in the DSC Model
For Total Decay Heat Load of 34.8 kW

Configuration 6

	1.068	1.168	1.168	1.068	
1.068	1.068	1.068	1.068	1.068	1.068
1.168	1.068	0.755	0.755	1.068	1.168
1.168	1.068	0.755	0.755	1.068	1.168
1.068	1.068	1.068	1.068	1.068	1.068
	1.068	1.168	1.168	1.068	

Configuration 7

	0.935	1.5	1.5	0.935	
0.935	0.935	0.935	0.935	0.935	0.935
1.5	0.935	0.775	0.775	0.935	1.5
1.5	0.935	0.775	0.775	0.935	1.5
0.935	0.935	0.935	0.935	0.935	0.935
	0.935	1.5	1.5	0.935	

Figure 4-15 – Continued
Thermally Bounding Loading Configurations Considered in the DSC Model
For Total Decay Heat Load of 33.8 kW, CE14x14 Fuel Assemblies

For Total Decay Heat of 34.8 kW

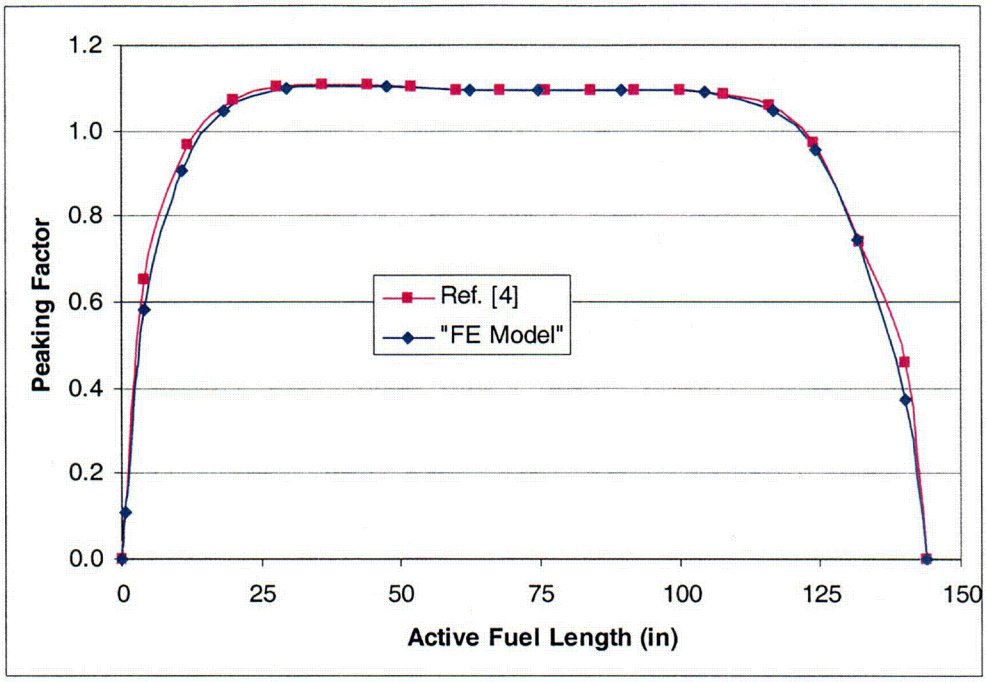

For Total Decay Heat of 33.8 kW, CE14x14 Fuel Assemblies

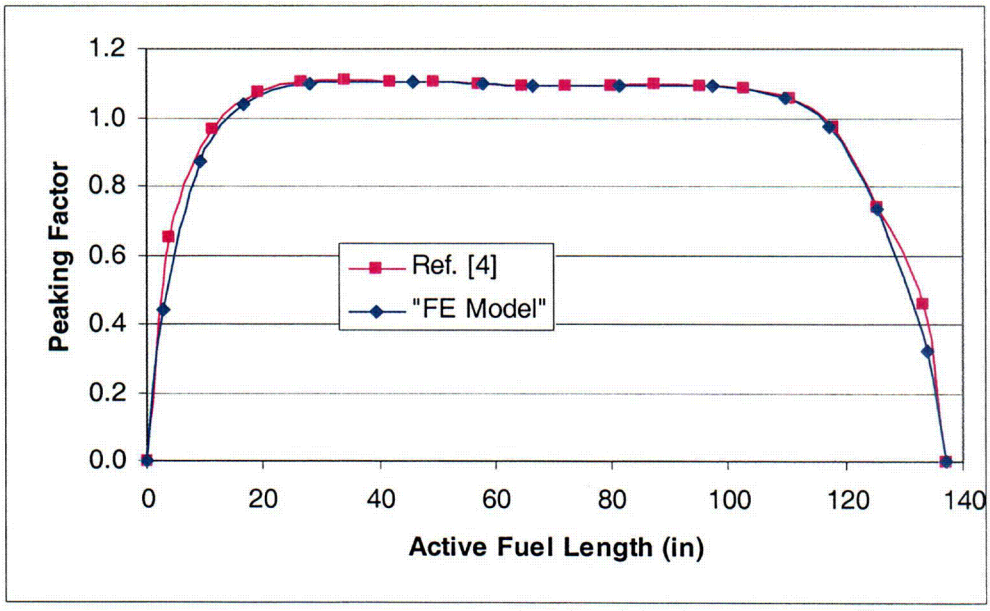

Figure 4-39
Comparison of the Axial Heat Profiles in the FE Model and in Ref. [4]

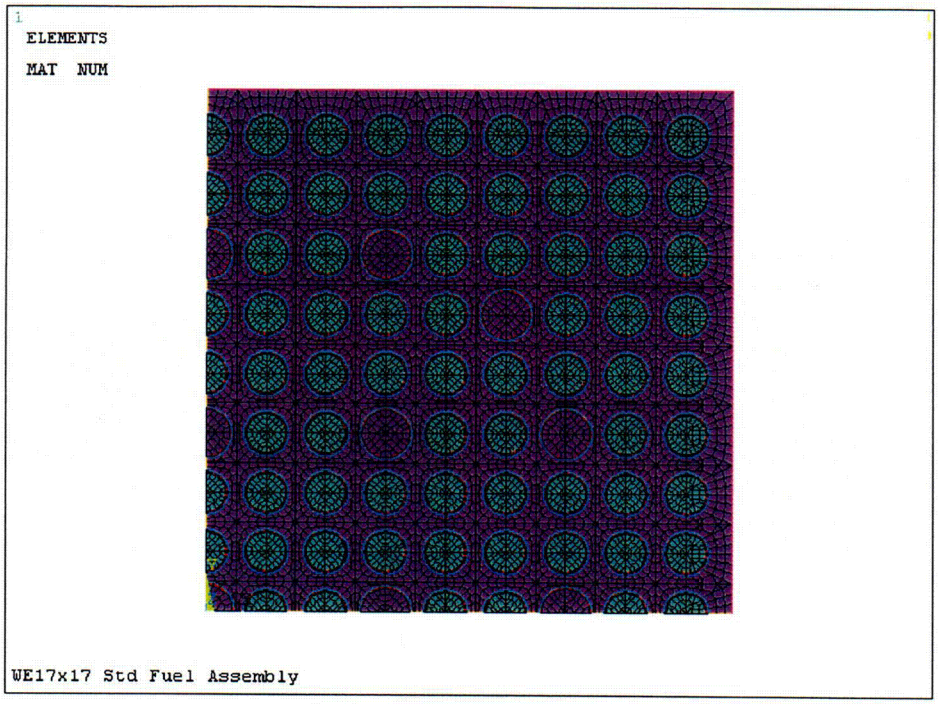

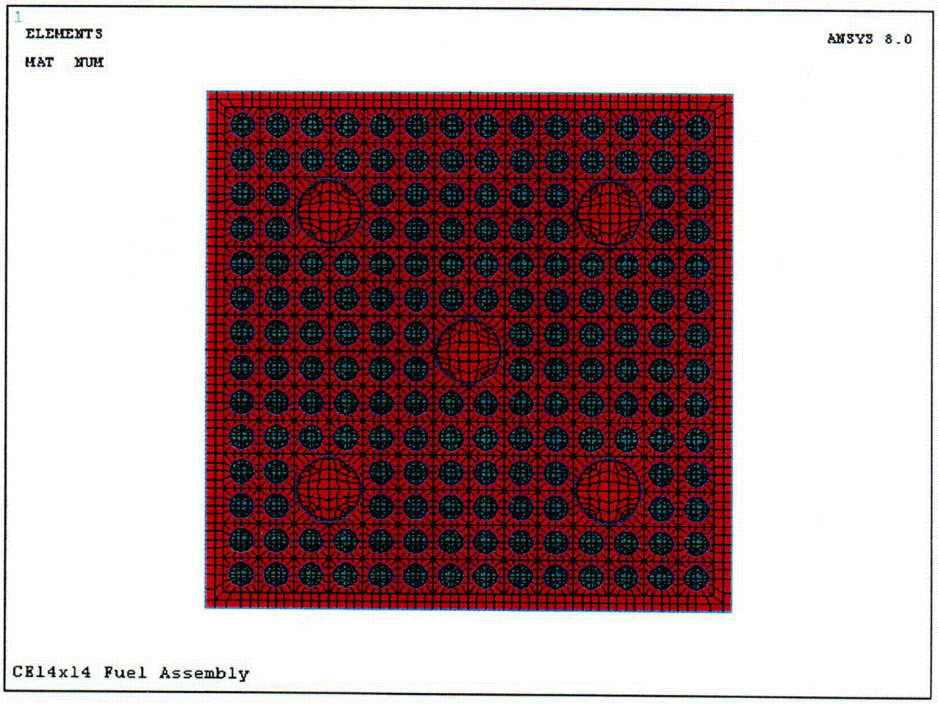

Figure 4-40
Finite Element Model of Fuel Assemblies

C03

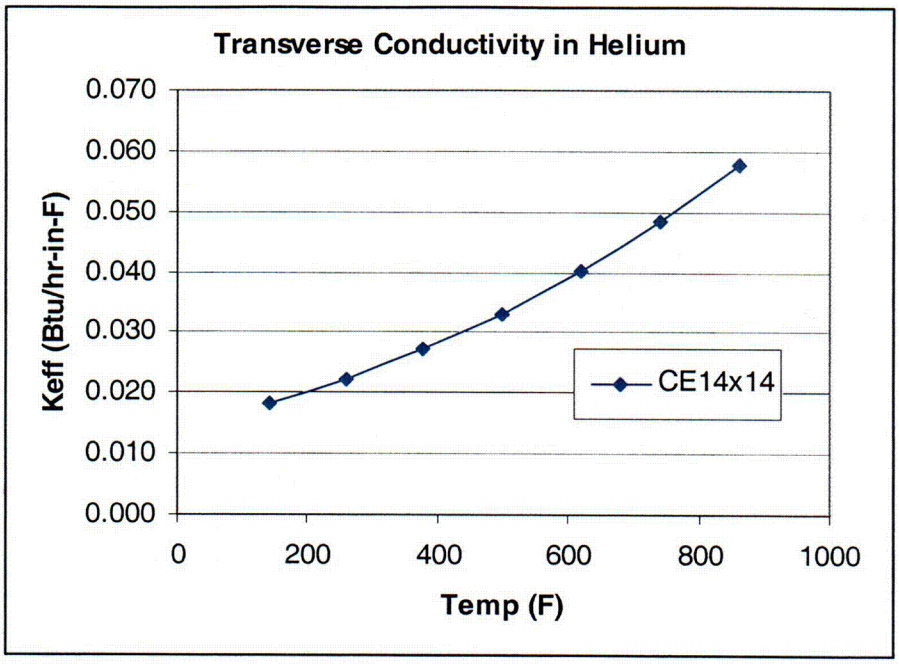

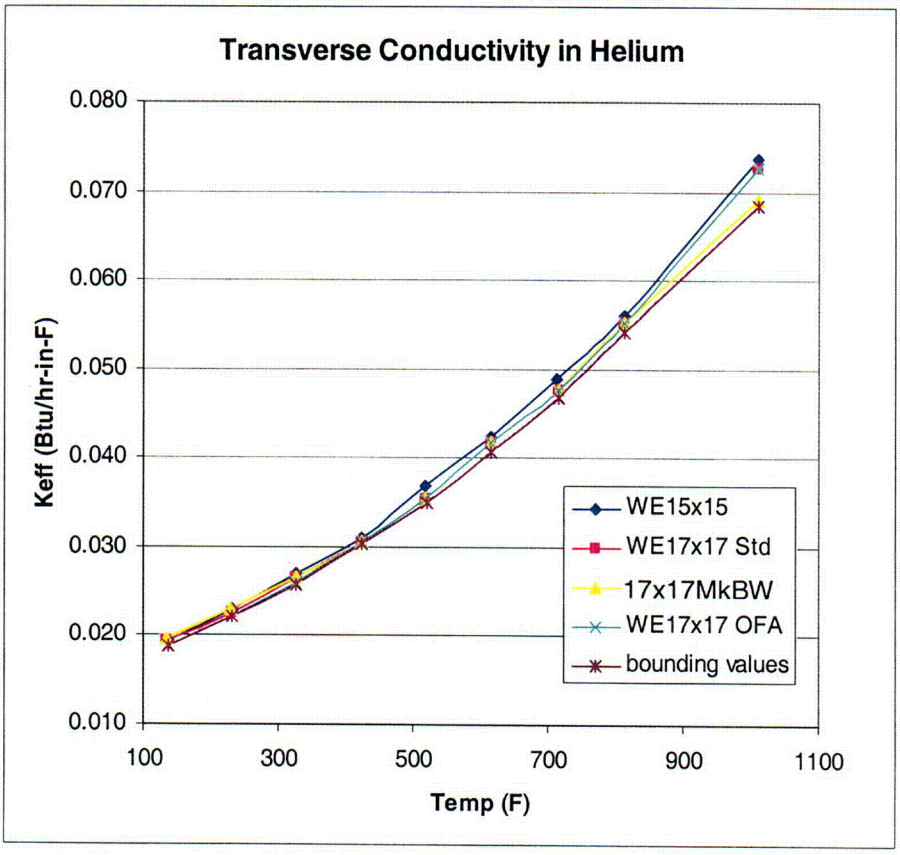

Figure 4-41
Effective Transverse Fuel Conductivity in Helium

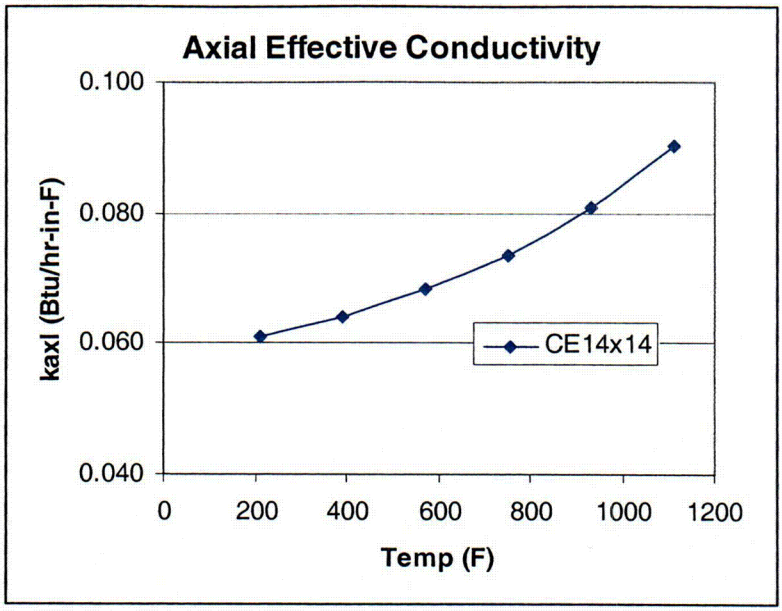

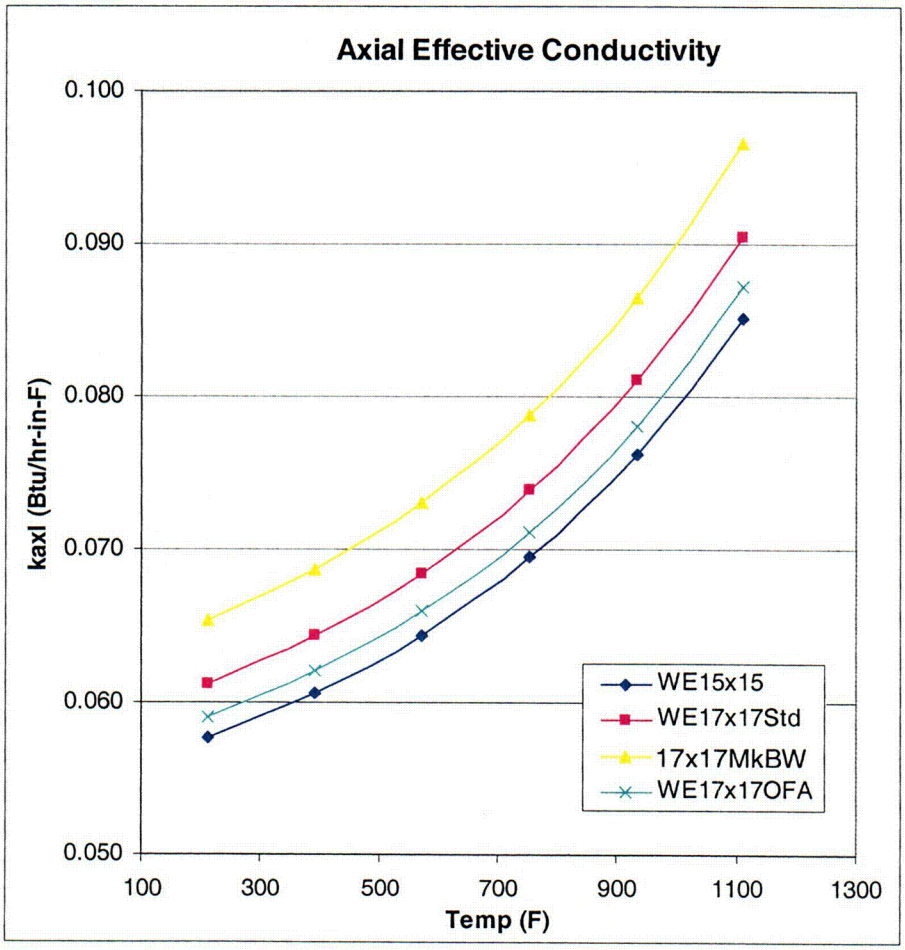

Figure 4-43
Effective Axial Fuel Conductivity

C05

5. SHIELDING EVALUATION

The shielding evaluation presented for the NUHOMS® 32PTH System demonstrates adequacy of the shielding design for the payload described in Chapter 2. The geometry of the NUHOMS® System is described in Chapter 1. The heavy concrete walls and roof of the Horizontal Storage Module (HSM-H) provide the bulk of the shielding for the payload in the storage condition. During fuel loading and transfer operations, the combination of thick steel shield plugs at the ends of the 32PTH-DSC and heavy steel/lead/neutron shield material of the OS187H transfer cask provide shielding for personnel loading and transferring the 32PTH-DSC to the HSM-H. Figure 5-1 through Figure 5-4 and Table 5-1 provide the general configuration and material thicknesses of the important components of the NUHOMS® 32PTH System.

For this shielding evaluation, source terms are calculated for the bounding Framatome Mk BW 17x17 fuel assembly. This fuel assembly is bounding because it contains the greatest mass of fuel.

Also included in the source term is the bounding Non-Fuel Assembly Hardware (NFAH) which is the BPRA.

Several burnup/enrichment combinations with minimum 5 year cooling times are addressed for the fuel to provide more flexibility in qualifying fuel for storage. These combinations form the basis for the NUHOMS® 32PTH System fuel specifications in Chapter 12. Bounding operating histories are assumed for the NFAH with a minimum cooling time of 4 days. The methodology, assumptions, and criteria used in this evaluation are summarized in the following subsections.

Section 5.4 provides a three dimensional (3-D) shielding analysis for the NUHOMS® 32PTH System using MCNP [2,6]

5.1 Discussion and Results

The maximum and average dose rates due to 32 design basis PWR fuel assemblies stored with 32 design basis NFAH (BPRAs) in the NUHOMS® 32PTH System are summarized in Table 5-2 through Table 5-5. Table 5-2 provides the dose rates on the surface of the HSM-H while Table 5-3 through Table 5-5 provide the dose rates on and around the Transfer Cask (top, bottom and sides) during fuel loading, and transfer operations.

As previously stated, the NUHOMS® HD System is capable of storing PWR spent fuel, and non-fuel assembly hardware (NFAH) such as the Burnable Poison Rod Assemblies (BPRAs), Thimble Plug Assemblies (TPAs), and Vibration Suppresser Inserts (VSIs). Based on the source term calculations presented in Section 5.2, the design basis fuel source term is the Framatome MK BW 17x17 fuel assembly with 60 GWd/MTU burnup, a minimum initial enrichment of 4.0 weight % U-235 and a cooling time of 7 years. The design basis NFAH source term is a BPRA assembly irradiated to 30 GWD/MTU and a cooled for 4 days.

A discussion of the method used to determine the design basis fuel and NFAH source terms is included in Section 5.2. The model specification and shielding material densities are given in Section 5.3. The method used to determine the dose rates due to 32 design basis fuel assemblies with 32 design basis NFAH in the NUHOMS® 32PTH System is provided in Section 5.4.

Normal and off-normal conditions are modeled with the NUHOMS® 32PTH System intact, including the filled neutron shield in the transfer cask. The shielding calculations are performed using the MCNP Monte Carlo transport code [2]. Average and peak dose rates on the front, side, top and back of the HSM-H and the OS187H Transfer Cask System are calculated. Occupational doses during loading, transfer to the ISFSI, and maintenance and surveillance operations are provided in Chapter 10. Locations where streaming could occur are discussed in Chapter 10.

For accident conditions (e.g., cask drop, fire), the transfer cask neutron shield water (shown in Figure 5-4 is assumed to be removed and a 1 inch void in the lead due to "lead slump' is also assumed at the top and/or bottom. Site dose and occupational dose analyses are addressed in Chapter 10 (including requirements for site specific 72.104 and 72.106 analyses).

5.2 Source Specification

Source terms are calculated with the SAS2H (ORIGEN-S) module of SCALE 4.4 1. The following sub-sections provide a discussion of the fuel assembly and Non-Fuel Assembly Hardware (NFAH) material weights and composition, gamma and neutron source terms and energy spectrum. The SAS2H results are used to develop source terms suitable for use in the shielding calculations.

There are five principal sources of radiation associated with the NUHOMS® 32PTH System that are of concern for radiation protection. These are:

1. Primary gamma radiation from the spent fuel
2. Primary gamma radiation from activation products in the structural materials found in the spent fuel assembly and the NFAH
3. Primary neutron radiation from the spent fuel
4. Neutrons produced from sub-critical multiplication in the fuel
5. Capture gammas from (n,γ) reactions in the NUHOMS® 32PTH System materials

The first three sources of radiation are evaluated using SAS2H. The capture gamma radiation and sub-critical multiplication are handled as part of the shielding analysis which is performed with MCNP.

The neutron flux during reactor operation is peaked in the active fuel (in-core) region of the fuel assembly and drops off rapidly outside the in-core region. Much of the fuel assembly hardware is outside of the in-core region of the fuel assembly. To account for this reduction in neutron flux, each fuel assembly type is divided into four exposure zones. A neutron flux (fluence) correction is applied to each region to account for this reduction in neutron flux outside the in-core region. The correction factors are given in Table 5-6. The four exposure zones, or regions are 4:

Bottom—location of fuel assembly bottom nozzle and fuel rod end plugs
In-core—location of active fuel
Plenum—location of fuel rod plenum spring and top plug
Top—location of top nozzle

The Framatome MK BW 17x17 assembly is the bounding fuel assembly design for shielding purposes because it has the highest initial heavy metal loading as compared to the 14x14, 15x15, and other 17x17 fuel assemblies which are also authorized contents of the NUHOMS®-32PTH DSC and described in Chapter 2. The SAS2H/ORIGEN-S modules of the SCALE code with the 44 group ENDF/B-IV library are used to generate the gamma and neutron source terms. For the bounding MK BW 17x17 fuel assembly, an initial enrichment of 4.0 wt% U-235 is assumed. The fuel assembly is irradiated with a constant specific power of 25 MW/MTU to a total burnup of 60 GWD/MTU. A conservative three-cycle operating history is utilized with a 20 day down time between each cycle. The fuel assembly masses for each irradiation region are listed in Table 5-7.

Data for the 17x17 assembly is from Reference [7]. Some values for the 15x15 were assumed to be the same as the 17x17. The design-basis heavy metal weight is 0.476 MTU. These masses are irradiated in the appropriate fuel assembly region in the SAS2H/ORIGEN-S models.

TPA

The TPA materials and masses for each irradiation zone are listed in Table 5-8. These materials are irradiated in the appropriate zone for fourteen cycles of operation. The TPA is irradiated to an equivalent assembly life burnup of 210 GWd/MTU over 14 cycles. The model assumes that the TPA is irradiated in an assembly each with an initial enrichment of 3.50 weight % U-235.The fuel assembly, containing the TPA, is burned for three cycles with a burnup of 15 GWd/MTU per cycle. This is equivalent to an assembly life burnup of 45 GWd/MTU over the three cycles. The results for a cooling time of 20 years are increased by the ratio of 14/3 to achieve the equivalent 210 GWD/MTU source.

BPRA

The BPRA materials and masses for each irradiation zone are also listed in Table 5-8. These materials are irradiated in the appropriate zone for three cycles of operation. The model assumes that the BPRA is irradiated in an assembly each with an initial enrichment of 3.50 weight % U-235. The fuel assembly containing the BPRA is burned for three cycles with a burnup of 10 GWd/MTU per cycle. This is equivalent to an assembly life burnup of 30 GWd/MTU over the three cycles. The source term for the BPRA is taken at 4 days cooling time.

VSI

VSIs are very similar in design to burnable poison rod assemblies: the stainless steel baseplate and hold-down spring assembly designs are identical to those used on older Westinghouse BPRAs. Each VSI contains 24 solid Zircalloy-4 damper rods that are attached to the hold-down assembly using a crimp nut top connector. The damper rods are the same diameter and length as BPRA rodlets. The VSIs are assumed to be equivalent in source strength to BPRAs.

Elemental Compositions of Structural Materials

To account for the source terms due to the elemental composition of the fuel assembly and NFAH structural materials the following methodology is used:

1) The material composition for each irradiation region is determined for the assembly and NFAH type.

2) The elemental compositions for each of the structural materials present in each region is determined by multiplying the total weight of each material in a specific irradiation zone (Table 5-7) by the elemental compositions. The fuel assembly and NFAH elemental composition, including impurities, for each material are taken from Reference [7].

CHAPTER 6
CRITICALITY EVALUATION

TABLE OF CONTENTS

6. CRITICALITY EVALUATION 6-1

6.1 Discussion and Results 6-2

6.2 Spent Fuel Loading 6-4

6.3 Model Specification 6-5

6.3.1 Description of Criticality Analysis Model 6-5

6.3.2 Package Regional Densities 6-7

6.4 Criticality Calculation 6-8

6.4.1 Calculational Method 6-8

6.4.2 Fuel Loading Optimization 6-13

6.4.3 Criticality Results 6-22

6.5 Critical Benchmark Experiments 6-23

6.5.1 Benchmark Experiments and Applicability 6-23

6.5.2 Results of the Benchmark Calculations 6-24

6.6 Supplemental Information 6-25

6.6.1 References 6-25

6.6.2 KENO Input Files 6-27

LIST OF TABLES

Table 6-1 Maximum Initial Enrichment for Each Fuel Design for both Intact and Damaged Fuel Assemblies
Table 6-2 Summary of Limiting Criticality Evaluations for all Fuel Assemblies
Table 6-3 Authorized Contents for NUHOMS®-32PTH DSC
Table 6-4 Fuel Assembly Design Parameters(2) for Criticality Analysis 8
Table 6-5 NUHOMS®-32PTH - Basket and DSC Dimensions
Table 6-6 NUHOMS® OS187H Transfer Cask Dimensions
Table 6-7 NUHOMS®-32PTH - Fixed Poison Loading Requirements
Table 6-8 Description of the Basic KENO Model Units
Table 6-9 Material Property Data
Table 6-10 Results of the Fuel Assembly Positioning Studies
Table 6-11 Results of the Rail Material Variation Studies
Table 6-12 Results of the Poison Plate Thickness Variation Studies
Table 6-13 Results of the Fuel Compartment Width Variation Studies
Table 6-14 Results of the Fuel Compartment Thickness Variation Studies
Table 6-15 WE 15x15 Class Intact Assemblies Without BPRAs - Final Results
Table 6-16 WE 15x15 Class Intact Assemblies With BPRAs - Final Results
Table 6-17 WE 17x17 Class Intact Assemblies Without BPRAs - Final Results
Table 6-18 WE 17x17 Class Intact Assemblies With BPRAs - Final Results
Table 6-19 Limiting Parameters for Damaged Fuel Calculations
Table 6-20 Results of Optimum Pitch Studies
Table 6-21 Results of the Single Ended Rod Shear Studies
Table 6-22 Results of the Double Ended Rod Shear Studies
Table 6-23 Evaluation of the Shifting of Fuel Rods Beyond the Poison
Table 6-24 Most Reactive Damaged Assembly Configuration
Table 6-25 Double Ended Rod Shear Study with BPRAs
Table 6-26 WE 15x15 Class Damaged Assemblies With BPRAs - Final Results
Table 6-27 WE 17x17 Class Damaged Assemblies With BPRAs - Final Results
Table 6-28 Maximum k_{eff} for Intact Assemblies - Final Results
Table 6-29 Maximum k_{eff} for Damaged Assemblies - Final Results
Table 6-30 Benchmark Results
Table 6-31 USL-1 Results
Table 6-32 USL Determination for Criticality Analysis
Table 6-33 CE 14x14 Class Intact Assemblies - Final Results
Table 6-34 CE 14x14 Class Damaged Assemblies - Final Results

LIST OF FIGURES

Figure 6-1 Basket Views and Dimensions
Figure 6-2 Basket Model Compartment Wall (View G)
Figure 6-3 Basket Model Compartment Wall (View F)
Figure 6-4 Basket Model Compartment Wall With Fuel Assembly (View G)
Figure 6-5 Basket Model Compartment Wall With Fuel Assembly (View F)
Figure 6-6 Basket Compartment With Fuel (Section A)
Figure 6-7 Basket Compartment With Fuel (Section B)
Figure 6-8 Fuel Assembly Positions and Poison Plate Locations in the Basket
Figure 6-9 Fuel Assembly Positions by KENO Unit ID
Figure 6-10 Canister and Transfer Cask Description in the KENO Model
Figure 6-11 Radial Cross Section of the Detailed KENO Model
Figure 6-12 WE 15x15 Fuel Assemblies in the Centered Position
Figure 6-13 WE 15x15 Fuel Assemblies in the Inward Position
Figure 6-14 CE 14x14 Fuel Assembly : Optimum Pitch Study
Figure 6-15 WE 17x17 Fuel Assembly : Single Ended Rod Shear Study
Figure 6-16 WE 15x15 Fuel Assembly : Double Ended Rod Shear Study
Figure 6-17 WE 17x17 Fuel Assembly : 4-inch Shift of Fuel Assembly
Figure 6-18 WE 15x15 Fuel Assembly : 6-inch Shift of Fuel Rods
Figure 6-19 WE 15x15 Fuel Assembly : Double Ended Rod Shear with BPRAs

Then criticality calculations evaluate a variety of fuel assembly types, initial enrichments and poison loadings (fixed and soluble poison). Finally, the maximum allowed initial enrichment and the number of damaged assemblies per DSC for each fuel assembly type as a function of soluble boron concentration and fixed poison loading is determined and is also shown in Table 6-1.

These calculations determine k_{eff} with the CSAS25 control module of SCALE-4.4 3 for each assembly type and initial enrichment, including all uncertainties to assure criticality safety under all credible conditions.

The results of these calculations demonstrate that the maximum expected k_{eff}, including statistical uncertainty, will be less than the Upper Subcritical Limit (USL) determined from a statistical analysis of benchmark criticality experiments. The statistical analysis procedure includes a confidence band with an administrative safety margin of 0.05. A series of benchmark calculations were performed with the SCALE 4.4 PC/CSAS25 3 package using the 44-group cross-section library as presented in Section 6.5. The minimum value of the Upper Subcritical Limit (USL) was determined to be 0.9419.

The results of the limiting criticality analyses are summarized in Table 6-2. The maximum k_{eff} for the normal fuel geometry is 0.9404 ($k_{eff}+2\sigma$) and is based on the Westinghouse 17x17 (WE 17x17) fuel assembly design. The maximum k_{eff} for the damaged fuel geometry is 0.9402 ($k_{eff}+2\sigma$) and is based on the WE 17x17 fuel assembly design.

6.2 Spent Fuel Loading

This section provides a summary of the maximum spent fuel loading and spent fuel parameters for the 32PTH DSC.

The NUHOMS®-32PTH DSC is capable of transferring and storing a maximum 32 intact PWR fuel assemblies. Additionally, a maximum of 16 locations (out of the 32 locations) per DSC can be loaded with damaged PWR fuel assemblies with the remaining locations loaded with intact PWR fuel assemblies. The required placement of the damaged fuel assemblies is defined in Chapter 12. Damaged fuel includes assemblies with known or suspected cladding defects greater than hairline cracks or pinhole leaks. The reactivity of a DSC loaded with less than 32 PWR fuel assemblies is expected to be lower than that calculated in this report since the more absorbing borated water replaces the fuel in the empty locations. Reconstituted fuel assemblies, where the fuel pins are replaced by stainless steel (or Zircaloy) pins that displace the same amount of borated water, are considered intact fuel assemblies. Table 6-3 lists the fuel assemblies considered as authorized contents of the NUHOMS®-32PTH DSC.

Table 6-4 lists the fuel design parameters for the PWR fuel assemblies. Reload fuel from other manufacturers with the same parameters are also considered as authorized contents.

For the fuel assemblies to be loaded in the NUHOMS®-32PTH DSC (except the CE 14x14 class), Burnable Poison Rod Assemblies (BPRAs) are also included as authorized contents. The only change to the package fuel loading is the addition of BPRAs that are modeled as $^{11}B_4C$. Since BPRAs displace borated moderator in the assembly guide tubes, an evaluation is performed to determine the potential impact of BPRA storage on the system reactivity. No credit is taken for BPRA cladding and absorbers; rather the BPRA is modeled as $^{11}B_4C$ in the entire guide tube of the respective design. Thus, the highly borated moderator between the guide tube and the BPRA rodlet is modeled as $^{11}B_4C$. The inclusion of more Boron-11 and carbon enhances neutron scattering causing the neutron population in the fuel assembly to be slightly increased which increases reactivity. The fuel assembly dimensions reported in Table 6-4 remains unchanged for the BPRA cases. The models that include BPRAs only differ in that the region inside the guide tubes and instrument tube are modeled as $^{11}B_4C$ instead of moderator.

Other Non Fuel Assembly Hardware (NFAH) like the Thimble Plug Assemblies (TPAs), and Vibration Suppressor Inserts (VSI) are considered as authorized contents for loading. Integral fuel burnable absorber (IFBA, ZrB_2 coating on fuel pellets) fuel assemblies may also be stored. These components are considered identical to BPRAs for criticality purposes and will be referred to as BPRAs for the rest of the report.

6.3.2 Package Regional Densities

The Oak Ridge National Laboratory (ORNL) SCALE code package 3 contains a standard material data library for common elements, compounds, and mixtures. All the materials used for the TC and canister analysis are available in this data library.

Table 6-9 provides a complete list of all the relevant materials used for the criticality evaluation. The material density for the B-10 in the poison plates includes a 10% reduction.

6.4 Criticality Calculation

This section describes the analysis methodology utilized for the criticality analysis. The analyses are performed with the CSAS25 module of the SCALE system. A series of calculations are performed to determine the relative reactivity of the various fuel assembly designs evaluated and to determine the most reactive configuration without BPRAs. The most reactive intact fuel design, for a given enrichment, as demonstrated by the analyses, is the WE 17x17 standard assembly. The most reactive credible configuration is an infinite array of flooded casks, each containing 32 fuel assemblies, with minimum fuel compartment ID, minimum basket structure thickness and minimum assembly-to-assembly pitch.

A series of calculations are also performed to determine the relative reactivity of the various damaged fuel configurations for each fuel assembly class. The most reactive damaged fuel configuration for the WE17 and WE15 class occurs due to a postulated double-ended shear. The most reactive damaged fuel configuration for the CE14 class occurs when the fuel rods are arranged in an optimum pitch configuration. The most reactive credible configuration analyzed in this calculation is an infinite array of flooded casks, each containing a maximum of 32 damaged fuel assemblies with BPRAs, with minimum fuel compartment ID, minimum basket structure thickness and minimum assembly-to-assembly pitch.

As mentioned in Section 6.1, the NUHOMS®-32PTH DSC is evaluated to determine the maximum initial enrichment of the fuel assemblies (both damaged and intact) per DSC for each assembly class as a function of fixed poison loading and soluble boron concentration levels.

6.4.1 Calculational Method

6.4.1.1 Computer Codes

Criticality analyses were performed using the microcomputer application KENO-Va and the 44 neutron group library based on ENDF-B Version 5 cross-section data that are part of the SCALE 4.4 code package 3. Validation and benchmarking of these codes is performed in accordance with applicable QA program requirements (see Chapter 13) and is discussed in Section 6.5.

SCALE 4.4 3 is an extensive computer package which has many applications including cross section processing, criticality studies, and heat transfer analyses among others. The package is comprised of many functional modules, which can be run independently of each other. Control Modules were created to combine certain functional modules in order to make the input requirements less complex. For the purpose of criticality analysis, only four functional modules are used and one control module. These Modules are CSAS25, which includes the three dimensional criticality code KENO-Va and the preprocessing codes BONAMI-S, NITAWL-II and XSDRNPM-S.

KENO-Va, in conjunction with a suitable working library of nuclear cross section data, is used to calculate the multiplication factor, k_{eff}, of systems of fissile material. It can also compute lifetime and generation time, energy dependent leakages, energy and region-dependent absorptions, fissions, fluxes, and fission densities. KENO-Va utilizes a three-dimensional Monte-Carlo computation scheme. KENO-Va is capable of modeling complex geometries including facilities for handling arrays, arrays of arrays, and holes.

SCALE 4.4 is set up so that any number of cross-section libraries may be used with the preprocessing functional and control modules. For the purpose of this analysis, only the 44-group ENDF/B Version 5 library is used.

The preprocessing codes used for this analysis are the functional modules BONAMI-S, NITAWL-II and XSDRNPM-S. They are consolidated into the control module CSAS25. BONAMI-S has the function of performing Bondarenko calculations for resonance self-shielding. The cross sections and Bondarenko factor data are pulled from an AMPX master library. The output is placed into a master library as well. Dancoff approximations allow for different fuel lattice cell geometries. The main function of NITAWL-II is to change the format of the master cross-section libraries to one which the criticality code (KENO-Va) can access. It also provides the Nordheim Integral Treatment for resonance self-shielding. XSDRNPM-S provides cell-weighted cross sections based on the specified unit cell.

The criticality analysis, using the above computer codes, is performed in compliance with the 10CFR 72 [1] requirements. Specifically, all cases are analyzed assuming that the basket in fully flooded with borated water and the neutron shield of the transfer cask is eliminated and the cask is flooded with fresh water. Finally, KENO V.a calculates the k_{eff} of the system that is modeled. A sufficiently large number of neutron histories are run so that the standard deviation is below 0.0010 for all calculations.

6.4.1.2 Physical and Nuclear Data

The physical and nuclear data required for the criticality analysis include the fuel assembly data and cross-section data as described below.

Table 6-4 provides the pertinent data for criticality analysis for each fuel assembly evaluated for the NUHOMS® HD System.

The criticality analysis used the 44-group cross-section library built into the SCALE system. ORNL used ENDF/B-V data to develop this broad-group library specifically for criticality analysis of a wide variety of thermal systems.

6.4.1.3 Bases and Assumptions

The analytical results reported in Section 3.7 demonstrate that the TC containment boundary and canister basket structure do not experience any significant distortion under hypothetical accident conditions. Therefore, for both normal and hypothetical accident conditions the TC geometry is identical except for the neutron shield and skin. As discussed above, the neutron shield and skin are conservatively removed and the interstitial space modeled as water.

The TC is modeled with KENO V.a using the available geometry input. This option allows a model to be constructed that uses regular geometric shapes to define the material boundaries. The following conservative assumptions are also incorporated into the criticality calculations:

(1) No burnable poisons like IFBA, Gadolinia, Erbia or any other absorber, accounted for in the fuel.

(2) The fuel insert hardware like BPRA, TPA, and VSI are conservatively assumed to exhibit neutronic properties similar to $^{11}B_4C$. There is no neutron absorption from any of these hardware and are collectively referred to as BPRAs.

(3) Water density at optimum moderator density.

(4) Unirradiated fuel – no credit taken for fissile depletion due to burnup or fission product poisoning.

(5) The fuel pins are modeled assuming a stack density of 97.5% theoretical density with no allowance for dishing or chamfer. This assumption conservatively increases the total fuel content in the model.

(6) Temperature at 20°C (293K).

(7) The maximum fuel enrichment is modeled as uniform everywhere throughout the assembly. Natural Uranium blankets and axial or radial enrichment zones are modeled as enriched uranium with an average enrichment.

(8) All fuel rods are filled with full density water in the pellet/cladding gap.

(9) Only a 15.03-inch section of the basket with fuel assemblies is explicitly modeled with periodic axial boundary conditions, therefore the model is effectively infinitely long.

(10) It is assumed that for all cases the neutron shield and stainless steel skin of the cask are stripped away and the infinite array of casks are pushed close together with moderator in the interstitial spaces.

6.4.2 Fuel Loading Optimization

The criticality analysis is performed for the 32PTH DSC loaded with 32 intact or 32 damaged fuel assemblies. The following sub-sections describe the various analyses performed with the intact fuel assemblies.

6.4.2.1 Most Reactive Fuel Assembly and Assembly Position Studies

The first series of analyses determines the most reactive fuel assembly design and the most reactive fuel positioning within the steel tubes. The first KENO run models the fuel assemblies as being centered within the basket compartment tubes. The off-center fuel assembly positioning is modeled by shifting all the fuel assemblies radially inward such that the fuel pins come in contact with the two faces of the compartment tubes. This is "inward" positioning and the fuel assemblies are at the closest approach relative to the center of the basket.

These calculations are repeated for all four fuel assembly designs listed in Table 6-3. These runs are carried out at nominal compartment dimensions with varying internal moderator density assuming a Type B basket and fuel at 4.30 wt% U-235 and a boron concentration of 2500 ppm. All input and output files are included on the attached compact disk. In all other respects, the model is the same as that described in Sections 6.3.1 and 6.3.2. The 2D KENO plots are shown in Figure 6-12 and Figure 6-13 and the results are shown in Table 6-10.

The peripheral rails were not modeled for these calculations. The rail material was assumed to be completely replaced by the internal moderator (borated water at 2500 ppm). This assumption does not affect this parametric study.

The most reactive fuel assembly design is the WE 17x17 standard fuel assembly for the WE17 class, the WE 15x15 standard fuel assembly for the WE15 class and the CE 14x14 Fort Calhoun Fuel assembly for the CE14 class of fuel assemblies. The "inward" positioning of fuel assemblies is most reactive.

6.4.2.2 Determination of the Most Reactive Configuration

The fuel loading configuration of the canister/cask affects the reactivity of the package. Several series of analyses determined the most reactive configuration for the canister/cask.

For this analysis, the most reactive fuel type is used to determine the most reactive configuration. The canister/cask is modeled, with the WE 17x17 standard assembly, over a 15.03-inch axial section with periodic axial boundary conditions and reflective radial boundary conditions. This represents an infinite array in the x-y direction of canister/casks that are infinite in length which is conservative for criticality analysis. The starting model is identical to the model used above. The canister/cask model for this evaluation differs from the actual design in the following ways:

- The boron 10 content in the poison plates is 10% lower than the minimum required,
- The stainless steel and aluminum basket rails, which provide support to the fuel compartment grid, are modeled using a homogenized material and,

- The neutron shield and the skin of the cask are conservatively replaced with water between the casks.

Each evaluation is performed at various internal moderator density (IMD) values to determine the optimum moderator density where the reactivity is maximized. All input and output files are included on the attached compact disk.

The first set of analyses determines the effect of rail material composition variation on the reactivity of the basket. The most reactive configuration from the previous section is utilized as the base case for this evaluation. Four different variations in the rail material compositions are considered in this evaluation. The previous evaluation utilized borated water as the rail material. In this evaluation, the rail materials used are unborated water at 100% density, composition 3 (30% water, 35% aluminum, 35% ss304 by volume), composition 4 (40% water, 30% aluminum, 30% ss304 by volume) and composition 5 (50% water, 25% aluminum, 25% ss304 by volume). The rails are also modeled discretely based on the detailed model, as shown in Figure 6-11, for a comparison of the results.

Based on the actual volume fraction of rail materials, it is expected that the volume of water does not go below 30%. Also, such a variation (composition 3 through 5) adequately accounts for the fabrication tolerances associated with the rail materials. The results of this evaluation are shown in Table 6-11 including the most reactive results from the previous study and the results based on the detailed model. These results indicate that the most reactive rail composition is the one based on composition 3. The results also indicate that the change is k_{eff} due to variation in composition is statistically insignificant. The comparison of k_{eff} results with composition 3 and detailed model indicates that the simplified model (based on homogenous rail) is both adequate and conservative. Therefore, for the rest of the calculation, the rail assemblies will be modeled with a homogenous rail assumption with the material based on composition 3.

The next set of calculations determines the effect of variation in the poison plate thickness in the reactivity of the system. The poison plate thickness is varied from a maximum of 0.187 inches (for the Type D basket) to a minimum of 0.050 inches (for the Type A basket) based on a poison loading of 15.0 mg B-10/cm^2 (Borated Aluminum poison, Type B basket loading). Even though, this large variation in thickness is not expected for a single basket type, these calculations are intended to demonstrate that the effect of variation is statistically insignificant. The variation in the poison plate thickness also results in a compensatory variation in the aluminum plate thickness in order to maintain the total thickness of 0.25 inches. Therefore, the study also indirectly evaluates the effect of variation in the aluminum plate thickness. The results of these calculations are shown in Table 6-12 along with the most reactive results from the previous evaluation.

The results of this evaluation indicate that the effect of variation in the poison plate thickness is statistically insignificant and that the maximum k_{eff} values at all plate thicknesses are about the same. As stated above, the variation in the thickness considered in this evaluation is not expected to represent physical reality; however, the results demonstrate that within the tolerance band for the thicknesses of various basket types, the variation in k_{eff} is statistically insignificant.

These results also indicate that there would be no significant effect on k_{eff} due to the presence of aluminum cladding in case of Boral® poison due to the fact that this study also evaluates the effect of aluminum plate thickness.

The next set of analyses determines the effect of fuel compartment size on the system reactivity. The model starts with the most reactive geometry determined from the previous study. For this evaluation, the compartment size is varied from 8.650 inches to 8.750 inches square. These results are shown in Table 6-13. These results indicate that the most reactive configuration is with the minimum fuel compartment size because the assembly-to-assembly pitch is minimized.

The next set of analyses determines the effect of fuel compartment box thickness on the system reactivity. The model starts with the minimum fuel compartment width from the previous study and the compartment thickness is varied from 0.1775 inches to 0.2325 inches. The results in Table 6-14 show that the most reactive calculated condition occurs with nominal compartment box thickness. The results indicate that the system reactivity is not very sensitive to the box thickness and that the difference in k_{eff} between the nominal and minimum thickness cases is within statistical uncertainty. The balance of this evaluation uses the nominal box thickness because it represents the most reactive configuration from this study.

6.4.2.3 Determination of Maximum Initial Enrichment for Intact Assemblies

The most reactive configuration determined based on parametric studies is with the rail structure represented with Composition 3, poison and aluminum plates at nominal thickness, fuel compartment at minimum width and nominal thickness and the fuel assemblies positioned in the "inward" position. The following analysis uses this configuration to determine the maximum allowable initial enrichment as a function of poison plate loading and soluble boron concentration for the two fuel assembly classes. Only the fuel assembly type, the fixed and soluble poison loading is changed for each model. In addition, the internal moderator density is varied to determine the peak reactivity for the specific configuration.

The canister / cask model for this evaluation differs from the actual design in the following ways:

- the boron-10 content in the borated aluminum poison plates is 10% lower than the minimum required and the boron-10 content in the Boral® poison plates is 25% lower than the minimum required
- the neutron shield and the skin of the cask are conservatively replaced with water between the casks, and
- the worst case geometry and material conditions, as determined in the previous sections, are modeled.

Five different fixed poison loadings are analyzed in the criticality calculations as described in Section 6.3, corresponding to the five different types of basket based on fixed poison loading (Type A, B, C, D and E). Four different soluble boron concentration levels are analyzed -2000 ppm, 2300 ppm, 2400 ppm and 2500 ppm. The maximum analyzed initial enrichment is 5.0 wt. % U-235.

Calculations are also performed with the presence of BPRAs (bounding for all NFAH) in the guide tubes to determine the maximum allowable enrichment for the WE15 and WE17 fuel assembly classes with NFAH. These calculations are applicable to intact fuel assemblies only. Reconstituted fuel assemblies, where the fuel pins are replaced by non-fuel pins are also considered intact fuel assemblies provided they displace the same amount of moderator.

CE 14x14 Class Assemblies

The most reactive CE 14x14 class assembly is the CE 14x14 Fort Calhoun type fuel assembly with the larger fuel pellet OD. The results for the CE 14x14 class of fuel assemblies are shown in Table 6-33.

WE 15x15 Class Assemblies

The most reactive WE 15x15 class assembly is the WE 15x15 standard fuel assembly. The results for the WE 15x15 class of fuel assemblies without BPRAs are shown in Table 6-15. The results for WE 15x15 class of fuel assemblies with BPRAs are shown in Table 6-16. These results indicate that the presence of BPRAs increases the reactivity of the system and consequently a reduction in the allowable enrichment.

WE 17x17 Class Assemblies

The most reactive WE 17x17 class assembly is the WE 17x17 standard fuel assembly. The results for the WE 17x17 class of fuel assemblies without BPRAs are shown in Table 6-17. The results for WE 17x17 class of fuel assemblies with BPRAs are shown in Table 6-18. These results also indicate that the presence of BPRAs increases the reactivity of the system and consequently a reduction in the allowable enrichment. For calculations with Type C basket, the WE 17x17 assembly results are conservatively applied to WE 15x15 assembly.

6.4.2.4 Determination of the Most Reactive Damaged Fuel Configuration

There are several mechanisms by which a fuel rod may be breached. These mechanisms may occur while the fuel is loaded in the reactor core, in the spent fuel pool, during transport, while in temporary dry storage, and while in permanent dry storage. In addition, the type and extent of fuel rod breach can be broken down into several categories. For this calculation, the method by which the fuel rod is breached is not as important as the extent of the resultant damage. The worst case gross damage resulting from a cask drop accident is assumed to be either a single-ended or double-ended rod shear with moderator intrusion. The bent or bowed fuel rod cases assume that the fuel is intact but not in its nominal fuel rod pitch. It is possible that the fuel rods may be crushed inwards or bowed outwards to a certain degree. Therefore, this will be evaluated by varying the fuel rod pitch from a minimum pitch (based on clad OD) to a maximum based on the fuel compartment size for each fuel assembly class. All pitch variations assume a uniform rod pitch throughout the entire fuel matrix.

The single-ended fuel rod shear cases assume that a fuel rod shears in one place and is displaced to a new location. The fuel pellets are assumed to remain in the fuel rod. This case will be evaluated by displacing one row of rods from the base fuel assembly matrix at small increments towards the side of the fuel compartment. The base fuel assembly matrix will be at nominal

pitch and positioned in the "inward" position within the 32PTH DSC to maximize the separation distance between the fuel array and the sheared row of fuel rods. A smaller rod pitch for the base fuel assembly matrix was not chosen because it has been shown from the pitch cases that decreasing the rod pitch decreases reactivity. Increasing the base fuel assembly rod pitch will increase reactivity, however, the resulting model is similar to and is bounded by the rod pitch varying cases presented above and therefore will not be duplicated here. The single shear cases are analyzed for the two fuel assembly classes.

The double-ended fuel rod shear cases assume that the fuel rod shears in two places and the intact fuel rod piece is separated from the parent fuel rod. Three resulting conditions are exhibited by the occurrence of a double-ended rod shear. These are, the fuel rod piece can remain in place, it can be displaced in the same plane, or it can be displaced to a different plane. The "remain in place" situation results in no deviation from the base fuel assembly matrix, and is therefore considered trivial and will not be evaluated separately. The fuel rod piece displaced in the same plane is equivalent to the single-ended rod shear case discussed above and will not be reevaluated in these cases. The fuel rod piece displaced in a different plane results in two possibilities: an added rod or a removed rod. As in the single-ended shear cases, the base fuel assembly matrix will be positioned in the "inward" position of the 32PTH DSC to allow room for a row of displaced fuel rods. One row of fuel rods of different lengths will be removed from a section of the assembly and added to another to determine if the system exhibits any trends. The nominal rod pitch is used for the base fuel matrix just as in the single-ended shear rod cases. The two fuel assembly classes are analyzed for the double-ended shear configuration.

In order to determine the effect of an axial shift in the fuel assemblies beyond the poison during transfer, bounding calculations that consider a 4" axial shift of fuel assemblies are performed. The nominal rod pitch is used for these cases and both the fuel assembly classes are analyzed for this configuration.

The first step is to determine the most reactive damaged fuel assembly geometry. This was completed using limiting fixed poison loading, soluble boron concentration and assembly enrichment for the various fuel assembly classes. The limiting parameters used for this study are shown in Table 6-19. All 32 assembly locations were filled with damaged fuel assemblies. The intent of these calculations was to determine the most reactive geometry, not to meet the USL. The following is a breakdown of runs made in this analysis:

- Optimum Rod Pitch Study (for fuel assemblies and rod storage baskets).
- Single-ended Shear Study.
- Double-ended Shear Study.
- Shifting of fuel assemblies beyond (4 inches above) the poison sheet height.

With the selection of the most reactive damaged fuel assembly geometry, the next set of analyses determined the maximum k_{eff} for various damaged fuel assembly loading configurations in the NUHOMS® 32PTH DSC. The most reactive damaged fuel assembly geometry for each fuel assembly class determined will be used to determine the maximum enrichment as a function of

fixed poison loading and soluble boron concentration for loading 32 damaged fuel assemblies in the basket. In other words, cases are analyzed for all the configurations described in Table 6-1.

Rod Pitch Study:

The first set of damaged fuel analyses involved a study on the effect of the fuel rod pitch on system reactivity. KENO models with rod pitches ranging from a minimum corresponding to the clad OD to a maximum limited by the fuel compartment size are developed for each fuel assembly class. The results of the rod pitch study are shown in Table 6-20 and a discussion of these results is as follows. For the CE14 fuel assembly class, the optimum pitch was calculated to be 0.620". For the WE15 fuel assembly class, the largest pitch (limited by the fuel compartment size) resulted in the most reactive configuration. For the WE17 fuel assembly class, the second largest pitch resulted in the most reactive configuration.

This study also bounds damaged fuel configurations with missing rods. A separate study to determine the effect on reactivity due to removal of fuel rods at optimum pitch is not necessary due to the presence of soluble boron in the moderator. The removal fuel rods would ensure that the fissile fuel rods are replaced with boron poison and would result in a reduction in k_{eff}. Therefore, the rod pitch study is completed by determining the optimum pitch and the associated maximum k_{eff} at optimum moderator density. The 2D KENO plot for the CE14 fuel assembly is shown in Figure 6-14.

Single Ended Rod Shear Study:

The next set of analyses performed is for the Single-ended rod shear. The Single-ended rod shear study depicts the fuel assembly with its last row of rods separated from the rest of the assembly. The displacement of the sheared row of rods varies radially from fuel assembly up to a maximum that is governed by the fuel assembly width and the fuel compartment size.

To model this in KENO, the base case was slightly modified. First, for a given fuel lattice, the fuel assemblies are modeled as a XX by (XX-1) array where XX corresponds to the fuel assembly class. For example, the WE 15 fuel assembly is modeled as a 15x14 array. Unit 200 is a XX by 1 array comprising of the single sheared row of rods. The units 201, 204, 211 and 214, therefore consist of two arrays, the array describing the truncated fuel assembly and the sheared row of fuel rods. The displaced row of rod array is then shifted (separation distance is "d") away from the fuel assembly. The amount of fuel remains the same, i.e. no new fuel is added to the system. Nominal rod pitch for all of the fuel assembly classes is used for the base XX by (XX-1) fuel assembly. In the cask drop accident scenarios, it is more likely that the fuel assembly will be crushed as a result of the drop and therefore cause local decreases in the rod pitch of the assembly. However, the rod pitch studies outlined above show that a decrease in the fuel rod pitch results in a decrease in system reactivity, therefore for the single-ended rod shear study runs, rod pitch is modeled at nominal value. The study is repeated for all the fuel assembly classes and at varying moderator density for important separation distances. An example plot of a single ended shear configuration with WE 17x17 fuel assembly is shown in Figure 6-15. The results of this evaluation are shown in Table 6-21. The results indicate that there exists an optimum shear row separation distance for each class of fuel assembly where the reactivity is highest.

Double Ended Rod Shear Study:

The three Double-ended Rod Shear cases model a row (XX by 1 array) of dislocated rods severed at different sections axially and then displacing to other sections of the DSC in order to define a conservative bounding condition for fuel rod location subsequent to a double-ended rod shear. To model this in KENO, the base case was accordingly modified. A new KENO unit, UNIT 11 forms one axial section of the basket that models the un-sheared fuel assemblies. The sheared fuel assemblies depleted by one row of fuel rods are modeled as a XX by (XX-1) array where XX corresponds to the fuel assembly class. The corresponding KENO units for the fuel assembly positions are 301, 304, 311, 314, 302, 303, 305 and 312. The unit 12 forms the axial section of the basket that models this depleted array of fuel assemblies. The fuel assemblies that contain the sheared-migrated row of fuel rods are modeled as a XX by (XX+1) array where XX corresponds to the fuel assembly class. The corresponding KENO units for the fuel assembly positions are 401, 404, 411 414, 402, 403, 405 and 412. The unit 13 forms the axial section of the basket that models this depleted array of fuel assemblies. Depending on the fraction of double shear, the array 11 (an axial array of units 11, 12 and 13) is constructed to calculate the reactivity effect. Due to the height of a single axial segment (15.03"), the total axial height of the model for these studies is 150.30" (15.03*10). However, periodic axial boundary conditions are applied making the model essentially infinite. The same rod pitch assumptions made for the Single-ended Shear runs also apply here.

Basically three types of double ended shear studies are evaluated. The first is a half shear where the sheared row breaks into two equal sections resulting in one-half of the fuel assembly being defined by a rod array containing an extra row of fuel rods while the other half is defined by an array depleted by one row of fuel rods. The half shear is represented in this calculation as a $(5/10)^{th}$ shear. The second is a one-third shear where the sheared row breaks into two unequal sections measuring a third of the fuel assembly length and two-third of the fuel assembly length respectively. Therefore, the fuel assembly can be defined by three axially equal sections, one with a regular array of fuel rods, one with an extra row of fuel rods and the other with a depleted row of fuel rods. This is modeled as $(3/10)^{th}$ which is about the same as one-third. The same mechanism can be extended to other shear ratios but the effect on reactivity is expected to reduce with reduction in the shear ratio. The one-fifth shear is also analyzed in this study as $(2/10)^{th}$ shear. The internal moderator density is varied to determine the k_{eff} at optimum density.

Results of the double-ended rod shear study show that the movement of one exterior row of half of the fuel assembly length is the most reactive. The CE14 fuel is only evaluated for the half shear condition since the evaluation results show this is the most reactive. An example plot of a double ended shear configuration with WE 15x15 fuel assembly is shown in Figure 6-16. The results of the evaluation are shown Table 6-22.

Shifting of Fuel Beyond Fixed Poison:

This study analyzes the effect of shifting of loose rods beyond the height of the poison plates. Two types of shifting of fuel rods beyond the poison plates are analyzed in this study. The first calculational model assumes that a four-inch axial section of the entire fuel assembly shifts beyond the poison plates. The height of the axial shift, four-inches, is more than the maximum difference between the basket height and the canister cavity height (about 2.5 inches). The

second calculational model involves a shifting of 8 of the outermost rows of fuel rods (basically two concentric rings of fuel rods) beyond the poison plates by six inches. In KENO, this six-inch section is modeled like a regular fuel assembly with fuel pins defining the 8 outer most rows (and columns) with aluminum occupying the space in the middle. This is done to simulate the sliding of fuel rods around the inlet or outlet nozzle during an accident. These models conservatively bound all the cases associated with the shifting of fuel rods beyond poison like sliding of a single rod, sliding of a row of single sheared rods etc.

To model these in KENO, the base case was modified. First, a new KENO unit, UNIT 11 forms one axial section of the basket that models the fuel assemblies covered with poison. For the shifting of fuel assemblies (first model), a four-inch axial section of the fuel assemblies containing the uncovered fuel assemblies are modeled with the KENO units 301, 304, 311 and 314. The unit 12 forms the axial section of the basket that models this uncovered section of fuel assemblies. Finally, the array 11 (an axial array of units 11 and 12) is constructed to calculate the reactivity effect. Periodic axial boundary conditions are utilized to make this model essentially infinite in length. For the sliding of fuel assemblies (second model), a six-inch axial section of the fuel assemblies containing the eight uncovered rows of fuel rods with aluminum in the middle portion are modeled with the KENO units 301, 304, 311 and 314. The unit 12 forms the axial section of the basket that models this uncovered section of fuel assemblies. Finally, the array 11 (an axial array of units 11 and 12) is constructed to calculate the reactivity effect. Periodic axial boundary conditions are utilized to make this model essentially infinite in length. This study is performed for the two fuel assembly classes with varying moderator density.

The results of these evaluations are shown in Table 6-23. An example plot of a shifting configuration with WE 17x17 fuel assembly is shown in Figure 6-17. An example plot of a sliding configuration with WE 15x15 fuel assembly is shown in Figure 6-18.

6.4.2.5 Determination of the Most Reactive Damaged Configuration

The fuel-loading configuration of the canister/cask affects the reactivity of the package. Several series of analyses performed in the previous sections evaluated the various damaged assembly configurations. A comparison of the maximum k_{eff} due to the various damaged assembly configurations is shown in Table 6-24. The most reactive damaged assembly configuration for the CE14 fuel is the optimum pitch configuration of the rods and for the WE15 and WE17 fuel is the double-ended rod shear with a shear ratio of one-half.

Additionally, the one-half (5/10) double-ended shear configuration is modified to include BPRAs to obtain a bounding damaged assembly configuration. The results of this evaluation, shown in Table 6-25, demonstrate that the configuration with BPRAs is bounding. Therefore, this configuration is the design basis configuration for the WE15 and WE17 fuel assembly classes and will be utilized to determine the k_{eff} of the NUHOMS®-32PTH DSC containing damaged fuel assemblies. An example plot of a double ended shear configuration with WE 15x15 fuel assembly with BPRAs is shown in Figure 6-19.

6.4.2.6 Determination of Maximum Initial Enrichment for Damaged Assemblies

The most reactive damaged assembly configuration for the WE15 and WE17 fuel is based on the double-ended shear model with a shear ratio of one-half with BPRAs while the most reactive damaged assembly configuration for the CE14 fuel is based on an optimum pitch arrangement of rods. The following analysis uses these configurations to determine the maximum allowable initial enrichment as a function of poison plate loading and soluble boron concentration for all the fuel assembly classes. The analysis is carried out with the NUHOMS®-32PTH DSC containing 32 design basis damaged assemblies. Only the fuel assembly type, the fixed and soluble poison loading is changed for each model. In addition, the internal moderator density is varied to determine the peak reactivity for the specific configuration. All calculations for the WE15 and WE17 fuel are performed with the presence of BPRAs (bounding for all NFAH and no NFAH cases) in the guide tubes to determine the maximum allowable enrichment for these two fuel assembly classes with and without NFAH.

The canister / cask model for this evaluation differs from the actual design in the following ways:

- the boron-10 content in the borated aluminum poison plates is 10% lower than the minimum required and the boron-10 content in the boral® poison plates is 25% lower than the minimum required
- the neutron shield and the skin of the cask are conservatively replaced with water between the casks, and
- the worst case geometry and material conditions as determined in Section 6.4.2.2 and the worst case damaged assembly configuration as determined in Section 6.4.2.5, are modeled.

Five different fixed poison loadings are analyzed in the criticality calculations as described in Section 4.2, corresponding to the four different types of basket based on fixed poison loading (Type A, B, C, D and E). Four different soluble boron concentration levels are analyzed - 2000 ppm, 2300 ppm, 2400 ppm and 2500 ppm. The maximum analyzed initial enrichment is 5.0 wt. % U-235.

CE 14x14 Class Assemblies

The results for CE 14x14 class of fuel assemblies are shown in Table 6-34.

WE 15x15 Class Assemblies

The results for WE 15x15 class of fuel assemblies with BPRAs are shown in Table 6-16.

WE 17x17 Class Assemblies

The most reactive WE 17x17 class assembly is the WE 17x17 standard fuel assembly. The results for the WE 17x17 class of fuel assemblies with BPRAs are shown in Table 6-17. For calculations with Type C basket, the WE 17x17 assembly results are conservatively applied to WE 15x15 assembly.

6.4.3 Criticality Results

This section presents the results of the analyses used to demonstrate the acceptability of storing qualified fuel in the 32PTH DSC under normal, off-normal, and accident conditions for fuel loading, handling, and storage.

Table 6-28 lists the bounding results for intact fuel assemblies for all conditions of storage. The highest calculated k_{eff}, including 2σ uncertainty, is for the WE 17x17 Standard fuel assembly with an initial enrichment of 3.80 wt. % U-235, 2300 ppm soluble boron and a poison loading of 7.0 mg B-10/cm^2 (Type A Basket) without BPRAs. The maximum allowable initial enrichment with BPRAs for the WE15 and WE17 (bounding for cases without BPRAs) fuel assembly types and without BPRAs for the CE14 fuel assembly type as a function of fixed poison loading and soluble boron concentration is given in Table 6-1. The input files for the cases with the highest calculated reactivity (with and without BPRAs) are included in the Appendix A.

Table 6-29 lists the bounding results for damaged fuel assemblies for all conditions of storage. The highest calculated k_{eff}, including 2σ uncertainty for the damaged assembly calculations, is 0.9402 and it occurs for the WE 17x17 Standard fuel assembly with an initial enrichment of 4.80 wt. % U-235, 2400 ppm soluble boron and a poison loading of 50.0 mg B-10/cm^2 (Type E Basket). The maximum allowable initial enrichment with BPRAs for the WE15 and WE17 (bounding for cases without BPRAs) fuel assembly types and without BPRAs for the CE14 fuel assembly type as a function of fixed poison loading and soluble boron concentration is given in Table 6-1. The input file for the case with the highest calculated reactivity is included in the Appendix A.

ANS/ANSI-8.1 5 recommends that calculational methods used in determining criticality safety limits for applications outside reactors be validated by comparison with appropriate critical experiments. An Upper Subcritical Limit (USL) provides a high degree of confidence that a given system is subcritical if a criticality calculation based on the system yields a k_{eff} below the USL.

The criterion for subcriticality is that

$$k_{KENO} + 2\sigma_{KENO} \leq USL,$$

Where USL is the upper subcritical limit established by an analysis of benchmark criticality experiments. In Section 6.5, the minimum USL over the parameter range is determined to be is 0.9419. From Table 6-28 and Table 6-29, for the most reactive case,

$$k_{KENO} + 2\sigma_{KENO} = 0.9390 + 2\ (0.0007) = 0.9404 \leq 0.9419.$$

This indicates that the fuel will remain subcritical. Conclusions regarding specific aspects of the methods used or the analyses presented can be drawn from the quantitative results presented in the associated tables.

Table 6-1
Maximum Initial Enrichment for Each Fuel Design
for both Intact and Damaged Fuel Assemblies

Assembly Class and Type	Maximum Initial enrichment of U-235 as a Function of Soluble Boron Concentration and Fixed Poison Loading (Basket Type)				
	Basket Type[1]	Minimum Soluble Boron Concentration			
		2000 ppm	2300 ppm	2400 ppm	2500 ppm
CE 14x14 Fuel Assembly (Intact Fuel Loading)	A	4.05	4.40	4.45	4.55
	B	4.55	4.90	5.00	-
	C	4.70	5.00	-	-
	D	5.00	-	-	-
	E	-	-	-	-
WE 15x15 Fuel Assembly (with BPRAs - bounds all Intact Fuel Loading)	A	3.50	3.70	3.80	3.90
	B	3.80	4.10	4.20	4.30
	C	3.95	4.25	4.35	4.45
	D	4.20	4.50	4.70	4.80
	E	4.50	4.80	4.90	5.00
WE 17x17 Fuel Assembly (with BPRAs - bounds all Intact Fuel Loading)	A	3.50	3.70	3.80	3.90
	B	3.80	4.10	4.20	4.30
	C	3.95	4.25	4.35	4.45
	D	4.20	4.50	4.60	4.70
	E	4.45	4.70	4.90	5.00
CE 14x14 Fuel Assembly (Damaged Fuel Loading)	A	3.90	4.20	4.25	4.35
	B	4.35	4.70	4.80	4.90
	C	4.50	4.85	4.95	5.00
	D	4.85	5.00	-	-
	E	5.00	-	-	-
WE 15x15 Fuel Assembly (with BPRAs - bounds all Damaged Fuel Loading)	A	3.40	3.60	3.70	3.80
	B	3.75	4.00	4.10	4.20
	C	3.85	4.15	4.25	4.35
	D	4.10	4.40	4.50	4.60
	E	4.35	4.70	4.80	4.90
WE 17x17 Fuel Assembly (with BPRAs - bounds all Damaged Fuel Loading)	A	3.40	3.60	3.70	3.80
	B	3.75	4.00	4.10	4.20
	C	3.85	4.15	4.25	4.35
	D	4.10	4.40	4.50	4.60
	E	4.30	4.65	4.80	4.90

(1) Basket Type are classified according to the fixed poison loading

Table 6-2
Summary of Limiting Criticality Evaluations for all Fuel Assemblies

Limiting Assembly Position- The fuel assembly is located in the corner of each compartment tube closest to the 32PTH DSC centerline.				
CE 14x14 Fuel Assembly				
Case	**K_{eff}**	**σ**	**$K_{eff} + 2\sigma$**	**USL**
Intact Fuel - 70% IMD, Type A Basket (7.0 mg B-10/cm^2), 2300 ppm Boron, 4.4 wt. % U-235	0.9383	0.0007	0.9397	0.9419
Damaged Fuel – Optimum Pitch, 70% IMD Type B Basket (15.0 mg B-10/cm^2), 2400 ppm Boron, 4.8 wt. % U-235	0.9386	0.0007	0.9400	0.9419
WE 15x15 Fuel Assembly				
Case	**K_{eff}**	**σ**	**$K_{eff} + 2\sigma$**	**USL**
Intact Fuel - 90% IMD, No BPRA, Type D Basket (32.0 mg B-10/cm^2), 2500 ppm Boron, 4.9 wt. % U-235	0.9383	0.0008	0.9399	0.9419
Intact Fuel - Full IMD, With BPRA, Type D Basket (32.0 mg B-10/cm^2), 2400 ppm Boron, 4.7 wt. % U-235	0.9388	0.0007	0.9402	0.9419
Damaged Fuel - Double Ended Shear Full IMD, With BPRA, Type E Basket (50.0 mg B-10/cm^2), 2300 ppm Boron, 4.7 wt. % U-235	0.9361	0.0007	0.9375	0.9419
WE 17x17 Fuel Assembly				
Case	**K_{eff}**	**σ**	**$K_{eff} + 2\sigma$**	**USL**
Intact Fuel - 70% IMD, No BPRA, Type A Basket (7.0 mg B-10/cm^2), 2300 ppm Boron, 3.8 wt. % U-235	0.9390	0.0007	0.9404	0.9419
Intact Fuel - 80% IMD, With BPRA, Type A Basket (7.0 mg B-10/cm^2), 2500 ppm Boron, 3.9 wt. % U-235	0.9381	0.0008	0.9397	0.9419
Damaged Fuel - Double Ended Shear Full IMD, With BPRA, Type E Basket (50.0 mg B-10/cm^2), 2400 ppm Boron, 4.8 wt. % U-235	0.9388	0.0007	0.9402	0.9419

Table 6-3
Authorized Contents for NUHOMS®-32PTH DSC

Assembly Type[1]	Array
Westinghouse 17x17 Standard (WE 17x17) Westinghouse 17x17 Vantage 5H (WEV 17x17)	17x17
Westinghouse 17x17 OFA (WEO 17x17)	17x17
Framatome ANP Advanced MK BW 17x17 (FR 17x17)	17x17
Westinghouse 15x15 Standard (WE 15x15) Westinghouse 15x15 Surry Improved (WES15x15)	15x15
CE 14x14 Standard (CE 14x14 Std)	14x14

(1) Reload fuel from other manufacturers with these parameters are also acceptable.

Table 6-4
Fuel Assembly Design Parameters[2] for Criticality Analysis

Manufacturer[1]	Array	Version	Active Fuel Length (inches)	# Fuel Rods per Assembly	Pitch (inches)	Fuel Pellet OD (inches)
Westinghouse	17x17	Standard Vantage	144	264	0.4960	0.3225
Westinghouse	17x17	OFA	144	264	0.4960	0.3088
Framatome	17x17	MK BW	144	264	0.4960	0.3195
Westinghouse	15x15	Std / Surry	144	204	0.5630	0.3669
CE	14x14	Std	137	176	0.5800	0.3765
CE	14x14	Ft. Calhoun	128	176	0.5800	0.3815
Manufacturer[1]	**Array**	**Version**	**Clad Thickness (inches)**	**Clad OD (inches)**	**Guide Tube OD Inst. Tube OD (inches)**	**Guide Tube ID Inst. Tube ID (inches)**
Westinghouse	17x17	Standard Vantage	0.0225	0.374	24 @ 0.4820 1 @ 0.4740	24 @ 0.4500 1 @ 0.4440
Westinghouse	17x17	OFA	0.0225	0.360	24 @ 0.4820 1 @ 0.4740	24 @ 0.4500 1 @ 0.4440
Framatome	17x17	MK BW	0.0240	0.374	24 @ 0.4820 1 @ 0.4820	24 @ 0.4500 1 @ 0.4500
Westinghouse	15x15	Std / Surry	0.0243	0.422	20 @ 0.5450 1 @ 0.5450	20 @ 0.5100 1 @ 0.5100
CE	14x14	Std	0.0280	0.440	5 @ 1.115	5 @ 1.035
CE	14x14	Ft. Calhoun	0.0280	0.440	5 @ 1.115	5 @ 1.035

(1) Reload Fuel Assemblies from other manufacturers with these fuel parameters are also acceptable

(2) All Dimensions shown are nominal

Table 6-7
NUHOMS®-32PTH - Fixed Poison Loading Requirements

Basket Type	Borated Aluminum Loading	Boral® Loading
A	7.0 mg B-10/cm^2 Thickness = 0.050"	9.0 mg B-10/cm^2 Thickness = 0.075"
B	15.0 mg B-10/cm^2 Thickness = 0.075"	19.0 mg B-10/cm^2 Thickness = 0.075"
C	20.0 mg B-10/cm^2 Thickness = 0.075"	25.0 mg B-10/cm^2 Thickness = 0.075"
D	32.0 mg B-10/cm^2 Thickness = 0.125"	Not Applicable
E	50.0 mg B-10/cm^2 Thickness = 0.187"	Not Applicable

Table 6-10
Results of the Fuel Assembly Positioning Studies
(Continued)

Description	K_{keno}	σ_{keno}	K_{eff}	Filename
Westinghouse 17x17 Standard Fuel Assembly				
Centered, 70% IMD	0.9212	0.0008	0.9228	we17std_c070.out:
Centered, 80% IMD	0.9264	0.0007	0.9278	we17std_c080.out:
Centered, 90% IMD	0.9233	0.0007	0.9247	we17std_c090.out:
Centered, 100% IMD	0.9194	0.0007	0.9208	we17std_c100.out:
Inward, 70% IMD	0.9245	0.0008	0.9261	we17std_o070.out:
Inward, 80% IMD	**0.9289**	**0.0008**	**0.9305**	**we17std_o080.out:**
Inward, 90% IMD	0.9277	0.0007	0.9291	we17std_o090.out:
Inward, 100% IMD	0.9217	0.0007	0.9231	we17std_o100.out:
CE 14x14 Standard Fuel Assembly				
Centered, 60% IMD	0.8799	0.0007	0.8813	ce14std_c060.out:
Centered, 70% IMD	0.8834	0.0007	0.8848	ce14std_c070.out:
Centered, 80% IMD	0.8807	0.0007	0.8821	ce14std_c080.out:
Centered, 90% IMD	0.8723	0.0007	0.8737	ce14std_c090.out:
Centered, 100% IMD	0.8619	0.0007	0.8633	ce14std_c100.out:
Inward, 60% IMD	0.8826	0.0008	0.8842	ce14std_o060.out:
Inward, 70% IMD	**0.8862**	**0.0007**	**0.8876**	**ce14std_o070.out:**
Inward, 80% IMD	0.8842	0.0007	0.8856	ce14std_o080.out:
Inward, 90% IMD	0.8772	0.0008	0.8788	ce14std_o090.out:
Inward, 100% IMD	0.8676	0.0007	0.8690	ce14std_o100.out:
CE 14x14 Fort Calhoun Fuel Assembly				
Centered, 60% IMD	0.8808	0.0008	0.8824	ce14ftc_c060.out:
Centered, 70% IMD	0.8851	0.0007	0.8865	ce14ftc_c070.out:
Centered, 80% IMD	0.8828	0.0007	0.8842	ce14ftc_c080.out:
Centered, 90% IMD	0.8756	0.0008	0.8772	ce14ftc_c090.out:
Centered, 100% IMD	0.8679	0.0007	0.8693	ce14ftc_c100.out:
Inward, 60% IMD	0.8826	0.0008	0.8842	ce14ftc_o060.out:
Inward, 70% IMD	**0.8883**	**0.0007**	**0.8897**	**ce14ftc_o070.out:**
Inward, 80% IMD	0.8865	0.0008	0.8881	ce14ftc_o080.out:
Inward, 90% IMD	0.8815	0.0008	0.8831	ce14ftc_o090.out
Inward, 100% IMD	0.8717	0.0008	0.8733	ce14ftc_o100.out:

Table 6-18
WE 17x17 Class Intact Assemblies With BPRAs - Final Results
(Continued)

Description	K_{keno}	σ_{keno}	K_{eff}	Filename
Type D Basket (32.0 mg B-10/cm^2), 2500 ppm Boron, 4.7 wt. % U-235				
60% IMD	0.8992	0.0007	0.9006	we17bp25_p32e47_060.out:
70% IMD	0.9154	0.0007	0.9168	we17bp25_p32e47_070.out:
80% IMD	0.9272	0.0007	0.9286	we17bp25_p32e47_080.out:
90% IMD	0.9341	0.0007	0.9355	we17bp25_p32e47_090.out:
100% IMD	0.9356	0.0008	0.9372	we17bp25_p32e47_100.out:
Type E Basket (50.0 mg B-10/cm^2), 2500 ppm Boron, 5.0 wt. % U-235				
60% IMD	0.8871	0.0008	0.8887	we17bp25_p50e50_060.out:
70% IMD	0.9102	0.0007	0.9116	we17bp25_p50e50_070.out:
80% IMD	0.9260	0.0007	0.9274	we17bp25_p50e50_080.out:
90% IMD	0.9343	0.0008	0.9359	we17bp25_p50e50_090.out:
100% IMD	0.9379	0.0008	0.9395	we17bp25_p50e50_100.out:

Table 6-19
Limiting Parameters for Damaged Fuel Calculations

Fuel Assembly Type	Enrichment	Boron Concentration	Fixed Poison Loading
CE 14x14	4.90 wt. % U-235	2300 ppm	15 mg B-10/cm^2
Westinghouse 15x15	4.90 wt. % U-235	2500 ppm	32 mg B-10/cm^2
Westinghouse 17x17	4.80 wt. % U-235	2500 ppm	32 mg B-10/cm^2

Table 6-20
Results of Optimum Pitch Studies
(Continued)

Description	K_{keno}	σ_{keno}	K_{eff}	Filename
CE 14x14, 4.9 wt. % U-235, 2300 ppm, 15 mg B-10/cm^2 (Type B Basket)				
Pitch = 0.4400", 70% IMD	0.6852	0.0007	0.6866	ce14_pitch_min_070.out:
Pitch = 0.4400", 80% IMD	0.6915	0.0008	0.6931	ce14_pitch_min_080.out:
Pitch = 0.4700", 70% IMD	0.7560	0.0008	0.7576	ce14_pitch_470_070.out:
Pitch = 0.4700", 80% IMD	0.7626	0.0009	0.7644	ce14_pitch_470_080.out:
Pitch = 0.5000", 70% IMD	0.8196	0.0008	0.8212	ce14_pitch_500_070.out:
Pitch = 0.5000", 80% IMD	0.8245	0.0008	0.8261	ce14_pitch_500_080.out:
Pitch = 0.5400", 70% IMD	0.8872	0.0008	0.8888	ce14_pitch_540_070.out:
Pitch = 0.5400", 80% IMD	0.8886	0.0009	0.8904	ce14_pitch_540_080.out:
Pitch = 0.5800", 70% IMD	0.9337	0.0007	0.9351	ce14_pitch_nom_070.out:
Pitch = 0.5800", 80% IMD	0.9336	0.0007	0.9350	ce14_pitch_nom_080.out:
Pitch = 0.6000", 70% IMD	0.9473	0.0007	0.9487	ce14_pitch_600_070.out:
Pitch = 0.6000", 80% IMD	0.9468	0.0007	0.9482	ce14_pitch_600_080.out:
Pitch = 0.6100", 60% IMD	0.9457	0.0008	0.9473	ce14_pitch_610_060.out:
Pitch = 0.6100", 70% IMD	0.9491	0.0008	0.9507	ce14_pitch_610_070.out:
Pitch = 0.6100", 80% IMD	0.9467	0.0007	0.9481	ce14_pitch_610_080.out:
Pitch = 0.6100", 90% IMD	0.9383	0.0008	0.9399	ce14_pitch_610_090.out:
Pitch = 0.6100", 100% IMD	0.9290	0.0007	0.9304	ce14_pitch_610_100.out:
Pitch = 0.6200", 60% IMD	0.9500	0.0007	0.9514	ce14_pitch_620_060.out:
Pitch = 0.6200", 70% IMD	**0.9512**	**0.0007**	**0.9526**	**ce14_pitch_620_070.out:**
Pitch = 0.6200", 80% IMD	0.9471	0.0007	0.9485	ce14_pitch_620_080.out:
Pitch = 0.6200", 90% IMD	0.9368	0.0008	0.9384	ce14_pitch_620_090.out:
Pitch = 0.6200", 100% IMD	0.9250	0.0007	0.9264	ce14_pitch_620_100.out:
Pitch = 0.6250", 60% IMD	0.9499	0.0007	0.9513	ce14_pitch_625_060.out:
Pitch = 0.6250", 70% IMD	0.9506	0.0007	0.9520	ce14_pitch_625_070.out:
Pitch = 0.6250", 80% IMD	0.9476	0.0008	0.9492	ce14_pitch_625_080.out:
Pitch = 0.6250", 90% IMD	0.9372	0.0007	0.9386	ce14_pitch_625_090.out:
Pitch = 0.6250", 100% IMD	0.9234	0.0008	0.9250	ce14_pitch_625_100.out:
Pitch = 0.6315", 60% IMD	0.9499	0.0007	0.9513	ce14_pitch_max_060.out:
Pitch = 0.6315", 70% IMD	0.9500	0.0008	0.9516	ce14_pitch_max_070.out:
Pitch = 0.6315", 80% IMD	0.9445	0.0007	0.9459	ce14_pitch_max_080.out:
Pitch = 0.6315", 90% IMD	0.9340	0.0008	0.9356	ce14_pitch_max_090.out:
Pitch = 0.6315", 100% IMD	0.9187	0.0007	0.9201	ce14_pitch_max_100.out:

Table 6-21
Results of the Single Ended Rod Shear Studies
(Continued)

Description	K_{keno}	σ_{keno}	K_{eff}	Filename
CE 14x14, 4.9 wt. % U-235, 2300 ppm, 15 mg B-10/cm^2 (Type B Basket)				
D=0.00 cm, 60% IMD	0.9309	0.0008	0.9325	ce14_ss000_060.out:
D=0.00 cm, 70% IMD	0.9348	0.0009	0.9366	ce14_ss000_070.out:
D=0.00 cm, 80% IMD	0.9343	0.0007	0.9357	ce14_ss000_080.out:
D=0.00 cm, 90% IMD	0.9289	0.0007	0.9303	ce14_ss000_090.out:
D=0.00 cm, 100% IMD	0.9214	0.0008	0.9230	ce14_ss000_100.out:
D=0.20 cm, 60% IMD	0.9303	0.0007	0.9317	ce14_ss020_060.out:
D=0.20 cm, 70% IMD	0.9383	0.0007	0.9397	ce14_ss020_070.out:
D=0.20 cm, 80% IMD	0.9357	0.0007	0.9371	ce14_ss020_080.out:
D=0.20 cm, 90% IMD	0.9311	0.0008	0.9327	ce14_ss020_090.out:
D=0.20 cm, 100% IMD	0.9230	0.0007	0.9244	ce14_ss020_100.out:
D=0.40 cm, 60% IMD	0.9336	0.0008	0.9352	ce14_ss040_060.out:
D=0.40 cm, 70% IMD	0.9391	0.0008	0.9407	ce14_ss040_070.out:
D=0.40 cm, 80% IMD	0.9400	0.0008	0.9416	ce14_ss040_080.out:
D=0.40 cm, 90% IMD	0.9335	0.0007	0.9349	ce14_ss040_090.out:
D=0.40 cm, 100% IMD	0.9254	0.0007	0.9268	ce14_ss040_100.out:
D=0.60 cm, 60% IMD	0.9335	0.0008	0.9351	ce14_ss060_060.out:
D=0.60 cm, 70% IMD	0.9407	0.0008	0.9423	ce14_ss060_070.out:
D=0.60 cm, 80% IMD	0.9402	0.0008	0.9418	ce14_ss060_080.out:
D=0.60 cm, 90% IMD	0.9345	0.0007	0.9359	ce14_ss060_090.out:
D=0.60 cm, 100% IMD	0.9248	0.0007	0.9262	ce14_ss060_100.out:
D=0.80 cm, 60% IMD	0.9340	0.0008	0.9356	ce14_ss080_060.out:
D=0.80 cm, 70% IMD	0.9403	0.0007	0.9417	ce14_ss080_070.out:
D=0.80 cm, 80% IMD	**0.9411**	**0.0008**	**0.9427**	**ce14_ss080_080.out:**
D=0.80 cm, 90% IMD	0.9342	0.0007	0.9356	ce14_ss080_090.out:
D=0.80 cm, 100% IMD	0.9252	0.0007	0.9266	ce14_ss080_100.out:
D=1.00 cm, 60% IMD	0.9351	0.0008	0.9367	ce14_ss100_060.out:
D=1.00 cm, 70% IMD	0.9410	0.0008	0.9426	ce14_ss100_070.out:
D=1.00 cm, 80% IMD	0.9401	0.0008	0.9417	ce14_ss100_080.out:
D=1.00 cm, 90% IMD	0.9336	0.0007	0.9350	ce14_ss100_090.out:
D=1.00 cm, 100% IMD	0.9233	0.0008	0.9249	ce14_ss100_100.out:

Table 6-21
Results of the Single Ended Rod Shear Studies
(Continued)

Description	K_{keno}	σ_{keno}	K_{eff}	Filename
CE 14x14, 4.9 wt. % U-235, 2300 ppm, 15 mg B-10/cm^2 (Type B Basket)				
D=1.20 cm, 60% IMD	0.9336	0.0007	0.9350	ce14_ss120_060.out:
D=1.20 cm, 70% IMD	0.9402	0.0008	0.9418	ce14_ss120_070.out:
D=1.20 cm, 80% IMD	0.9384	0.0007	0.9398	ce14_ss120_080.out:
D=1.20 cm, 90% IMD	0.9325	0.0007	0.9339	ce14_ss120_090.out:
D=1.20 cm, 100% IMD	0.9235	0.0007	0.9249	ce14_ss120_100.out:
D=1.35 cm, 60% IMD	0.9341	0.0007	0.9355	ce14_ssmax_060.out:
D=1.35 cm, 70% IMD	0.9386	0.0007	0.9400	ce14_ssmax_070.out:
D=1.35 cm, 80% IMD	0.9363	0.0008	0.9379	ce14_ssmax_080.out:
D=1.35 cm, 90% IMD	0.9291	0.0008	0.9307	ce14_ssmax_090.out:
D=1.35 cm, 100% IMD	0.9203	0.0007	0.9217	ce14_ssmax_100.out:

Table 6-22
Results of the Double Ended Rod Shear Studies

CE 14x14, 4.9 wt. % U-235, 2300 ppm, 15 mg B-10/cm^2 (Type B Basket)				
Description	**K_{keno}**	**σ_{keno}**	**K_{eff}**	**Filename**
No Shear				
Ratio=0, 60% IMD	0.9289	0.0008	0.9305	ce14_ds000_060.out:
Ratio=0, 70% IMD	0.9340	0.0008	0.9356	ce14_ds000_070.out:
Ratio=0, 80% IMD	0.9336	0.0007	0.9350	ce14_ds000_080.out:
Ratio=0, 90% IMD	0.9284	0.0008	0.9300	ce14_ds000_090.out:
Ratio=0, 100% IMD	0.9224	0.0007	0.9238	ce14_ds000_100.out:
Double Ended Shear with Minimum Distance Between the Sheared and Intact Rows				
Ratio=5/10, 60% IMD	0.9349	0.0007	0.9363	ce14_ds001_060.out:
Ratio=5/10, 70% IMD	0.9406	0.0009	0.9424	ce14_ds001_070.out:
Ratio=5/10, 80% IMD	0.9442	0.0007	0.9456	ce14_ds001_080.out:
Ratio=5/10, 90% IMD	0.9398	0.0008	0.9414	ce14_ds001_090.out:
Ratio=5/10, 100% IMD	0.9328	0.0008	0.9344	ce14_ds001_100.out:
Double Ended Shear with Maximum Distance Between the Sheared and Intact Rows				
Ratio=5/10, 60% IMD	0.9373	0.0007	0.9387	ce14_ds011_060.out:
Ratio=5/10, 70% IMD	0.9453	0.0008	0.9469	ce14_ds011_070.out:
Ratio=5/10, 80% IMD	**0.9492**	**0.0008**	**0.9508**	**ce14_ds011_080.out:**
Ratio=5/10, 90% IMD	0.9443	0.0007	0.9457	ce14_ds011_090.out:
Ratio=5/10, 100% IMD	0.9365	0.0007	0.9379	ce14_ds011_100.out:

Table 6-22
Results of the Double Ended Rod Shear Studies
(Continued)

Description	K_{keno}	σ_{keno}	K_{eff}	Filename
WE 15x15, 4.9 wt. % U-235, 2500 ppm, 32 mg B-10/cm^2 (Type D Basket)				
Ratio=0, 60% IMD	0.9209	0.0007	0.9223	we15_ds000_060.out:
Ratio=0, 70% IMD	0.9320	0.0008	0.9336	we15_ds000_070.out:
Ratio=0, 80% IMD	0.9382	0.0007	0.9396	we15_ds000_080.out:
Ratio=0, 90% IMD	0.9384	0.0007	0.9398	we15_ds000_090.out:
Ratio=0, 100% IMD	0.9335	0.0008	0.9351	we15_ds000_100.out:
Ratio=2/10, 60% IMD	0.9204	0.0007	0.9218	we15_ds210_060.out:
Ratio=2/10, 70% IMD	0.9321	0.0008	0.9337	we15_ds210_070.out:
Ratio=2/10, 80% IMD	0.9388	0.0008	0.9404	we15_ds210_080.out:
Ratio=2/10, 90% IMD	0.9381	0.0008	0.9397	we15_ds210_090.out:
Ratio=2/10, 100% IMD	0.9334	0.0007	0.9348	we15_ds210_100.out:
Ratio=3/10, 60% IMD	0.9214	0.0008	0.9230	we15_ds310_060.out:
Ratio=3/10, 70% IMD	0.9350	0.0008	0.9366	we15_ds310_070.out:
Ratio=3/10, 80% IMD	0.9408	0.0008	0.9424	we15_ds310_080.out:
Ratio=3/10, 90% IMD	0.9421	0.0008	0.9437	we15_ds310_090.out:
Ratio=3/10, 100% IMD	0.9367	0.0008	0.9383	we15_ds310_100.out:
Ratio=5/10, 60% IMD	0.9239	0.0008	0.9255	we15_ds510_060.out:
Ratio=5/10, 70% IMD	0.9371	0.0007	0.9385	we15_ds510_070.out:
Ratio=5/10, 80% IMD	**0.9438**	**0.0008**	**0.9454**	**we15_ds510_080.out:**
Ratio=5/10, 90% IMD	0.9425	0.0007	0.9439	we15_ds510_090.out:
Ratio=5/10, 100% IMD	0.9404	0.0009	0.9422	we15_ds510_100.out:

Table 6-23
Evaluation of the Shifting of Fuel Rods Beyond the Poison

Description	K_{keno}	σ_{keno}	K_{eff}	Filename
CE 14x14, 4.9 wt. % U-235, 2300 ppm, 15 mg B-10/cm^2 (Type B Basket)				
Shift 4-inches, 60% IMD	0.9320	0.0008	0.9336	ce14_nopoison_04_060.out
Shift 4-inches, 70% IMD	0.9372	0.0008	0.9388	ce14_nopoison_04_070.out
Shift 4-inches, 80% IMD	**0.9371**	**0.0009**	**0.9389**	**ce14_nopoison_04_080.out**
Shift 4-inches, 90% IMD	0.9321	0.0008	0.9337	ce14_nopoison_04_090.out
Shift 4-inches, 100% IMD	0.9224	0.0008	0.9240	ce14_nopoison_04_100.out
Slide 6-inches, 60% IMD	0.9279	0.0008	0.9295	ce14_slide_06_060.out:
Slide 6-inches, 70% IMD	**0.9341**	**0.0007**	**0.9355**	**ce14_slide_06_070.out:**
Slide 6-inches, 80% IMD	0.9329	0.0008	0.9345	ce14_slide_06_080.out:
Slide 6-inches, 90% IMD	0.9276	0.0007	0.9290	ce14_slide_06_090.out:
Slide 6-inches, 100% IMD	0.9198	0.0007	0.9212	ce14_slide_06_100.out:
WE 15x15, 4.9 wt. % U-235, 2500 ppm, 32 mg B-10/cm^2 (Type D Basket)				
Shift 4-inches, 60% IMD	0.9271	0.0009	0.9289	we15_np004_060.out:
Shift 4-inches, 70% IMD	0.9382	0.0008	0.9398	we15_np004_070.out:
Shift 4-inches, 80% IMD	**0.9424**	**0.0008**	**0.9440**	**we15_np004_080.out:**
Shift 4-inches, 90% IMD	0.9397	0.0008	0.9413	we15_np004_090.out:
Shift 4-inches, 100% IMD	0.9341	0.0007	0.9355	we15_np004_100.out:
Slide 6-inches, 60% IMD	0.9190	0.0007	0.9204	we15_sl006_060.out:
Slide 6-inches, 70% IMD	0.9324	0.0008	0.9340	we15_sl006_070.out:
Slide 6-inches, 80% IMD	**0.9378**	**0.0008**	**0.9394**	**we15_sl006_080.out:**
Slide 6-inches, 90% IMD	0.9372	0.0008	0.9388	we15_sl006_090.out:
Slide 6-inches, 100% IMD	0.9319	0.0007	0.9333	we15_sl006_100.out:
WE 17x17, 4.8 wt. % U-235, 2500 ppm, 32 mg B-10/cm^2 (Type D Basket)				
Shift 4-inches, 60% IMD	0.9241	0.0009	0.9259	we17_np004_060.out:
Shift 4-inches, 70% IMD	0.9362	0.0007	0.9376	we17_np004_070.out:
Shift 4-inches, 80% IMD	0.9407	0.0007	0.9421	we17_np004_080.out:
Shift 4-inches, 90% IMD	**0.9411**	**0.0007**	**0.9425**	**we17_np004_090.out:**
Shift 4-inches, 100% IMD	0.9366	0.0008	0.9382	we17_np004_100.out:
Slide 6-inches, 60% IMD	0.9153	0.0007	0.9167	we17_sl006_060.out:
Slide 6-inches, 70% IMD	0.9283	0.0007	0.9297	we17_sl006_070.out:
Slide 6-inches, 80% IMD	0.9344	0.0007	0.9358	we17_sl006_080.out:
Slide 6-inches, 90% IMD	**0.9364**	**0.0008**	**0.9380**	**we17_sl006_090.out:**
Slide 6-inches, 100% IMD	0.9346	0.0008	0.9362	we17_sl006_100.out:

Table 6-24
Most Reactive Damaged Assembly Configuration

Description	K_{keno}	σ_{keno}	K_{eff}	Filename
CE 14x14, 4.9 wt. % U-235, 2300 ppm, 15 mg B-10/cm^2 (Type B Basket)				
Optimum Pitch	**0.9512**	**0.0007**	**0.9526**	**ce14_pitch_620_070.out:**
Single Ended Shear	0.9411	0.0008	0.9427	ce14_ss080_080.out:
Double Ended Shear	0.9492	0.0008	0.9508	ce14_ds011_080.out:
Shift 4-inches	0.9371	0.0009	0.9389	ce14_nopoison_04_080.out
Slide 6-inches	0.9341	0.0007	0.9355	ce14_slide_06_070.out:
WE 15x15, 4.9 wt. % U-235, 2500 ppm, 32 mg B-10/cm^2 (Type D Basket), No BPRA				
Optimum Pitch	0.9417	0.0007	0.9431	we15_pitch5877_080.out:
Single Ended Shear	0.9403	0.0007	0.9417	we15_ss035_080.out:
Double Ended Shear	**0.9438**	**0.0008**	**0.9454**	**we15_ds510_080.out:**
Shift 4-inches	0.9424	0.0008	0.9440	we15_np004_080.out:
Slide 6-inches	0.9378	0.0008	0.9394	we15_sl006_080.out:
WE 17x17, 4.8 wt. % U-235, 2500 ppm, 32 mg B-10/cm^2 (Type D Basket), No BPRA				
Optimum Pitch	0.9405	0.0008	0.9421	we17_pitch5100_090.out:
Single Ended Shear	0.9398	0.0008	0.9414	we17_ss015_090.out:
Double Ended Shear	**0.9444**	**0.0008**	**0.9460**	**we17_ds510_090.out:**
Shift 4-inches	0.9411	0.0007	0.9425	we17_np004_090.out:
Slide 6-inches	0.9364	0.0008	0.9380	we17_sl006_090.out:

Table 6-25
Double Ended Rod Shear Study with BPRAs

Description	K_{keno}	σ_{keno}	K_{eff}	Filename
WE 15x15, 4.9 wt. % U-235, 2500 ppm, 32 mg B-10/cm^2 (Type D Basket), BPRA				
Ratio=5/10, 60% IMD	0.9132	0.0008	0.9148	we15bp_ds510_060.out:
Ratio=5/10, 70% IMD	0.9316	0.0008	0.9332	we15bp_ds510_070.out:
Ratio=5/10, 80% IMD	0.9410	0.0009	0.9428	we15bp_ds510_080.out:
Ratio=5/10, 90% IMD	0.9483	0.0008	0.9499	we15bp_ds510_090.out:
Ratio=5/10, 100% IMD	**0.9514**	**0.0007**	**0.9528**	**we15bp_ds510_100.out:**
WE 17x17, 4.8 wt. % U-235, 2500 ppm, 32 mg B-10/cm^2 (Type D Basket), BPRA				
Ratio=5/10, 60% IMD	0.9052	0.0008	0.9068	we17bp_ds510_060.out:
Ratio=5/10, 70% IMD	0.9257	0.0007	0.9271	we17bp_ds510_070.out:
Ratio=5/10, 80% IMD	0.9387	0.0007	0.9401	we17bp_ds510_080.out:
Ratio=5/10, 90% IMD	0.9462	0.0008	0.9478	we17bp_ds510_090.out:
Ratio=5/10, 100% IMD	**0.9478**	**0.0008**	**0.9494**	**we17bp_ds510_100.out:**

Table 6-28
Maximum k_{eff} for Intact Assemblies - Final Results

Description	K_{keno}	σ_{keno}	K_{eff}	Filename
CE 14x14, No BPRA, Type D Basket (7.0 mg B-10/cm^2), 2300 ppm Boron, 4.4 wt. % U-235				
70% IMD	0.9383	0.0007	0.9397	ce14b23_p07e44_070.out:
WE 15x15, No BPRA, Type D Basket (32.0 mg B-10/cm^2), 2500 ppm Boron, 4.9 wt. % U-235				
90% IMD	0.9383	0.0008	0.9399	we15b25_p32e49_090.out:
Dry	0.5340	0.0004	0.5348	we15b25_p32e49_000.out:
WE 15x15, BPRA, Type D Basket (32.0 mg B-10/cm^2), 2400 ppm Boron, 4.7 wt. % U-235				
100% IMD	0.9388	0.0007	0.9402	we15bp24_p32e47_100.out:
Dry	0.5408	0.0005	0.5418	we15bp24_p32e47_000.out:
WE 17x17, No BPRA, Type A Basket (7.0 mg B-10/cm^2), 2300 ppm Boron, 3.8 wt. % U-235				
70% IMD	0.9390	0.0007	0.9404	we17b23_p07e38_070.out:
Dry	0.5286	0.0004	0.5294	we17b23_p07e38_000.out:
WE 17x17, BPRA, Type A Basket (7.0 mg B-10/cm^2), 2500 ppm Boron, 3.9 wt. % U-235				
80% IMD	0.9381	0.0008	0.9397	we17bp25_p07e39_080.out:
Dry	0.5554	0.0004	0.5562	we17bp25_p07e39_000.out:
Regulatory Requirements				
Dry Storage : Bounded by Infinite array of Dry Casks	0.5554	0.0004	0.5562	we17bp25_p07e39_000.out:
Normal Conditions: Wet Loading	0.9388	0.0007	0.9402	we15bp24_p32e47_100.out:
Accident Conditions: Damaged Transfer Cask While Fuel Still Wet	0.9390	0.0007	0.9404	we17b23_p07e38_070.out:

Table 6-29
Maximum k_{eff} for Damaged Assemblies - Final Results

Description	K_{keno}	σ_{keno}	K_{eff}	Filename
CE 14x14, No BPRA, Type D Basket (15.0 mg B-10/cm^2), 2400 ppm Boron, 4.8 wt. % U-235				
70% IMD	0.9386	0.0007	0.9400	ce14d24_p15e48_070.out:
WE 15x15, BPRA, Type B Basket (15.0 mg B-10/cm^2), 2000 ppm Boron, 3.75 wt. % U-235				
100% IMD	0.9372	0.0007	0.9386	we15bpds_p15e38_100.out:
WE 17x17, BPRA, Type E Basket (50.0 mg B-10/cm^2), 2400 ppm Boron, 4.8 wt. % U-235				
100% IMD	0.9388	0.0007	0.9402	we17bpds_p50e48_100.out:
Dry	0.5264	0.0004	0.5272	we17bpds_p50e48_000.out:
Regulatory Requirements				
Dry Storage : Bounded by Infinite array of Dry Casks	0.5264	0.0004	0.5272	we17bpds_p50e48_000.out:
Normal Conditions: Wet Loading	0.9388	0.0007	0.9402	we17bpds_p50e48_100.out:
Accident Conditions: Damaged Transfer Cask While Fuel Still Wet	0.9364	0.0007	0.9378	we17bpds_p15e42_090.out:

Table 6-31
USL-1 Results

Parameter	Range of Applicability	Formula to Determine USL
Pin Pitch (cm)	0.890 - 2.540	0.9366 + (4.2438E-03)*X (X < 1.796) 0.9442 (X ≥ 1.796)
Water to Fuel Volume Ratio	0.383 - 5.067	0.9421 + (7.6076E-04)*X (X < 2.146) 0.9438 (X ≥ 2.146)
Average Energy Group Causing Fission (AEG)	29.89 - 36.61	0.9466 - (8.5090E-05)*X (X < 32.548) 0.9438 (X ≥ 32.548)
Assembly Separation (cm)	1.640 - 20.78	0.9409 + (5.0514E-04)*X (X < 7.118) 0.9445 (X ≥ 7.118)
Boron Concentration (ppm)	15 - 3389	0.9435 + (5.3999E-07)*X (X < 2450) 0.9449 (X ≥ 2450)
Enrichment (wt. % U-235)	2.350 - 5.740	0.9403 + (1.0614E-03)*X (X < 3.597) 0.9442 (X ≥ 3.597)

Table 6-32
USL Determination for Criticality Analysis

Parameter	Value from Limiting WE 17x17 Analysis	Bounding USL-1
Pin Pitch (cm)	**1.25984**	**0.9419**
Water to Fuel Volume Ratio	1.6668	0.9433
Average Energy Group Causing Fission (AEG)	30.9147	0.9438
Assembly Separation (cm)	2.222	0.9420
Boron Concentration (ppm)	2300	0.9447
Enrichment (wt. % U-235)	3.700 (min)	0.9442
Parameter	**Value from Limiting WE 15x15 Analysis**	**Bounding USL**
Pin Pitch (cm)	1.43002	0.9426
Water to Fuel Volume Ratio	1.6751	0.9433
Average Energy Group Causing Fission (AEG)	31.3557	0.9438
Assembly Separation (cm)	2.222	0.9420
Boron Concentration (ppm)	2400	0.9448
Enrichment (wt. % U-235)	3.700 (min)	0.9442
Parameter	**Value from Limiting CE 14x14 Analysis**	**Bounding USL**
Pin Pitch (cm)	1.4732	0.9428
Water to Fuel Volume Ratio	1.6127	0.9433
Average Energy Group Causing Fission (AEG)	30.5980	0.9440
Assembly Separation (cm)	2.222	0.9420
Boron Concentration (ppm)	2400	0.9448
Enrichment (wt. % U-235)	3.700 (min)	0.9442

Table 6-33
CE 14x14 Class Intact Assemblies - Final Results

Description	K_{keno}	σ_{keno}	K_{eff}	Filename
Type A Basket (7.0 mg B-10/cm^2), 2000 ppm Boron, 4.05 wt. % U-235				
60% IMD	0.9290	0.0008	0.9306	ce14b20_p07e40_060.out:
70% IMD	0.9344	0.0009	0.9362	ce14b20_p07e40_070.out:
80% IMD	0.9338	0.0008	0.9354	ce14b20_p07e40_080.out:
90% IMD	0.9281	0.0007	0.9295	ce14b20_p07e40_090.out:
100% IMD	0.9192	0.0007	0.9206	ce14b20_p07e40_100.out:
Type B Basket (15.0 mg B-10/cm^2), 2000 ppm Boron, 4.55 wt. % U-235				
60% IMD	0.9239	0.0009	0.9257	ce14b20_p15e45_060.out:
70% IMD	0.9349	0.0008	0.9365	ce14b20_p15e45_070.out:
80% IMD	0.9364	0.0007	0.9378	ce14b20_p15e45_080.out:
90% IMD	0.9359	0.0008	0.9375	ce14b20_p15e45_090.out:
100% IMD	0.9299	0.0007	0.9313	ce14b20_p15e45_100.out:
Type C Basket (20.0 mg B-10/cm^2), 2000 ppm Boron, 4.70 wt. % U-235				
60% IMD	0.9183	0.0009	0.9201	ce14b20_p20e47_060.out:
70% IMD	0.9311	0.0007	0.9325	ce14b20_p20e47_070.out:
80% IMD	0.9357	0.0007	0.9371	ce14b20_p20e47_080.out:
90% IMD	0.9324	0.0007	0.9338	ce14b20_p20e47_090.out:
100% IMD	0.9294	0.0009	0.9312	ce14b20_p20e47_100.out:
Type D Basket (32.0 mg B-10/cm^2), 2000 ppm Boron, 5.00 wt. % U-235				
60% IMD	0.9091	0.0007	0.9105	ce14b20_p32e50_060.out:
70% IMD	0.9242	0.0009	0.9260	ce14b20_p32e50_070.out:
80% IMD	0.9320	0.0007	0.9334	ce14b20_p32e50_080.out:
90% IMD	0.9347	0.0008	0.9363	ce14b20_p32e50_090.out:
100% IMD	0.9317	0.0007	0.9331	ce14b20_p32e50_100.out:
Type A Basket (7.0 mg B-10/cm^2), 2300 ppm Boron, 4.40 wt. % U-235				
60% IMD	0.9356	0.0008	0.9372	ce14b23_p07e44_060.out:
70% IMD	**0.9383**	**0.0007**	**0.9397**	**ce14b23_p07e44_070.out:**
80% IMD	0.9338	0.0007	0.9352	ce14b23_p07e44_080.out:
90% IMD	0.9282	0.0008	0.9298	ce14b23_p07e44_090.out:
100% IMD	0.9159	0.0008	0.9175	ce14b23_p07e44_100.out:
Type B Basket (15.0 mg B-10/cm^2), 2300 ppm Boron, 4.90 wt. % U-235				
60% IMD	0.9286	0.0007	0.9300	ce14b23_p15e49_060.out:
70% IMD	0.9359	0.0009	0.9377	ce14b23_p15e49_070.out:
80% IMD	0.9377	0.0008	0.9393	ce14b23_p15e49_080.out:
90% IMD	0.9327	0.0007	0.9341	ce14b23_p15e49_090.out:
100% IMD	0.9256	0.0007	0.9270	ce14b23_p15e49_100.out:

Table 6-33
CE 14x14 Class Intact Assemblies - Final Results
(Continued)

Description	K_{keno}	σ_{keno}	K_{eff}	Filename
Type C Basket (20.0 mg B-10/cm^2), 2300 ppm Boron, 5.00 wt. % U-235				
60% IMD	0.9196	0.0007	0.9210	ce14b23_p20e50_060.out:
70% IMD	0.9295	0.0007	0.9309	ce14b23_p20e50_070.out:
80% IMD	0.9305	0.0008	0.9321	ce14b23_p20e50_080.out:
90% IMD	0.9285	0.0008	0.9301	ce14b23_p20e50_090.out:
100% IMD	0.9223	0.0007	0.9237	ce14b23_p20e50_100.out:
Type A Basket (07.0 mg B-10/cm^2), 2400 ppm Boron, 4.45 wt. % U-235				
60% IMD	0.9317	0.0007	0.9331	ce14b24_p07e44_060.out:
70% IMD	0.9347	0.0007	0.9361	ce14b24_p07e44_070.out:
80% IMD	0.9305	0.0008	0.9321	ce14b24_p07e44_080.out:
90% IMD	0.9221	0.0007	0.9235	ce14b24_p07e44_090.out:
100% IMD	0.9124	0.0008	0.9140	ce14b24_p07e44_100.out:
Type B Basket (15.0 mg B-10/cm^2), 2400 ppm Boron, 5.00 wt. % U-235				
60% IMD	0.9290	0.0007	0.9304	ce14b24_p15e50_060.out:
70% IMD	0.9358	0.0008	0.9374	ce14b24_p15e50_070.out:
80% IMD	0.9358	0.0007	0.9372	ce14b24_p15e50_080.out:
90% IMD	0.9306	0.0007	0.9320	ce14b24_p15e50_090.out:
100% IMD	0.9238	0.0007	0.9252	ce14b24_p15e50_100.out:
Type A Basket (07.0 mg B-10/cm^2), 2500 ppm Boron, 4.55 wt. % U-235				
60% IMD	0.9345	0.0007	0.9359	ce14b25_p07e45_060.out:
70% IMD	0.9370	0.0008	0.9386	ce14b25_p07e45_070.out:
80% IMD	0.9295	0.0008	0.9311	ce14b25_p07e45_080.out:
90% IMD	0.9237	0.0007	0.9251	ce14b25_p07e45_090.out:
100% IMD	0.9139	0.0007	0.9153	ce14b25_p07e45_100.out:

Table 6-34
CE 14x14 Class Damaged Assemblies - Final Results

Description	K_{keno}	σ_{keno}	K_{eff}	Filename
Type A Basket (7.0 mg B-10/cm^2), 2000 ppm Boron, 3.90 wt. % U-235				
60% IMD	0.9371	0.0007	0.9385	ce14d20_p07e39_060.out:
70% IMD	0.9375	0.0007	0.9389	ce14d20_p07e39_070.out:
80% IMD	0.9304	0.0007	0.9318	ce14d20_p07e39_080.out:
90% IMD	0.9181	0.0007	0.9195	ce14d20_p07e39_090.out:
100% IMD	0.9046	0.0008	0.9062	ce14d20_p07e39_100.out:
Type B Basket (15.0 mg B-10/cm^2), 2000 ppm Boron, 4.35 wt. % U-235				
60% IMD	0.9331	0.0008	0.9347	ce14d20_p15e43_060.out:
70% IMD	0.9381	0.0007	0.9395	ce14d20_p15e43_070.out:
80% IMD	0.9354	0.0008	0.9370	ce14d20_p15e43_080.out:
90% IMD	0.9282	0.0007	0.9296	ce14d20_p15e43_090.out:
100% IMD	0.9180	0.0007	0.9194	ce14d20_p15e43_100.out:
Type C Basket (20.0 mg B-10/cm^2), 2000 ppm Boron, 4.50 wt. % U-235				
60% IMD	0.9293	0.0007	0.9307	ce14d20_p20e45_060.out:
70% IMD	0.9348	0.0007	0.9362	ce14d20_p20e45_070.out:
80% IMD	0.9342	0.0007	0.9356	ce14d20_p20e45_080.out:
90% IMD	0.9273	0.0007	0.9287	ce14d20_p20e45_090.out:
100% IMD	0.9187	0.0007	0.9201	ce14d20_p20e45_100.out:
Type D Basket (32.0 mg B-10/cm^2), 2000 ppm Boron, 4.85 wt. % U-235				
60% IMD	0.9263	0.0007	0.9277	ce14d20_p32e48_060.out:
70% IMD	0.9370	0.0008	0.9386	ce14d20_p32e48_070.out:
80% IMD	0.9385	0.0006	0.9397	ce14d20_p32e48_080.out:
90% IMD	0.9338	0.0007	0.9352	ce14d20_p32e48_090.out:
100% IMD	0.9257	0.0008	0.9273	ce14d20_p32e48_100.out:
Type E Basket (50.0 mg B-10/cm^2), 2000 ppm Boron, 5.00 wt. % U-235				
60% IMD	0.9111	0.0007	0.9125	ce14d20_p50e50_060.out:
70% IMD	0.9240	0.0008	0.9256	ce14d20_p50e50_070.out:
80% IMD	0.9296	0.0008	0.9312	ce14d20_p50e50_080.out:
90% IMD	0.9253	0.0007	0.9267	ce14d20_p50e50_090.out:
100% IMD	0.9197	0.0008	0.9213	ce14d20_p50e50_100.out:
Type A Basket (7.0 mg B-10/cm^2), 2300 ppm Boron, 4.20 wt. % U-235				
60% IMD	0.9382	0.0007	0.9396	ce14d23_p07e42_060.out:
70% IMD	0.9363	0.0007	0.9377	ce14d23_p07e42_070.out:
80% IMD	0.9280	0.0008	0.9296	ce14d23_p07e42_080.out:
90% IMD	0.9161	0.0007	0.9175	ce14d23_p07e42_090.out:
100% IMD	0.8999	0.0007	0.9013	ce14d23_p07e42_100.out:

Table 6-34
CE 14x14 Class Damaged Assemblies - Final Results
(Continued)

Description	K_{keno}	σ_{keno}	K_{eff}	Filename
Type B Basket (15.0 mg B-10/cm^2), 2300 ppm Boron, 4.70 wt. % U-235				
60% IMD	0.9369	0.0009	0.9387	ce14d23_p15e47_060.out:
70% IMD	0.9380	0.0007	0.9394	ce14d23_p15e47_070.out:
80% IMD	0.9349	0.0007	0.9363	ce14d23_p15e47_080.out:
90% IMD	0.9242	0.0007	0.9256	ce14d23_p15e47_090.out:
100% IMD	0.9118	0.0008	0.9134	ce14d23_p15e47_100.out:
Type C Basket (20.0 mg B-10/cm^2), 2300 ppm Boron, 4.85 wt. % U-235				
60% IMD	0.9314	0.0008	0.9330	ce14d23_p20e48_060.out:
70% IMD	0.9357	0.0008	0.9373	ce14d23_p20e48_070.out:
80% IMD	0.9346	0.0008	0.9362	ce14d23_p20e48_080.out:
90% IMD	0.9260	0.0007	0.9274	ce14d23_p20e48_090.out:
100% IMD	0.9135	0.0007	0.9149	ce14d23_p20e48_100.out:
Type D Basket (32.0 mg B-10/cm^2), 2300 ppm Boron, 5.00 wt. % U-235				
60% IMD	0.9170	0.0007	0.9184	ce14d23_p32e50_060.out:
70% IMD	0.9231	0.0007	0.9245	ce14d23_p32e50_070.out:
80% IMD	0.9237	0.0007	0.9251	ce14d23_p32e50_080.out:
90% IMD	0.9173	0.0007	0.9187	ce14d23_p32e50_090.out:
100% IMD	0.9081	0.0007	0.9095	ce14d23_p32e50_100.out:
Type A Basket (07.0 mg B-10/cm^2), 2400 ppm Boron, 4.25 wt. % U-235				
60% IMD	0.9356	0.0007	0.9370	ce14d24_p07e42_060.out:
70% IMD	0.9322	0.0007	0.9336	ce14d24_p07e42_070.out:
80% IMD	0.9235	0.0007	0.9249	ce14d24_p07e42_080.out:
90% IMD	0.9113	0.0007	0.9127	ce14d24_p07e42_090.out:
100% IMD	0.8952	0.0006	0.8964	ce14d24_p07e42_100.out:
Type B Basket (15.0 mg B-10/cm^2), 2400 ppm Boron, 4.80 wt. % U-235				
60% IMD	0.9366	0.0007	0.9380	ce14d24_p15e48_060.out:
70% IMD	**0.9386**	**0.0007**	**0.9400**	**ce14d24_p15e48_070.out:**
80% IMD	0.9323	0.0007	0.9337	ce14d24_p15e48_080.out:
90% IMD	0.9242	0.0007	0.9256	ce14d24_p15e48_090.out:
100% IMD	0.9115	0.0007	0.9129	ce14d24_p15e48_100.out:
Type C Basket (20.0 mg B-10/cm^2), 2400 ppm Boron, 4.95 wt. % U-235				
60% IMD	0.9318	0.0008	0.9334	ce14d24_p20e49_060.out:
70% IMD	0.9354	0.0008	0.9370	ce14d24_p20e49_070.out:
80% IMD	0.9313	0.0008	0.9329	ce14d24_p20e49_080.out:
90% IMD	0.9247	0.0007	0.9261	ce14d24_p20e49_090.out:
100% IMD	0.9121	0.0007	0.9135	ce14d24_p20e49_100.out:

Table 6-34
CE 14x14 Class Damaged Assemblies - Final Results
(Continued)

Description	K_{keno}	σ_{keno}	K_{eff}	Filename
Type A Basket (07.0 mg B-10/cm^2), 2500 ppm Boron, 4.35 wt. % U-235				
60% IMD	0.9364	0.0007	0.9378	ce14d25_p07e43_060.out:
70% IMD	0.9323	0.0007	0.9337	ce14d25_p07e43_070.out:
80% IMD	0.9235	0.0006	0.9247	ce14d25_p07e43_080.out:
90% IMD	0.9087	0.0007	0.9101	ce14d25_p07e43_090.out:
100% IMD	0.8926	0.0007	0.8940	ce14d25_p07e43_100.out:
Type B Basket (15.0 mg B-10/cm^2), 2500 ppm Boron, 4.90 wt. % U-235				
60% IMD	0.9375	0.0009	0.9393	ce14d25_p15e49_060.out:
70% IMD	0.9380	0.0007	0.9394	ce14d25_p15e49_070.out:
80% IMD	0.9327	0.0008	0.9343	ce14d25_p15e49_080.out:
90% IMD	0.9220	0.0007	0.9234	ce14d25_p15e49_090.out:
100% IMD	0.9077	0.0008	0.9093	ce14d25_p15e49_100.out:
Type C Basket (20.0 mg B-10/cm^2), 2500 ppm Boron, 5.00 wt. % U-235				
60% IMD	0.9297	0.0007	0.9311	ce14d25_p20e50_060.out:
70% IMD	0.9326	0.0007	0.9340	ce14d25_p20e50_070.out:
80% IMD	0.9277	0.0007	0.9291	ce14d25_p20e50_080.out:
90% IMD	0.9178	0.0007	0.9192	ce14d25_p20e50_090.out:
100% IMD	0.9059	0.0007	0.9073	ce14d25_p20e50_100.out:

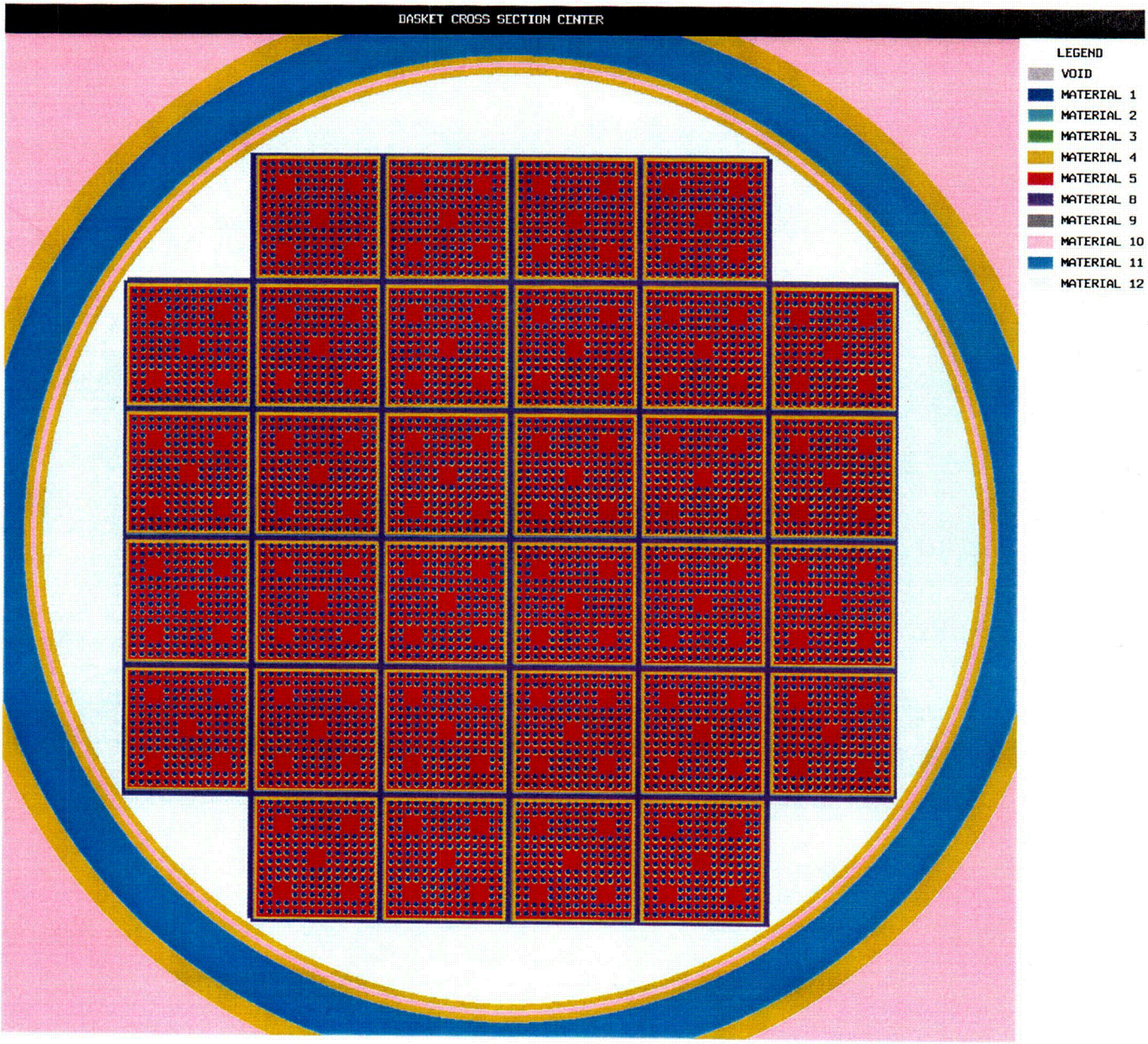

Figure 6-14
CE 14x14 Fuel Assembly : Optimum Pitch Study

12.2 Functional and Operating Limits

12.2.1 Fuel to be Stored in the 32PTH DSC

The spent nuclear fuel to be stored in each 32PTH DSC/HSM-H at the ISFSI shall meet the following requirements:

a. Fuel shall be INTACT FUEL ASSEMBLIES or DAMAGED FUEL ASSEMBLIES. DAMAGED FUEL ASSEMBLIES shall be placed in basket fuel compartments which contain top and bottom end caps. Damaged fuel assemblies shall be stored in the 16 inner-most basket fuel compartments, as shown in Figure 12-1.

b. Fuel types shall be limited to the following:

Westinghouse 15 x 15 (WE 15 x 15) Standard Assemblies
Westinghouse Surry Improved 15 x 15 (WES 15 x 15) Assemblies
Westinghouse 17 x 17 (WE 17 x 17) Standard Assemblies
Westinghouse 17 x 17 Vantage 5H (WEV 17 x 17) Assemblies
Westinghouse 17x17 OFA Assemblies (WEO 17x17)
Framatome ANP Advanced MK BW 17 x 17 Assemblies
Combustion Engineering 14x14 (CE 14x14) Assemblies

The fuel assemblies are specified in Table 12-1

Fuel burnup and cooling time is to be consistent with the limitations specified in Table 12-4.

NFHAs stored integral to the assemblies in a 32PTH DSC, shall be limited to Burnable Poison Rod Assemblies (BPRAs), Thimble Plug Assemblies (TPAs), and Vibration Suppressor Inserts (VSIs). The NFHAs stored shall have acceptable combinations of burnup and cooling time described in Table 12-5.

c. The maximum heat load for a single fuel assembly, including insert components, is 1.5 kW. The maximum heat load per 32PTH DSC, including any integral insert components, shall not exceed 34.8 kW for 15x15 or 17x17 assemblies and 33.8 kW for CE 14x14 assembies. Fuel assemblies may be qualified for four (4) heat load zones designated as Zones 1a, 1b, 2 and 3. Figure 12-2 shows the heat load zone locations. Table 12-4 identifies the acceptable combinations of enrichment, burnup and cooling times. Any fuel assembly that is thermally qualified from Table12-4 is acceptable from a shielding (Table2-3) perspective, since the maximum decay heat load is 1.5 kW and only 8 are allowed in the 32PTH DSC. The shielding analysis assumes 32, 1.5kW assemblies are in the 32PTH DSC.

d. Fuel can be stored in the 32PTH DSC in any of the following configurations:

1) A maximum of 32 INTACT fuel assemblies; or

2) Up to 16 DAMAGED FUEL ASSEMBLIES, with the balance INTACT FUEL ASSEMBLIES.

e. Fuel dimensions and weights are provided in Table 12-2.

f. The maximum neutron and gamma source terms are provided in Table 12-3.

12.2.2 Functional and Operating Limits Violations

If any Functional and Operating Limit of 12.1 is violated, the following actions shall be completed:

12.2.2.1 The affected fuel assemblies shall be placed in a safe condition.

12.2.2.2 Within 24 hours, notify the NRC Operations Center.

12.2.2.3 Within 30 days, submit a special report which describes the cause of the violation and the actions taken to restore compliance and prevent recurrence.

Table 12-1
Fuel Specifications

Fuel Type	Maximum Assembly Average Initial Enrichment	Cladding Material	Minimum Cooling Time	Minimum Assembly Average Initial Enrichment	Maximum Burnup
WE 15x15 WES 15x15	5.0 weight % U-235	Zircalloy-4 Zirlo	5 years	See Table 2-4 for Enrichment, Burnup, and Cooling Time Limits.	60 GWD/MTU
WE 17x17 WEV 17x17 WE 17x17 OFA	5.0 weight % U-235	Zircalloy-4 Zirlo	5 years	See Table 2-4 for Enrichment, Burnup, and Cooling Time Limits	60 GWd/MTU
Framatome MK BW 17x17	5.0 weight % U-235	M5	5 years	See Table 2-4 for Enrichment, Burnup, and Cooling Time Limits	60 GWd/MTU
CE 14x14	5.0 weight % U-235	Zircalloy-4 Zirlo	5 years	See Table 2-4 for Enrichment, Burnup, and Cooling Time Limits	60 GWd/MTU
NFHA	N/A	N/A	5 years	See Table 2-5	

Table 12-2
Fuel Dimension and Weights

Parameter	15x15 WE &WES	17 x 17 WE	17x17 MK BW	17x17 WEV	17x17 WEO	14x14 CE
Initial Enrichment, wt % U235 (max)	5.00	5.00	5.00	5.00	5.00	5.00
Clad Material	Zr-4/Zirlo	Zr-4/Zirlo	M5	Zr-4/Zirlo	Zr-4/Zirlo	Zr-4/Zirlo
No of fuel rods	204	264	264	264	264	176
No of guide/instrument tubes	21	25	25	25	25	5
Assembly Length[4]	162.2	162.4	162.4	162.4	162.4	159.5
Max Uranium Loading (MTU)	467	467	476	467	467	385
Assembly Cross Section	8.424 x 8.424	8.426 x 8.426	8.425 x 8.425	8.426 x 8.426	8.426 x 8.426	8.25 x 8.25
Max Assembly Weight with Insert components[4]	1528	1533	1554	1533	1533	1450[5]

(1) Nominal values shown unless stated otherwise
(2) All dimensions are inches
(3) Includes allowance for irradiation growth
(4) Weights of TPAs and VSIs are enveloped by BPRAs
(5) Without NHAHs

Table 12-7
Maximum Initial Enrichment for Intact and Damaged Fuel Loading

Assembly Class and Type	Maximum Initial enrichment of U-235 as a Function of Soluble Boron Concentration and Fixed Poison Loading (Basket Type)				
	Basket Type	Minimum Soluble Boron Concentration			
		2000 ppm	2300 ppm	2400 ppm	2500 ppm
CE 14x14 Fuel Assembly (Intact Fuel Loading)	A	4.05	4.40	4.45	4.55
	B	4.55	4.90	5.00	-
	C	4.70	5.00	-	-
	D	5.00	-	-	-
	E	-	-	-	-
WE 15x15 Fuel Assembly (with BPRAs)	A	3.50	3.70	3.80	3.90
	B	3.80	4.10	4.20	4.30
	C	3.95	4.25	4.35	4.45
	D	4.20	4.50	4.70	4.80
	E	4.50	4.80	4.90	5.00
WE 17x17 Fuel Assembly (with BPRAs)	A	3.50	3.70	3.80	3.90
	B	3.80	4.10	4.20	4.30
	C	3.95	4.25	4.35	4.45
	D	4.20	4.50	4.60	4.70
	E	4.45	4.70	4.90	5.00
CE 14x14 Fuel Assembly (Damaged Fuel Loading)	A	3.90	4.20	4.25	4.35
	B	4.35	4.70	4.80	4.90
	C	4.50	4.85	4.95	5.00
	D	4.85	5.00	-	-
	E	5.00	-	-	-
WE 15x15 Fuel Assembly (with BPRAs - bounds all Damaged Fuel Loading)	A	3.40	3.60	3.70	3.80
	B	3.75	4.00	4.10	4.20
	C	3.85	4.15	4.25	4.35
	D	4.10	4.40	4.50	4.60
	E	4.35	4.70	4.80	4.90
WE 17x17 Fuel Assembly (with BPRAs - bounds all Damaged Fuel Loading)	A	3.40	3.60	3.70	3.80
	B	3.75	4.00	4.10	4.20
	C	3.85	4.15	4.25	4.35
	D	4.10	4.40	4.50	4.60
	E	4.30	4.65	4.80	4.90

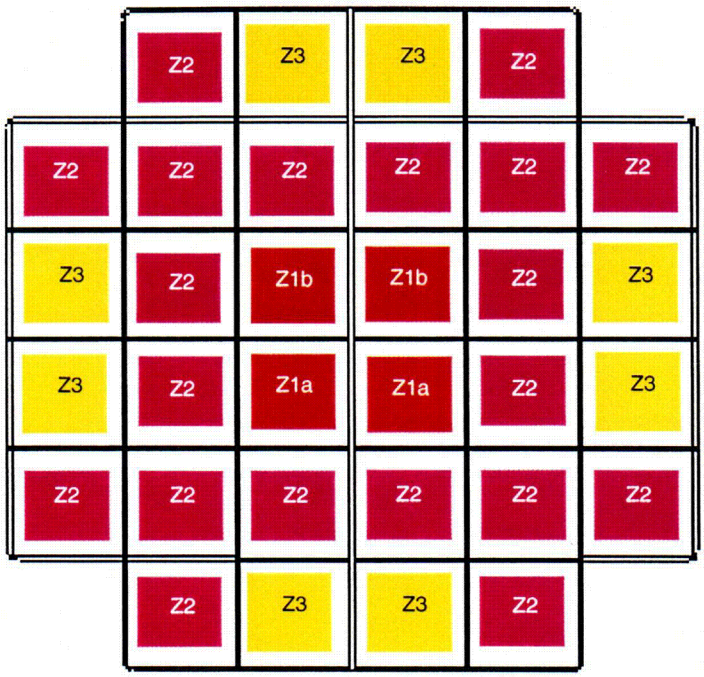

For CE 14x14 Assemblies

- Q_{zi} is the maximum decay heat per assembly in zone i
- Total Decay Heat ≤ 33.8 kW
- 4 fuel assemblies in zone 1 with Q_{z1} ≤0.775 kW
- 20 fuel assemblies in zone 2 with Q_{z2} ≤ 1.068 kW
- 8 fuel assemblies in zone 3 with Q_{z3} ≤ 1.5 kW
- $Q_{z1} \leq Q_{z2} \leq Q_{z3}$

For other Assemblies

- Q_{zi} is the maximum decay heat per assembly in zone i
- Total Decay Heat ≤ 34.8 kW
- 4 fuel assemblies in zone 1 with
  - total decay heat ≤ 3.2 kW
  - Q_{z1a} ≤ 1.05 kW in the lower compartments
  - Q_{z1b} ≤ 0.8 kW in the upper compartments
- 20 fuel assemblies in zone 2 with Q_{z2} ≤ 1.1 kW
- 8 fuel assemblies in zone 3 with Q_{z3} ≤ 1.5 kW
- $Q_{z1} \leq Q_{z2} \leq Q_{z3}$

Figure 12-2
Heat Load Zones